CEReS JUWOC ESTO

Proceedings of The International Symposium on Ocean Color Remote Sensing and Carbon Flux

December 13-15, 1999

Keyaki Hall, Chiba University, Japan

Center for Environmental Remote Sensing, Chiba Univ. (CEReS)

Japan-US Workshop on Ocean Color (JUWOC)

Earth Science & Technology Organization (ESTO)

International Symposium on Ocean Color Remote Sensing and Carbon Flux

December 13-15, 1999
Chiba University

1. Organizing Committee:

1) Chair

Dr. Yasuhiro Sugimori (CEReS, Chiba University)

2) Members

Dr. Janet Campbell (University of New Hampshire)

Dr. Joji Ishizaka (Nagasaki University)

Dr. Yasuhiro Senga (Tokai University / CEReS, Chiba University)

Dr. Ichio Asanuma (JAMSTEC / CEReS, Chiba University)

2. Sponsors:

CEReS : Center for Remote Sensing of Environmental Research

JUWOC : Japan U.S. Workshop on Ocean Color

ESTO: Earth Science & Technology Organization

Edited by Yasuhiro Sugimori and Ichio Asanuma

Published by

Center for Environmental Remote Sensing (CEReS), Chiba University

1-33, Yoyoi, Inage, 263-8522, JAPAN

Preface

The International Symposium on Ocean Color Remote Sensing and Carbon Flux was proposed to give oceanographers and related scientists a chance to exchange their ideas and research results on ocean color remote sensing and its application to carbon flux studies. Since the launch of the OCTS and SeaWiFS, ocean color data is flooding into our research fields and providing information related to climate change. At this time, carbon flux in the ocean is a serious research theme, which needs further research and study, especially on the control of carbon flux from fossil fuel consumption. In the near future, there will be improved spectral resolution ocean color data from the GLI and MODIS programs. This symposium was intended to provide opportunities to exchange ideas on these new data fields among scientists.

Through the symposium, we could invite scientists on this field from the U.S., Canada, Italy, and China and exchange each research status. It was a great pleasure to host this symposium under the joint sponsor ships of the Center for Remote Sensing of Environment (CEReS), the Japan-US Workshop on Ocean Color (JUWOC), and the Earth Science & Technology Organization (ESTO). This proceeding may contribute for the further studies on the ocean color remote sensing and carbon flux in the future.

Chair of the symposium
Prof. Yasuhiro Sugimori
CEReS, Chiba University

International Symposium on Ocean Color Remote Sensing and Carbon Flux at Chiba University

Dec.13 Monday

08:30 - Registration

Opening Session

Chairman : Yasuhiro Senga (Tokay Univ./CEReS, Chiba Univ.)

09:00 - 09:10 Opening session
1. Yasuhiro Sugimori (CEReS, Chiba University)
2. John Marra (NASA)

Session A1 : Ocean Color Remote Sensing System

Chairman : Yasuhiro Senga (Tokai Univ./CEReS, Chiba Univ.)

09:10 - 09:35 A1. OCTS summary
Tasuku Tanaka (Earth Observation Research Center/NASDA)

09:35 - 10:00 A2. An Overview of the SeaWiFS Mission
Bryan A. Franz (Goddard Space Flight Center/NASA)

10:00 - 10:25 A3. An Overview of SIMBIOS Project
Giulietta S. Fargion (SIMBIOS PROJECT, GSC-SAIC)

10:25 - 10:45 Coffee break

Session A2 : Ocean Color Remote Sensing System

Chairman : Yoshiaki Honda (CEReS, Chiba University)

10:45 - 11:10 A4. A Status of MODIS
Robert Evans (Miami University)

11:10 - 11:35 A5. GLI Project : Current Status
Vu Saito(Earth Observation Research Center/NASDA)

11:35 - 12:00 A6. Status of GLI
Masanobu Shimada
(Earth Observation Research Center/NASDA)

12:00 - 12:25 A7. International Coordination of Long-Term Ocean Biology Time Series Derived from Satellite Ocean Color Data
Janet W. Campbell (University of New Hampshire)
P.M.Schlittenhardt (ECJRC), T.Tanaka (EORC/NASDA)

12:25 - 13:30 Lunch

Session B1 : View from Ocean Color Sensors

Chairman : Ichio Asanuma (JAMSTEC/CEReS, Chiba University)

13:30 - 13:55 **B1. Early results from SeaWiFS observations of the NE Pacific nd BC coast**
Jim Gower (Institute of Ocean Science)

13:55 - 14:20 **B2. A hypothesis of Cloud-Phytoplankton-Ocean interaction in the subarctic North Pacific**
Hiroshi Kawamura (Tohoku Univ.)

14:20 - 14:45 **B3. Using Scatterometer winds to predict potential productivity in eastern boundary current regions**
Mary-Elena Carr (Jet Propulsion Laboratory/NASA)

14:45 - 15:10 **B4. Application of ocean color imagery for Japanese fisheries**
Hideo Tameishi (Japan Fisheries Information Service Center)

15:10 - 15:30 **Coffee Break**

Session B2: View from Ocean Color Sensor

Chairman : Hiroshi Kawamura (Tohoku University)

15:30 - 15:55 **B5. Variability of pigment biomass and mesoscale thermal features along First Oyashio Intrusion as determined from satellite and ship data**
Kedar N. Mahapatra & Yoshihiro Okada (Tokai Univ.)

16:20 - 16:45 **B6. Ocean Color Variability of Japan JGOFS time series station KNOT and its adjacent waters, northwestern North Pacific observed by OCTS and SeaWiFS**
Kosei Sasaoka, Sei-ichi Saitoh (Hokkaido Univ.),
Ichio Asanuma, Keiri Imai, Makio Honda and Toshiro Saino

16:45 - 17:10 **B7. Interannual Variability in the Optical Characteristics of the Equatorial Pacific: Consequences for the Upper Ocean Heat Budget**
Marlon Lewis (Dalhousie University) and Ichio Asanuma (CEReS)

17:30 - 19:00 **Reception**

Dec.14 Tuesday

Session C : Primary production

Chairman : Joji Ishizaka (Nagasaki University)

09:00 - 09:25 **C1. Photosynthetic characteristics of phytoplankton in the subarctic Pacific Ocean in summer**
Ken Furuya and Takashi Yoshikawa (University of Tokyo)

09:25 - 09:50 **C2. Remote Sensing of Primary Production**
Trevor Platt (Bedford Institute of Oceanography)

09:50 - 10:15 **C3. Chlorophyll and Primary Production in a Cyclonic Eddy off the Island of Hawaii**
Carrie L. Leonard and Robert R. Bidigare (University of Hawaii)

10:15 - 10:35 **Coffee break**

Session D: Optical Properties

Chairman : Sei-ichi Saitoh (Hokkaido University)

10:35 - 11:00 **D1. In-situ measurement of chlorophyll-a specific absorption coefficient in the sea**
S.Kobara, M.Kishino, and S.Taguchi (Soka Univ.)

11:00 - 11:25 **D2. Variations in the Absorption Characteristics of Phytoplankton: Implications for Remote Sensing**
Shubha Sathyendranath (Bedford Institute of Oceanography)

11:25 - 11:50 **D3. Evaluation of ocean color algorithms for the Sea of Japan using a merged Japan-Korea-US data set, and plans for East Asian regional algorithm Development**
Gregg Mitchell (Scripps Institution of Oceanography)
M.Kishino, S.Saitoh, J.Ishizaka, Yu-Hwan Ahn

11:50 - 12:15 **D4. Oceanic chlorophyll *a* algorithm for several cases of waters**
Toru Hirawake (National Institute of Polar Research)

12:15 - 13:30 **Lunch**

Session E : Carbon Flux

Chairman : Marlon Lewis (Dalhousie University)

13:30 - 13:55 **E1. Air-sea carbon flux simulated in an upper ocean biogeochemical model**
Y.Sasai and Motoyoshi Ikeda (Hokkaido Univ.)

13:55 - 14:20 **E2. Variations in CO2 outflux from the central and western equatorial Pacific**
H.Y.Inoue, M.Ishii, H.Matsueda, T.Tokieda, S.Saito (Meteolorgical Research Institude), T.Kawano, and A.Murata (JAMSTEC) I.Asanuma (JAMSTEC/CEReS)

14:20 - 14:45 **E3. Comparison between carbon fluxes collected by time-series sediment trap experiment and the primary productivity estimated with satellite data**
Makio C. Honda, Masashi Kusakabe, Fumiko Hoshi (JAMSTEC), Toshikatsu Sugawara (MWJ), and Ichio Asanuma (JAMSTEC/CEReS)

14:45 - 15:10 **Coffee Break**

Session F : Regional Study

Chairman : Giulietta S. Fargion (SIMBIOS PROJECT, GSC-SAIC)
Co-chairman : Koji Kajiwara (CEReS, Chiba University)

15:10 - 15:35 **F1. A comparison of CZCS, OCTS, POLDER and SeaWiFS chlorophyll imagery of the North Atlantic**
James Yoder (University of Road Island)

15:35 - 16:00 **F2. Chlorophyll control of sea-surface temperature in the Arabian Sea**
Robert Frouin (Scripps Institution of Oceanography), and Shoichiro Nakamoto (ESTO/JAMSTEC)

16:00 - 16:25 **F3. East China Sea**
Joji Ishizaka (Nagasaki University)

16:25 - 16:50 **F4. Banda Sea, Indonesia**
John Marra (NASA)

16:50 - 17:15 **F5. Blooming Mechanism off Lombok Strait**
Ichio ASANUMA (JAMSTEC/CEReS, Chiba University)

Closing Session

Chairman : John Marra (NASA)

17:15 - 17:25 **Closing Address: Yoshizumi YASUDA (CEReS, Chiba University)**

Dec.15 Wednesday

Japan-US Workshop on Ocean Color (JUWOC) 1999

09:00 - 11:00 Presentations from U.S. and Japan side are expected.

1. Opening: Objectives of JUWOC (Satsuki Matsumura)
2. NASA Oceanography NRA ideas (John Marra)
3. Calibration and vicarious calibration among Sensors, CZCS, OCTS, SeaWiFS, MODIS, GLI
4. Exchange of MODIS and GLI data between two agencies.
5. Consistent processing among sensors.
6. Assessment of algorithm among sensors.
7. Joint effort for vicarious calibration and validation.
8. Sharing of in-situ data.

11:00 - 15:00 Group discussion

1. Calibration, vicarious calibration and validation
2. Processing algorithm
3. Data exchange (Satellite and in-situ data)

15:00 - 15:30 Coffee break

15:30 - 16:30 Recommendations

16:30 - 17:00 Publication

(Prof.Sugimori suggested to publish papers in this meeting. We would like to organize a working group for publishing. Working group members will be assigned.

Adjourn

Table of Contents

An Overview of the SeaWiFS Mission

Bryan A. Franz
Goddard Space Flight Center, NASA
E-Mail: franz@orca.gsfc.nasa.gov

Abstracts

SeaWiFS has been operational since September 18, 1997. Since then, a number of improvements in the operational processing have been implemented, including changes to the sensor calibration and atmospheric correction algorithm. The presentation will review the activities of the SeaWiFS Project Office since launch, the improvements in the SeaWiFS processing algorithms, and the results of the product validation effort.

An overview of SIMBIOS Project

Giulietta S. Fargion
GSC SAIC, SIMBIOS Project

Abstracts

The Sensor Intercomparison and Merger for Biological and Interdisciplinary Oceanic Studies (SIMBIOS) Program was conceived in 1994 and consists of the SIMBIOS Science Team and the SIMBIOS Project (http://simbios.gsfc.nasa.gov). The SIMBIOS Science Team is the group of principal investigators defined by the NASA Research Announcements (NRA-96) selections. The SIMBIOS Project was established to provide support and coordination for the SIMBIOS Program such as administration, project documentation, and interagency and international coordination, and incorporates aspects of instrument calibration, round robins, algorithm development and evaluation, product merging, and data processing.

The SIMBIOS Project ongoing data collection takes place via the SIMBIOS Science Team (1997-2000 under NRA-96 and 2001-2003, under the new NRA-99) and the Aerosol Robotic Network (AERONET). The Project funds numerous investigators in order to obtain in situ atmospheric and bio-optical water characterization. Additional investigators are also supported to develop new algorithms or scientific approaches in accordance with the goals of the SIMBIOS Program. The Project has an extensive set of in situ data for match-up analysis from the SeaBASS database, which is presently comprised of data from over 250 cruises and includes 400,000 pigment records. The in situ data in SeaBASS include measurements of water-leaving radiance and other related optical and pigment measurements, from ships, moorings and drifters. SeaBASS data were used by the SIMBIOS Project to validate SeaWiFS and MOS, OCTS, POLDER postlaunch imagery and to develop new operational chlorophyll algorithms.

GLI Project: Current Status

Vu Saito
National Space Development Agency Of Japan
Earth Observation Research Center (NASDA/EORC)
E-Mail: vsaito@eorc.nasda.go.jp

ABSTRACT

Since January 1997, with the collaboration of its contracted PIs, the NASDA ADEOS-II/GLI Project has been developing a system used to generate L2 and higher level standard products making use of data acquired from GLI. As a result of the recent and new JRA (Joint Research Announcement) Program, about 29 PIs all around the world will be newly added to the current GLI PI Team very soon, to join its Cal/Val activities, and to conduct the researches related to the Earth Sciences. In this presentation, an outline of GLI sensor and some current topics of this Project will be given.

International Coordination of Long-Term Ocean Biology Time Series Derived from Satellite Ocean Color Data

Paper presented at the International Symposium on
Ocean Color Remote Sensing and Carbon Flux
Chiba University, Japan
13 December 1999

Janet W. Campbell
University of New Hampshire
Durham, New Hampshire, U.S.A.

Peter M. Schlittenhardt
Space Applications Institute of the
European Commission Joint Research Center
Ispra, Italy

Tasuku Tanaka
NASDA, EORC
Tokyo, Japan

Abstract

In this paper, we will describe plans to coordinate the initial development of long-term ocean biology time series derived from global ocean color observations acquired by the United States, Japan and Europe. Specifically, we have been commissioned by the International Ocean Color Coordinating Group (IOCCG) to coordinate the development of merged products derived from the OCTS, SeaWiFS, MODIS, MERIS and GLI imagers. Each of these missions will have been launched by the year 2002 and will have produced global ocean color data products. Our goal is to develop and document the procedures to be used by each space agency (NASA, NASDA, and ESA) to merge chlorophyll, primary productivity, and other products from these missions. This coordination is required to initiate the production of long-term ocean biology time series which will be continued operationally beyond 2002. The purpose of the time series is to monitor interannual to decadal-scale variability in oceanic primary productivity and to study the effects of environmental change on upper ocean biogeochemical processes.

Introduction

A multi-decadal time series of global ocean biological and biogeochemical measurements is needed to provide an observational basis for understanding and predicting the effects of environmental change on marine ecosystems. These observations will be relevant to both regional issues, such as land-ocean interactions and pollution, fisheries, and harmful algal blooms, as well as broader global issues, such as the global carbon cycle and whether marine primary productivity is changing in response to climate forcing. There are many practical benefits to be derived from such a time series, particularly if combined with time series of physical observations (ocean winds, temperature, sea surface height).

A major purpose of such observations is to provide input for global and regional ecosystem and biogeochemical models. The community of potential users of such data do not want to be concerned with the idiosyncracies of data sets generated by a particular space agency. They would prefer to have a single, self-consistent time series endorsed by all the agencies. There is merit in merging data from multiple mission to improve the space-time coverage of the global data products. This advantage accrues quickly over short time scales (fig. 1), but longer-term products (e.g., weekly or monthly means) derived from merged short-term products would also be improved (IOCCG Report 2).

Ocean color observations derived from satellite missions in the 1996-2002 period are largely experimental in nature. There are differences in atmospheric correction and bio-optical algorithms both within and between agencies. During this time period, we believe that each space agency will want to produce a suite of merged products compatible with its own products. Scientists can then compare different products created with the same data sets. There will likely be valuable information to be derived from systematic differences between products.

Our proposed approach will be to merge level-3 data. NASA and NASDA use different chlorophyll algorithms and also different level-3 binning (averaging) algorithms. These result in systematic differences between level-3 products produced by NASA and NASDA (figs. 2 and 3). ESA currently has no plans to produce level-3 products, and only limited plans for the production of level-2 products. They rely on the user community to develop and validate algorithms, but are willing to generate level-2 and level-3 products once the algorithms are developed and tested.

Importance of international coordination is clear. Thus, we propose to work together to develop and document the procedures to be used by each space agency to merge data products from international missions. Level-3 binned data products will be produced with the appropriate saved information to allow each agency to adjust the data furnished by the other two agencies to be compatible with its own algorithms and products.

Goals

Our long-term goal is to produce a time series of global-scale oceanic chlorophyll concentration and primary productivity, beginning with data from the ADEOS mission in 1996 and continuing indefinitely into the future, by merging global ocean-color satellite observations.

Our short-term goal is to coordinate the initial production of these time series by space agencies in the U.S., Japan and Europe. Specifically, we are proposing to develop and document procedures to be used operationally by NASA, NASDA, and ESA to create chlorophyll, primary productivity, and possibly other products by merging data from the OCTS, POLDER, SeaWiFS, MODIS, MERIS and GLI sensors.

Strategy

The three principal investigators will serve as team leaders within their respective communities, each identifying a team that will work toward developing the time series of merged products. The three team leaders will be responsible for coordinating the work within and between teams.

In the long-term, our strategy is to develop consensus algorithms, as well as consistent calibration and validation methods. In the short term we will share data to help understand differences and to begin creating merged products. Two types of data will be shared. There will be a diagnostic data set generated for selected sites containing all the information needed to process data from level 0 to level 2 (Table 1). These data will be generated during the routine processing of data by each space agency.

In addition, level 3 data will be shared. Our approach will be to merge level 3 (space and time binned) data. Each team will develop a methodology (merging algorithm) for the use of level-3 data from the different satellite missions. It is assumed that each space agency will want to produce a set of merged products that are consistent with its own products. As a minimum, there will be time series of global chlorophyll beginning with OCTS and POLDER data, and continuing with SeaWiFS, MODIS, MERIS, and GLI.

There are different chlorophyll algorithms being used and thus systematic differences between products (see comparison of OCTS and SeaWiFS, fig. 2). Also, there are different level-3 binning algorithms being used (fig. 3). For example, NASDA averages the logarithm of chlorophyll for level-3 OCTS data, whereas NASA's SeaWiFS Project averages chlorophyll. Differences between these methods were analyzed by Campbell et al. (1995) using CZCS data. They demonstrated that the average based on transforming the average logarithm is systematically less than the average chlorophyll.

We will investigate differences between algorithms and prescribe a way to derive chlorophyll from level-3 statistics saved by each sensor. This is likely to require that higher-order statistics be saved in the level-3 binning process. Each space agency will need to translate the "foreign" data to be compatible with its own products. The team for each community will define the input needed to produce its merged products. For example, to convert the average logarithm to a simple arithmetic average requires information on the variance of the logarithm (Campbell, 1995). Each space agency would agree to provide the data needed by the other agencies as a quid pro quo arrangement.

Table 1. Sites recommended for a Diagnostic Data Set to be generated by space agencies. All data within a two degree by two degree box surrounding each site will be saved and put into a separate file. These data will be used to compare algorithms and understand differences in data products generated by NASA, ESA, and NASDA.

MOBY (Hawaii), 20.8N, 157.2W
BATS/BTM (Bermuda), 32.0N, 64.5W
CALCOFI (California Current), 35N, 125W
Equatorial Pacific (EqPAC), 0N, 140W
Palmer LTER, 65S, 65W
LEO 15 (off New Jersey), 39N, 74W
Kashidoo (Maldives Islands), 5N, 73.5E
Lower Chesapeake Bay, 37N, 75.5W
NW African Upwelling, 21N, 17.5W
Ligurian Sea, 43.25 N, 7.05 E
North Adriatic ("Venice Tower"), 45.32N, 12.5E
Eastern Mediterranean, 33N, 32.5E
English Channel ("Plymbody"), 50.22 N, 4.08W
Helgoland/North Sea, 54N, 9E
Baltic Sea, 55N, 19.25E
East China Sea, 30N, 125E
Aline (Japan East Coast), 40N, 142E
KNOT (NW Pacific), 43N, 165E
Cariaco Basin, 11N, 65.1W
Gulf of Maine, 43N, 69W
Near Cape Town (St Helena Bay), 33S, 17.5E
Near Luderitz, Namibia 26S, 14.5E (World's strongest upwelling)
Philippine Sea, 17 N, 133 E
Cook Islands, 20 S, 163 W (World's deepest Secchi depth, 67m)

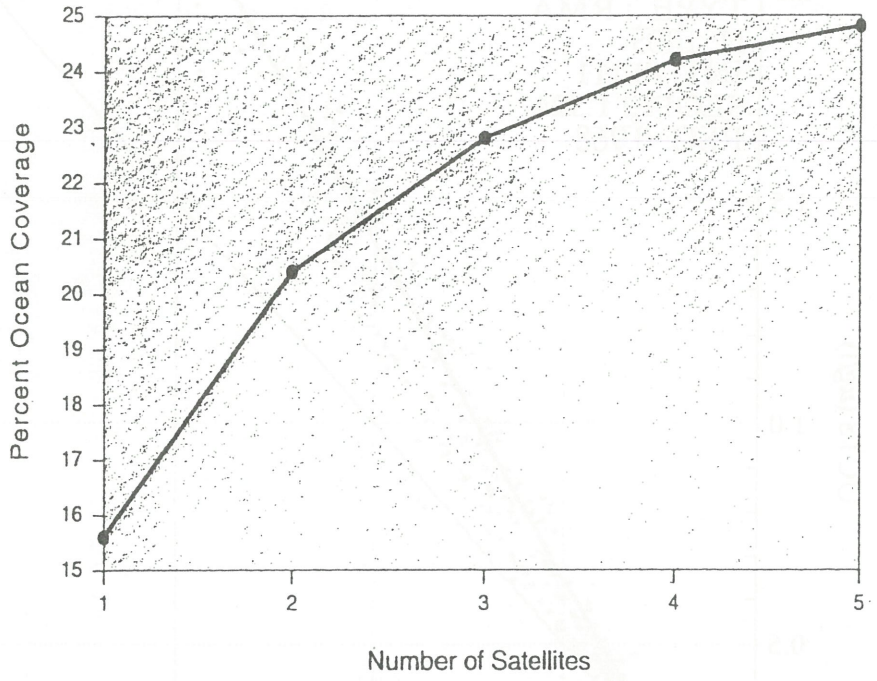

Figure 1. *Combined ocean coverage (in percent) by multiple satellites of the same design for one day. The satellite/sensor is SeaWiFS-type: noon descending node, 705 km altitude, scan width 45°, with a tilt capability. The satellite orbits differ only in the mean anomaly, which is set to produce average combined coverage. In this analysis, sun glint and clouds obscure observations of the ocean surface, producing the low estimates of ocean coverage. Sun glint is computed from climatological wind speeds as a function of viewing and solar geometry with respect to the satellite orbit. The sun-glint threshold is set to about four times the SeaWiFS Noise Equivalent Delta Radiance (NEΔL). This is an extreme estimate of sun glint contamination. However, sun glint can confuse the determination of aerosol characteristics, especially when the aerosol radiative characteristics are very different from those of sun glint, which may cause significant errors in chlorophyll retrieval. In the context of using data from multiple satellites, such possible errors need to be identified so they can be eliminated from the merged data set. Thus this estimate of sun glint supports the multi-mission application. Clouds are derived from global six-year climatology.*

From IOCCG, Report No. 2 entitled "Status and Plans for Satellite Ocean-Colour Missions: Considerations for Complementary Missions.

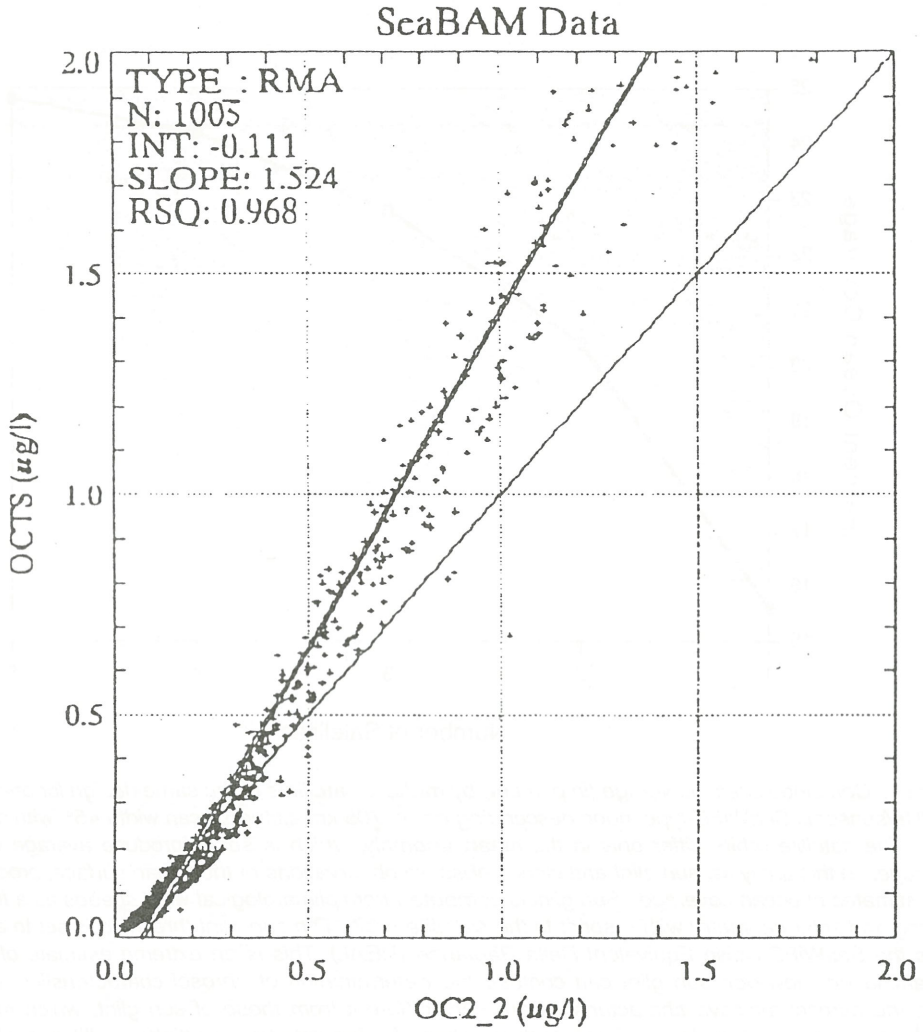

Figure. 2 Comparison of chlorophyll derived according to OCTS algorithm and chlorophyll derived according to SeaWiFS (OC2.V2) algorithm. Both algorithms were applied to the same data set (the SeaBAM data). Figure provided by John (Jay) O'Reilly and James (Jim) Yoder.

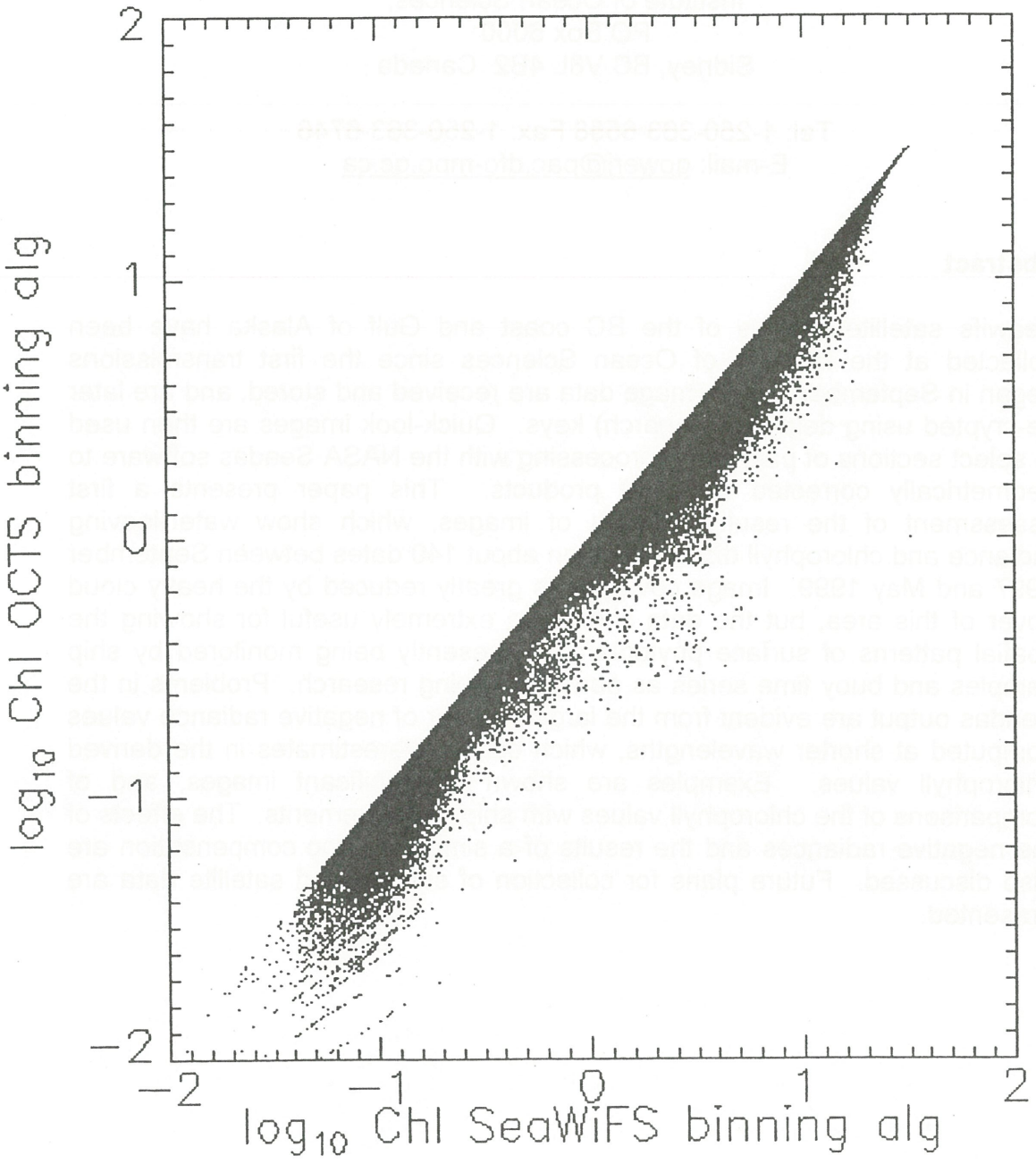

Figure. 3 Comparison of binning algorithms. The vertical axis is derived by transforming the average of the logarithm of chlorophyll. This is the binning algorithm used for OCTS data. The horizontal axis is the average of chlorophyll over the same set of images. This is the binning algorithm used by SeaWiFS. The data used were SeaWiFS data for Northwest Atlantic for the month of July 1998.

Early results from Seawifs observations of the NE Pacific and BC coast

J.F.R. Gower
Institute of Ocean Sciences,
PO Box 6000
Sidney, BC V8L 4B2 Canada

Tel: 1-250-363-6558 Fax: 1-250-363-6746
E-mail: gowerj@pac.dfo-mpo.gc.ca

Abstract

Seawifs satellite images of the BC coast and Gulf of Alaska have been collected at the Institute of Ocean Sciences since the first transmissions began in September 1997. Image data are received and stored, and are later de-crypted using delayed (research) keys. Quick-look images are then used to select sections of passes for processing with the NASA Seadas software to geometrically corrected (level 3) products. This paper presents a first assessment of the resulting series of images, which show water-leaving radiance and chlorophyll distributions on about 140 dates between September 1997 and May 1999. Image coverage is greatly reduced by the heavy cloud cover of this area, but the data should be extremely useful for showing the spatial patterns of surface phytoplankton presently being monitored by ship samples and buoy time series as part of on-going research. Problems in the Seadas output are evident from the large number of negative radiance values computed at shorter wavelengths, which cause overestimates in the derived chlorophyll values. Examples are shown of significant images, and of comparisons of the chlorophyll values with ship measurements. The effects of the negative radiances and the results of a simple ad-hoc compensation are also discussed. Future plans for collection of surface and satellite data are presented.

Introduction

The importance of satellite images of coastal and offshore water colour patterns for showing the spatial and temporal variability of primary productivity is now widely recognised. After the initial demonstration by NASA's CZCS imager, data were first provided by Japan's OCTS imager and are now being regularly provided by the Seawifs instrument. Improved satellite-born imagers (MODIS and MERIS) will soon be launched by both NASA and ESA.

Seawifs image data are available as global mosaiced products with about 10 km spatial resolution. Higher resolution (1 km) imagery can also be received directly using local tracking antennas. Seawifs satellite images of the BC coast and Gulf of Alaska have been collected at IOS since the first transmissions began in September 1997. Images are received and stored using low-cost hardware, and are de-crypted using delayed (research) keys provided over the internet as part of NASA's support to international research. Data are converted to level 0 and a copy is sent to NASA. A simple processing of the data gives quick-look images of an individual band (usually band 3, 490 nm) with a first-order atmospheric correction that shows water colour features in cloud-free areas. Images selected from these quick-looks are then processed to geometrically corrected (level 3) products using the Seadas software.

This paper reports on a first assessment of the resulting series of images, which show water-leaving radiance and chlorophyll distributions on about 140 dates (though with significant cloud cover) between September 1997 and May 1999.

Seadas results

The Seadas software produces Level 1 and Level 2 data of complete Seawifs passes, and also produces mapped (Level 3) products of specified areas. Level 2 and 3 data show derived products for each pixel, including normalised water-leaving radiances in the first 5 spectral bands (centered at 412, 443, 490, 510, and 555 nm) and chlorophyll concentrations. 16 flags for each pixel indicate conditions based on Seawifs data (blooms, turbidity and other anomalies), geometry (sun and satellite angles, sun glint) other data bases (land, shallow water), see table 1, below. These flags provide much of the diagnostic information useful in interpreting the images, and include one flag, for coccolithophores, that attempts an identification through the spectral signature measured by Seawifs.

Figure 1 shows four images (Level 3 data) derived from the Seawifs pass on 28 May 1998 of the Vancouver Island area, which was especially cloud-free at the time. The area is defined by 512 X 512 pixels each covering 1100 m square, centered at 49 N, 126 W (cylindrical projection with equal x and y scale at the image centre). The images show computed normalised water-leaving radiances at 443 nm (top left), 490 nm (top right) and 555 nm (bottom left). The chlorophyll concentration image, derived from the ratio of the 490 to

the 555 nm radiance, is shown at bottom right. Scales at the top of each image show the radiance or chlorophyll values corresponding to each colour. The radiance scale includes negative values, which are common in Seadas output in this geographic area.

A significant bloom of a strongly-scattering phytoplankton is in progress off the west coast of Vancouver Island. Land is masked (to dark blue) from a database included in Seadas. Cloud is masked to black using a Seawifs radiance threshold. A coastline and latitude/longitude grid has been added. The radiance images show high values between 49 and 50 degrees north latitude, indicating the presence of scattering material, presumably phytoplankton or its decay products. The chlorophyll image, in contrast, shows high values in areas where low radiance at 490 nm (top left image) is assumed to indicate strong absorption by high concentrations of chlorophyll a pigments. Off the north-west tip of Vancouver Island and in a strip along the west coast of Washington State (bottom right of the images) the high chlorophyll is associated with increased scatter at 555 nm (lower left image).

Three potential sources of error in the data are:

- overcompensation for atmospheric radiance (computed radiances at 490 nm are then too low)
- degradation of the Seawifs instrument leading to calibration errors, which are expected to have a greater effect at shorter wavelengths
- presence of other dissolved organic material in the water near the coast contributed by fresh water run-off from land (another cause of low radiance at 490 nm, but not indicating chlorophyll)

Errors in computed water-leaving radiances are clearly demonstrated by negative values. Seawifs measures radiance at a wavelength of 412 nm, where the atmospheric radiance contribution is extremely high, so that a small error can result in negative derived water-leaving radiances. If the negative values are due to an overestimate in the atmospheric correction, then this implies errors at longer wavelengths, most importantly in the 490 nm values used in calculation of chlorophyll concentrations.

The third source of error due to dissolved organic material, is known to be significant in all the areas showing high chlorophyll in the south-east of the imaged area. Surface water along the west coast of Washington State contains water from the Columbia and local coastal rivers. Sheltered water to the east of Vancouver Island is strongly affected by outflow from the Fraser River. The fresh water from the Fraser river contains very high concentrations of dissolved organic and suspended material. The suspended material causes a strong increase in water-leaving radiance, typically over an area 10 km by 10 km near the river mouth. This is masked in Seadas output, and is visible as the black area in the chlorophyll image. Dissolved organic material reduces water leaving radiance at short wavelengths over a much larger area.

Table 1: Flags provided for each pixel of Seawifs data by the Seadas software

1	Atmos. Correction failure
2	Land
3	Missing ancillary data
4	Sun glint
5	Radiance > knee
6	Large s/c zenith angle
7	Shallow water
8	Negative nLw
9	Stray light
10	Cloud or ice
11	Coccolithophores
12	Turbid case 2 waters
13	Large solar zenith Angle
14	High aerosol concn.
15	Low nLw at 555 nm
16	Chloro. Algorithm failure

Figure 2 shows the 16 masks computed by the Seadas software for the data shown in Figure 1. Masks are shown in the order listed in table 1. One interesting result is the identification of coccolithophores as being responsible for the area of elevated chlorophyll noted above off the north tip of Vancouver Island. A significant flag is that for negative radiances, showing that most other areas of high chlorophyll are affected by this error. This and other flags indicate small areas near edges of cloud and land where various problems occur. The only extended area where atmospheric correction failure is flagged is over the Fraser River plume where the high water-leaving radiance levels would be expected to cause problems. The shallow water flag is based on data with low spatial resolution and is not useful in the steep topography of this area.

Comparison with surface data

A series of chlorophyll measurements have been made during the Seawifs time period to provide data for Canadian studies of coastal productivity as part of the international JGOFS program. Cruises were undertaken in October 1997, May, July and October 1998 and May 1999. A program to provide time series of surface chlorophyll from surface meteorological buoys is underway at IOS, but the only test mooring so far instrumented is in sheltered water in an inlet too narrow to be imaged by Seawifs.

For this first comparison we consider ship measurements made near the location of the meteorological buoy on La Perouse Bank at 48° 50' North, 126° West, close to the edge of the area of highest chlorophyll on Figure 1. The value indicated for this location in the Figure 1 data is 6.2 $mg.m^{-3}$. These data

show a very low radiance at 443 at this location and a negative value at 412 nm, indicating that this chlorophyll concentration is probably overestimated.

Figure 3 shows the frequency distribution of chlorophyll values taken from Seadas output at this location for the 70 images at which the software indicated the area to be cloud-free. This is compared to a similar distribution derived from ship measurements over the shallow water of the continental shelf within 15 nautical miles of this buoy location over all available cruises. The distribution derived from satellite data shows a large number of high chlorophyll values, which do not appear in the ship data. Poor atmospheric correction or Seawifs calibration errors, as indicated by the presence of negative radiances, may explain this discrepancy.

Figure 4 shows the frequency distribution of radiances at 412 nm at this location. It can be seen that the vast majority are negative. In the absence of other information, a more accurate value of the negative radiance values at 412 nm can be taken as zero. One simple ad-hoc correction procedure is to then assume an error in the Rayleigh (λ^{-4} power) correction for atmospheric scattering, and apply a scaled additive correction to all Seawifs bands. If the error is in fact only in the 412 band (due to sensor degradation or a calibration change) then such a correction may over-compensate other bands. Inspection of the data shows negative values at 443 nm and occasional very low positive values at 490 nm, showing some link between bands.

The effect of this correction is indicated by the dotted frequency distribution in Figure 4, in which all values greater than 30 mg.m-3 are now removed and values between 10 and 30 are greatly reduced. However, the mean value is now shifted significantly below the mean of the ship observations, suggesting that a different method of propagating errors between bands may be more appropriate.

Figure 5 shows the data comparison as a time series. The original Seawifs data values are high in summer and also indicate a possible "spring bloom" peak in March. Average values computed for the months in which ship cruises occurred show much less contrast. The July 1998 cruise does not confirm the high summer values seen by Seawifs, but the Seawifs time series suggests that timing of the cruises may explain some of the lack of high values in Figure 4. Applying the same correction to Seawifs data as in Figure 4 results in the dotted time series in which summer values are reduced to better average agreement with ship data, but data at other months appears too low. The "spring bloom" observation in March 1998 has now disappeared, showing a strong effect of the "negative radiance" error on this observation.

Seawifs data internal consistency.

On 7 dates, usable data was collected as Seawifs observed the La Perouse site twice, once on the western edge of the swath (low pixel number) and once an orbit later, on the eastern edge of the swath (high pixel number). Since little or no change is expected in chlorophyll concentration in such a

short time (about 100 minutes) comparison of the two computed values provides a test of the accuracy of the Seadas results.

Table 2: Data from dates on which the La Perouse site was observed twice by Seawifs (on consecutive orbits). The table shows the two pixels numbers at which the site was imaged (in the range 1 to 1285), the two radiance values at 412 nm in units of $mw.cm^{-2}.\mu m^{-1}.sr^{-1}$, the two chlorophyll values computed by Seadas, and the two values after correction as above.

Date	Pixel 1	Pixel 2	L 412 1	L 412 2	Chl 1	Chl 2	Corr C1	Corr C2
980318	196	1185	-.32	-.80	4.4	54.0	2.5	2.8
980331	128	1141	-.52	-.83	1.1	1.7	0.9	0.9
980512	160	1160	-.31	-.74	1.2	1.0	1.0	0.8
980612	182	1170	-.46	-.53	46.1	30.0	6.4	6.0
980713	207	1182	+.03	-.59	3.9	21.6	4.1	3.2
980804	178	1179	-.25	-.58	10.1	15.0	6.4	5.2
990331	150	1157	-.42	-1.00	2.6	4.5	2.2	2.3

Table 2 shows that all but one of the radiance values are negative. There is a consistent bias in that radiances measured on the later pass are considerably more negative (they include the most negative value observed at this site of –1.0). Seadas chlorophyll output shows some high values with large inconsistency in the pairs. Corrected values are considerably more consistent, suggesting that some correction as proposed here should be able to improve the data at this site and at similar coastal sites round the world.

Future plans.

Seawifs data will continue to be received at IOS, and we anticipate improvements in data processing software which will correct the problems noted above. New data from MODIS and MERIS will be applied as they come available.

A program is underway at IOS to add optical sensors (including fluorometers) to some of the 17 surface meteorological buoys along and off the west coast of Canada. These buoys provide weather and ocean data for the Environment and the Fisheries departments of the Canadian federal government. The standard buoys measure wind speed and direction, wave height and spectrum, surface water and air temperature and atmospheric pressure and transmit the data hourly by satellite. The new sensors, installed on two buoys so far, measure insolation, water colour and fluorescence. This data is also transmitted hourly. A salinometer and acoustic profiler has been added to one package. The first time series from the prototype mooring started at the end of 1997 in Saanich Inlet, near the Institute of Ocean Sciences. This location is in too narrow an inlet to be imaged by Seawifs. Some data has also been collected from a second buoy off the Fraser River.

Fouling by marine growth is a major problem, but time series of data are available. Data from the prototype buoy can be viewed at http://www-sci.pac.dfo-mpo.gc.ca/ecobuoys.

Conclusions

Many projects with global implications such as JGOFS depend on research carried out in coastal areas. It is therefore important that Seawifs data should be calibrated and corrected adequately to provide good data near shore where water properties are complex and short wavelength radiances may be relatively low. Full resolution (1 km) Seawifs data are needed to resolve patterns in these areas. Future sensors such as MODIS and MERIS will provide higher spatial resolution and the spectral bands needed to detect solar-stimulated chlorophyll fluorescence and to better characterise intense plankton blooms (red tides).

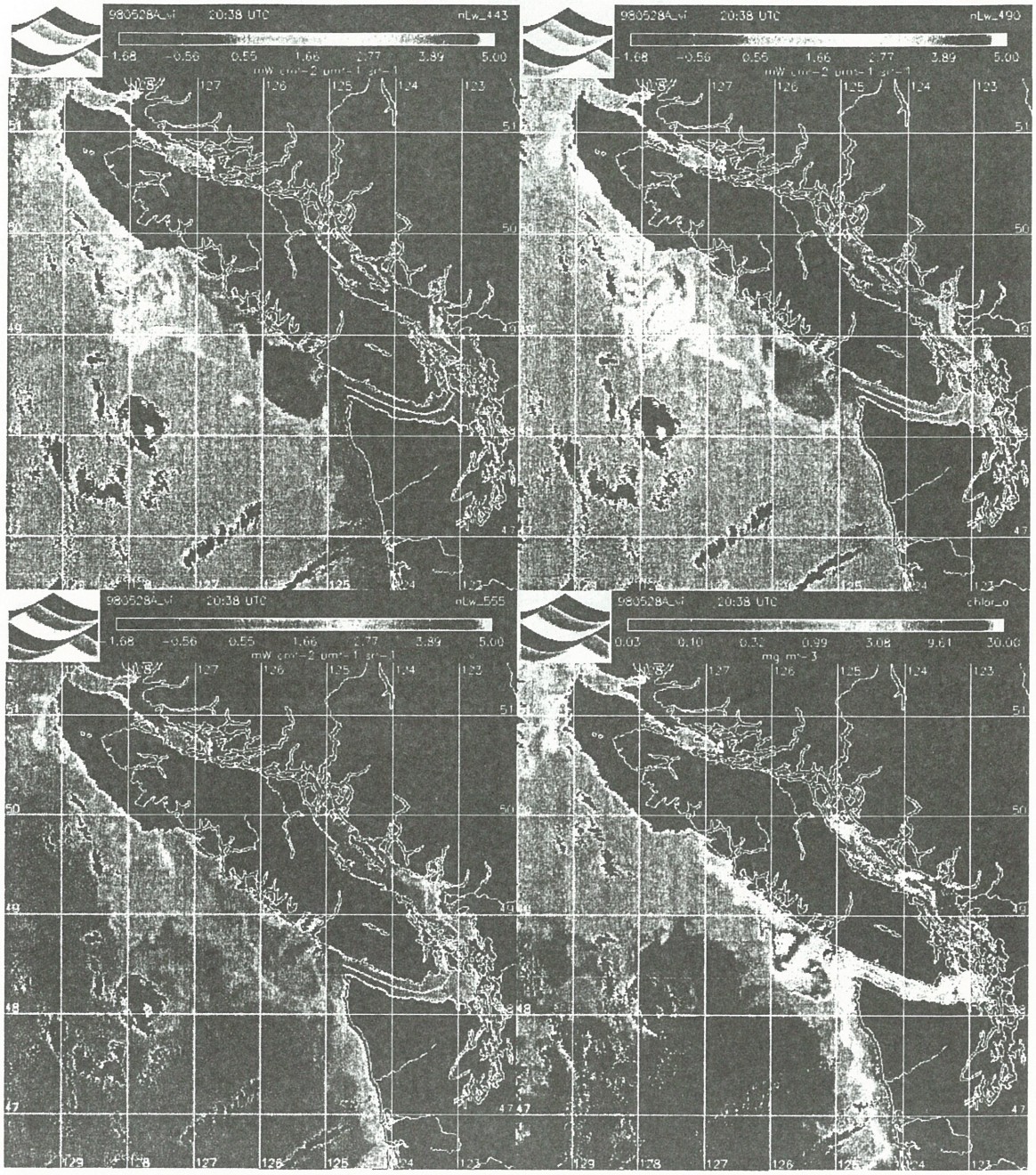

Figure 1. Seadas mapped output images (level3) showing normalised water-leaving radiances at 443, 490 and 555 nm (top left, right and bottom left),and computed chlorophyll concentrations (bottom right). Colour bars show the scales, which include negative radiances.

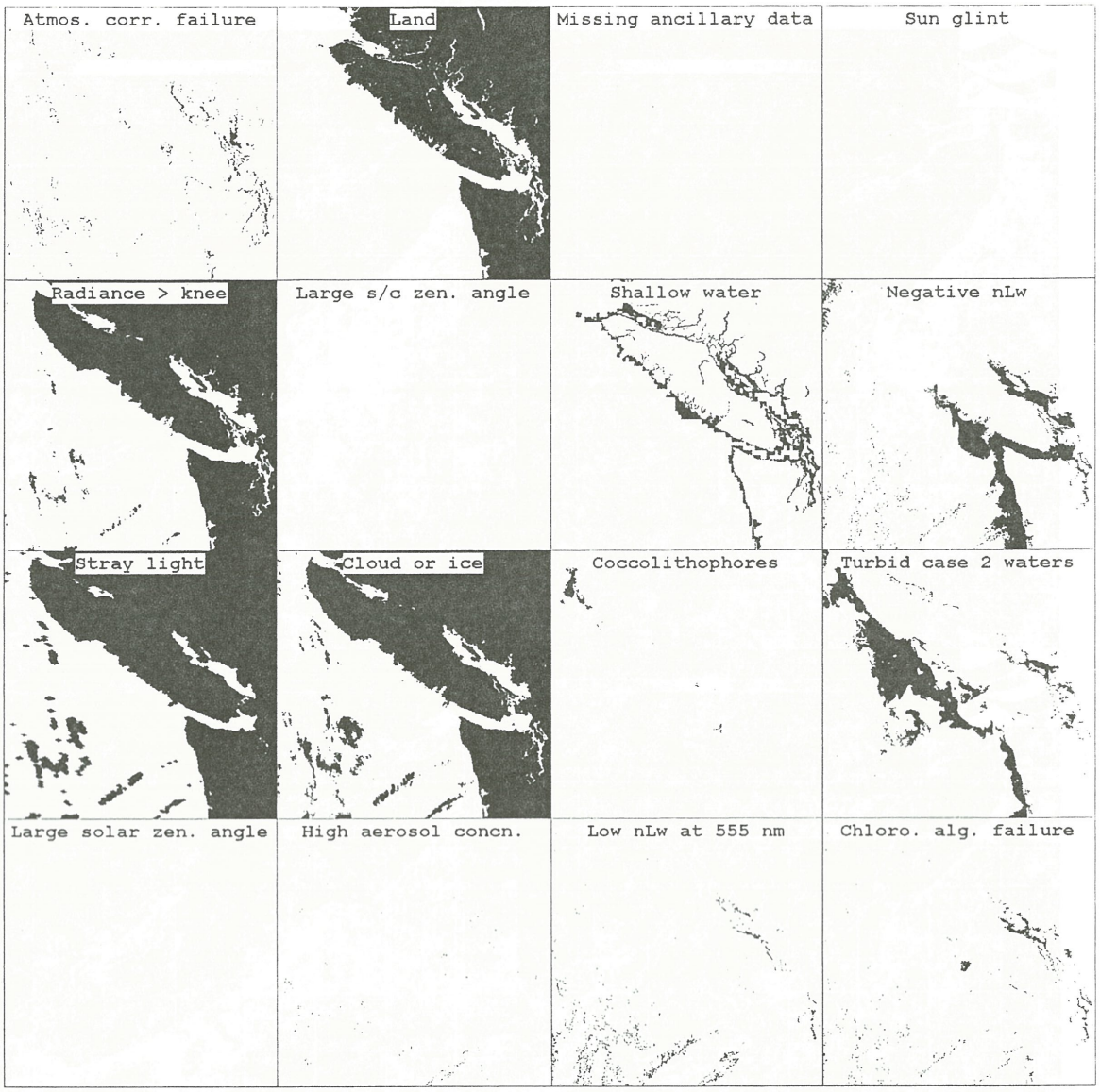

Figure 2. Binary (bitmap) images of all 16 flags in the order given in Table 1. Negative water-leaving radiances are flagged in coastal waters. The atmospheric correction algorithm fails over the bright water of the Fraser plume. Some high chlorophyll values are flagged as "algorithm failure."

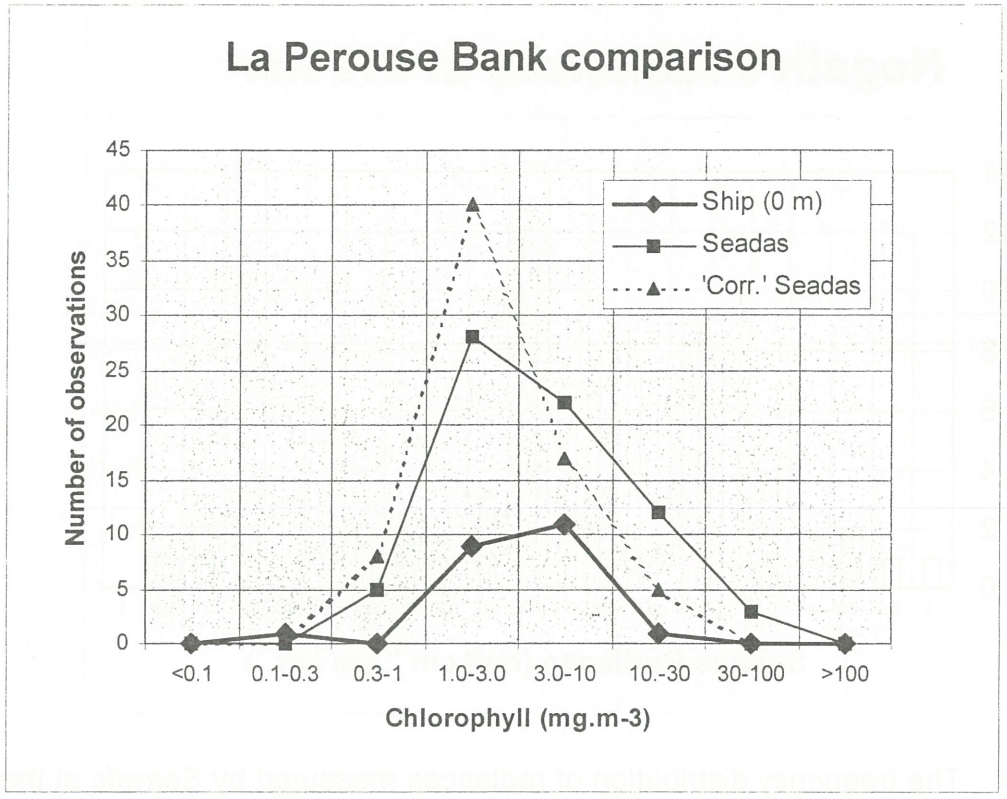

Figure 3. Frequency distributions of measured chlorophylls at the La Perouse Bank location at 49° 50' N, 126° W on the continental shelf off south west Vancouver Island. Data from Seawifs are compared with the limited ship data available. The effect of an ad-hoc correction for negative radiances is shown (dotted).

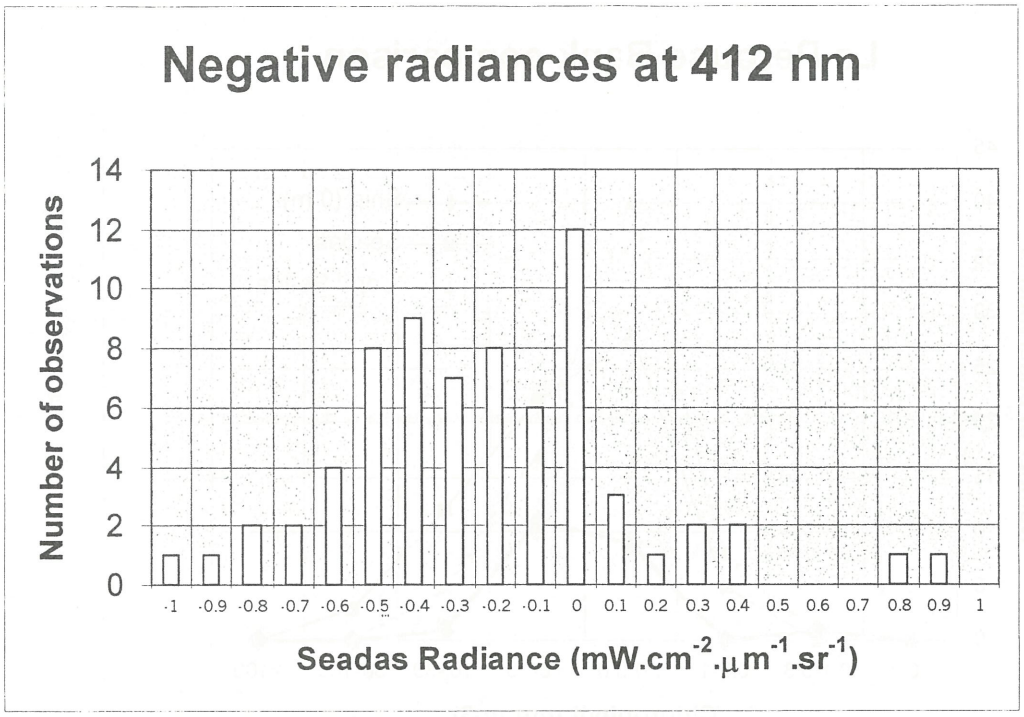

Figure 4. The frequency distribution of radiances measured by Seawifs at the La Perouse Bank location. Numbers on the x-axis are the maximum of each segment of the radiance range. Most computed radiances at 412 nm at this location are negative.

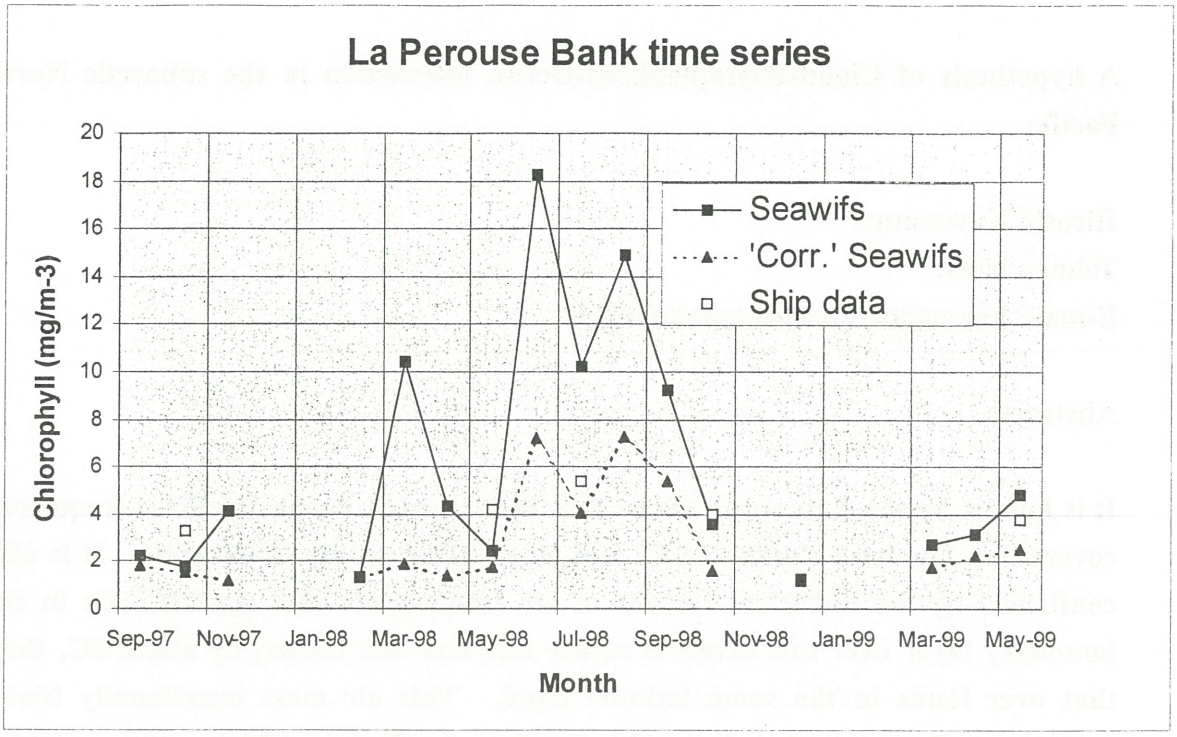

Figure 5. Time series (month average) of chlorophyll values deduced from Seawifs data at the la Perouse Bank location. Average ship measurements are shown for comparison. The effect of an ad-hoc correction for negative radiances is shown (dotted).

A hypothesis of Cloud-Phytoplankton-Ocean interaction in the subarctic North Pacific

Hiroshi Kawamura
Tohoku Univ.
E-mail: kamu@ocean.caos.tohoku.ac.jp

Abstracts

It is known by the ship observations that the subarctic North Pacific is frequently covered by low-level clouds (LLC) and fogs during spring to summer. It is also confirmed by the historical records of air temperature that the air-mass in the boundary layer over this ocean is rather uniform and colder, by about 5C, than that over lands in the same latitude band. This air mass occasionally blows toward southwest and bring cold summer to Japan, which causes serious agricultural damages and called "Yamase event". In order to understand formation process of the cold air-mass over the subarctic ocean, the role of LLCs is investigated using the ISCCP (International Cloud Climatrogy Project) data set. To estimate the LLC radiative forcing, radiation at the top of LLC and cloud-free surface is calculated by a radiative transfer code. The short wave radiation is reduced to 50% because of reflection at the cloud top. In contrast, the upward long wave radiation at the cloud top does not differ so much from that at the ocean surface because the altitude of cloud is low and the top temperature is close to SST. The strong contrast in the net radiation over the lands and oceans north of 40N is evident, and this is the main reason for generation of the cold air mass over the subarctic North Pacific during spring to summer. The satellite ocean color data shows that the surface Chl-a distribution also shows a front around 40N. A possible mechanism of interaction among the low-level cloud, phytoplankton and ocean will be presented.

Using Scatterometer Winds to Predict Potential Productivity in Eastern Boundary Current Regions

Mary-Elena Carr
Jet Propulsion Laboratory, MS 300-323
California Institute of Technology
4800 Oak Grove Dr.
Pasadena, CA 91109-8099

Abstracts

The coastal upwelling regions associated with the Eastern Boundary Currents (EBC) are characterized by very high primary productivity and contribute disproportionately for their small size to global carbon fluxes and fisheries. Various relationships between wind speed and ecosystem productivity have been proposed, ranging from linear increases of primary production and Ekman transport to optimal wind speeds for fish survival. Although intuitively valid, simple relationships tend to fail as more data become available. This is due in part to the role of mesoscale wind events and their timing. This study is part of an ongoing comparison of the four major coastal upwelling regions which utilizes satellite observations of wind and chlorophyll. Both the strength and the pattern (for example the number of calm periods) of wind forcing measured by NSCAT are compared with primary production estimated from chlorophyll concentrations measured by OCTS and contrasted with predictive relationships.

Application of ocean color imagery for Japanese fisheries

Hideo Tameishi
Japan Fisheries Information Service Center

Abstract

Warm streamer was first discovered by satellite imagery. Warm streamer would be utilized for migrating from offshore to near shore by fish schools. And then warm streamer was cold as Fish Way. It was found that this fish way have favorable temperature and favorable volume of phytoplankton for sardine schools migration by research vessel and aircraft survey. It was made sure that warm streamer had favorable temperature and favorable volume of phytoplankton by OCTS imageries.

On the other hand, it has been known that skipjack has favorable temperature and color by Satellite Data. The most favorable temperature and color range for skipjack corresponded to 20.5-23.0℃ and 0.12-0.16μg／l in Kuroshio. This is the most important information for the detection of fishing grounds. The skipjack fishing grounds were located at white area, which correspond to the water of both favorable temperature and color in the Kuroshio.

Furthermore, according to the movement of blooming area from middle of April to middle of May 1997, blooming would be regard as movement of frontal phenomena by satellite ADEOS/OCTS phytoplankton imageries, composed of 10 days imageries. Because, blooming was very much concerned with moving northward of isothermal map. The blooming was occurred by the temperature from 8 to 13℃. This temperature was very important factor for phytoplankton to occur blooming.

Variability of pigment biomass and mesoscale thermal features along First Oyashio Intrusion as determined from satellite and ship data

Kedarnath Mahapatra and Yoshihiro Okada

Center for Advanced Technology
Institute of Ocean Research and Development
Tokai University, 3-20-1 Orido, Shimizu, Shizuoka, 424-8610 Japan
e-mail: kedar@scc.u-tokai.ac.jp

Abstracts

A series of satellite data from the Sea-viewing Wide Field-of-view Sensor (SeaWiFS) and Advanced High Resolution Radiometer (AVHRR) over one year period, were examined to determine the relationship between the phytoplankton pigment distribution and sea surface temperature along the First Oyashio Intrusion. The structure of the temperature fronts and their role in phytoplankton pigment distribution was studied. The SST data showed generation of a thermal eddy during late fall, south east of Hokkaido and persisted for six moths before coalescence. The eddy had very little impact on the phytoplankton pigment distribution during the winter due to deep mixing. Stratification of water column during spring induced a phytoplankton bloom, which consequently led to formation of a phytoplankton eddy. Four sets of hydrographic data obtained from ship observations along two meridional transects were assessed to explore causal parameters for the spatio-temporal variability of phytoplankton distribution as delineated from the satellite images. Significant correlationship was marked between SST and phytoplankton pigment concentration during the fall and spring, however, nitrogen strongly related to pigment concentration during the winter and the summer. The relevance of such relationship was explored on the basis of the results from earlier investigations in the study area. Potential of complementary analysis of ocean color and thermal images in understanding meso-scale biological oceanographic phenomena was demonstrated in this study.

Ocean Color Variability of Japan JGOFS time series station KNOT and its adjacent waters, northwestern North Pacific observed by OCTS and SeaWiFS during 1996-1999

Kosei Sasaoka[1], Sei-ichi Saitoh[1] , Ichio Asanuma[2], Makio Honda[2], Keiri Imai[3], Toshiro Saino[4]

1 Faculty of Fisheries, Hokkaido University
2 Japan Marine Science and Technology Center
3 Japan Science and Technology corporation
4 Institute for Hydrospheric-Atmospheric Sciences, Nagoya University

Abstracts

The Subarctic North Pacific is well known as one of the highest biological productivity region in the world. Monitoring variability of the chlorophyll a (chl-a) distribution is very important to understand the role of biological pump in the ocean and to clarify the geochemical carbon cycles.

Our objectives of this study are, to grasp the temporal and spatial variability of chl-a distribution at the Japan JGOFS time series station KNOT (Kyo-do Northwest Pacific Ocean Time Series) (44-N, 155-E) and its adjacent waters in the Subarctic north-western North Pacific, and to understand the mechanisms of chl-a distribution during 1996 - 1999. We applied ocean color remote sensing data sets both OCTS (Ocean Color and Temperature Scanner) from Oct. 1996 to June 1997 and SeaWiFS (Sea-viewing wide Field-of-view Sensor) from Sep. 1997 to July 1999. Furthermore to analyze short-term variability, we carried out synoptic ship observations at Stn. KNOT and its adjacent waters.

Relatively low chl-a concentration (about 0.3 - 0.8mg/m3) dominated throughout the year at the Stn.KNOT, but remarkable peak was seen in bloom period (in May and October), winter (in November and December) and summer (in August 1998). In adjacent sea area, most remarkable high chl-a (more than 10mg/m3) was seen northward to Stn.KNOT along the Kuril-Islands and adjacent waters in May 1999, moreover high concentration remain over a month during the bloom season. Year-to-year variability of chl-a was seen. Chl-a (about 1.4mg/m3) at the Stn.KNOT in November 1997 was higher than that in November during 1996-1999. Chl-a around the center of Western Subarctic Gyre in October 1998 was higher than that in October 1997.

Interannual Variability in the Optical Characteristics of the Equatorial Pacific: Consequences for the Upper Ocean Heat Budget.

Marlon Lewis[1] and Ichio Asanuma[2]

1: Department of Oceanography, Dalhousie University, Halifax, Canada

2: JAMSTEC, Japan

Abstracts

The Equatorial Pacific undergoes strong interannual variations in physical dynamics associated with the El Nino/Southern Oscillation. These in turn cause changes in the ecosystem properties; in particular, a large decrease in the surface concentration of chlorophyll is associated with the El Nino phase, particularly in the central to eastern regions. The large decrease renders the waters more optically clear permitting solar energy to penetrate deeper into the water, and causes a redistribution of the irradiance divergence and resulting local heating rates. Along with changes in the surface heat fluxes, the changes in the penetration of solar energy has consequences for the upper ocean heat content, which, in closing the loop, alters the air-sea exchange of heat, moisture, momentum and gases.

In this presentation, we will use both in situ optical measurements from cruises spanning 5 years, and satellite ocean color observations from 3 years to evaluate this coupling between physical and biological dynamics in this critically important portion of the world's oceans.

Photosynthetic characteristics of phytoplankton in the subarctic North Pacific Ocean during summer

Ken Furuya*, Takashi Yoshikawa*, Hajime Obata* and Shigenobu Takeda**
***University of Tokyo**
****Central Research Institute of Electric Power Industry**

Abstracts

Geographical variability in the relationship between photosynthesis and irradiance in summer phytoplankton populations was examined in the subarctic North Pacific Ocean in July-August 1997 and July 1999. Photosynthesis versus irradiance (P-E) curves were obtained for seawater that were collected by trace metal clean techniques. Most region sampled during this study was characterized by high nutrient (> 8 . m nitrate) and low chlorophyll (0.2-0.6 μg l^{-1}) except the central western gyre in 1997 where high chlorophyll concentrations of 1.3-3.0 μg l^{-1}. Ambient iron concentration at the surface was consistently subnano molar during both the years (<0.22 nM). Maximum photosynthetic rates (P^B_m) varied between 1.79 and 5.24 mgC (mg chl)$^{-1}$ h^{-1} with no obvious geographical difference between the western and eastern gyres. In contrast however, there were noticeable east-west gradients in the initial slope of the P-E curves (α^B) for surface population during 1997: Station P (50° N, 145° W), located in the eastern gyre had the lowest α^B (0.088 ± 0.041 mgC (mg chl)$^{-1}$ h^{-1} (μmol $m^{-2}s^{-1}$)$^{-1}$, n=3) that increased westward. During July 1999, no major east-west gradient in α^B was seen which was observed to range between 0.012 and 0.029 mgC (mg chl)$^{-1}$ h^{-1} (μmol $m^{-2}s^{-1}$)$^{-1}$, while a high α^B was observed in the western gyre area. Significant enhancement of both PBm and α^B were observed with 1 - 2 nM iron enrichment signifying the role of iron in controlling the productivity potential of phytoplankton as well as the regional variability in P-E during summer.

Computation of primary production from remote sensing: Operational mode

Trevor Platt and Shubha Sathyendranath
Bedford Institute of Oceanography and Dalhousie University,
Halifax, Nova Scotia
Canada
e-mail: tplatt@is.dal.ca

ABSTRACT

Estimation of primary production from remotely-sensed data on ocean colour is a problem with two principal parts: construction of a local algorithm and definition of a protocol for extrapolating the local algorithm to large scales. By "local algorithm", we mean an algorithm that can be implemented at a fixed point provided that all necessary information (forcing variables, physiological parameters, chlorophyll profile parameters) is available. Such algorithms already exist. The remaining challenge is to define an extrapolation protocol that will lead to best estimates of the necessary parameters on all pixels in the image, that is on pixels for which we have no direct knowledge of the parameters.

Here, the extrapolation protocol under development for the Canadian Atlantic Coast is presented and discussed.

Acknowledgements: Carla Caverhill, Glen Harrison, Heidi Maass, Linda Payzant and George White have all contributed to the progress of this work.

INTRODUCTION

In Canada, one of the applications of remote sensing is to produce bi-weekly information on the state of the marine ecosystem for the Atlantic Zone, with the continental shelves put into their oceanographic context. The intended uses are first, for research (establish a time series that can be exploited to address various scientific questions); and second, development of information and conceptual bases for coastal-zone management, including fisheries management. The time series is based on ocean-colour data and on sea-surface temperature data, which can both be received through the same dish and analysed to produce images at the same time and space scales (Figure 1). The images comprise some 1.8×10^6 ocean pixels each. The total area covered (land and ocean) is some 5×10^6 km^2.

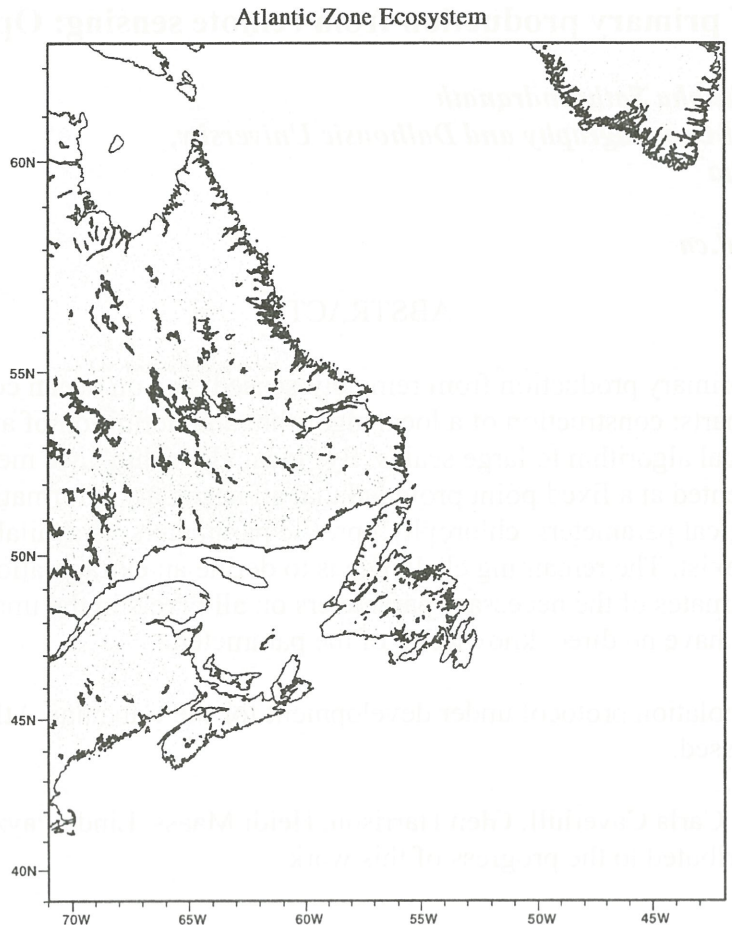

Figure 1.

It was considered that the value of the project would be enhanced if it could include bi-weekly images of primary production computed, on the same spatial scales, using the remotely-sensed fields as inputs. Whereas several authors have computed primary production from remotely-sensed data on ocean colour, to our knowledge the routine calculation for a particular area, with a view to production of a time series, has not been attempted.

BACKGROUND

Estimation of primary production from ocean-colour data is a problem with two components. First, we must construct a local algorithm that will make reliable estimates of primary production, given biomass, provided that all necessary information (forcing variables, physiological parameters, chlorophyll profile parameters) is available. Next, we must establish a protocol for extrapolation of the local algorithm to large horizontal scale, that is a protocol for applying the local algorithm on all pixels in the target image, where, typically, we have no direct knowledge of the parameters required.

In our view, the construction of a local algorithm is a solved problem. An array of models is available according to the degree of approximation that can be tolerated and the computing time that is acceptable.

EXTRAPOLATION PROTOCOL

The extrapolation protocol, however, is a different matter, especially for implementation in the routine mode. One of the factors that must be weighed is the existing knowledge about the phytoplankton (vertical profile of chlorophyll, photosynthetic performance) for the region under consideration. In the case of the Atlantic Zone of Canada, some 835 stations are available in the archive for photosynthesis parameters, and some 495 for the vertical structure of chlorophyll.

In deciding on a protocol for assignment of parameters, the following options may be considered.

1 According to some objective function of a continuous variable such as depth, latitude or SST.

2 According to partition of region into dynamic domains wherein parameters are piecewise constant or piecewise continuous (suite of biogeochemical provinces).

3 According to a match between given remotely-sensed fields (chlorophyll, SST) and information in archive of ship observations for the same region.

In choosing between these options, we must acknowledge that the region is complex and dynamic, with cold water from the Labrador Current and warm water from the Gulf Stream in close proximity. No suitable objective function yet exists that will assign the parameters we need. We have not yet succeeded in finding a suitable dynamic partition into provinces, where the qualifier "dynamic" implies that the boundaries of the provinces are free to vary from image to image.

Thus, we resort to the third option, assigning the parameters according to matches between the image data and the archived station data. For any pixel in the images (Figure 2), we know the biomass and the SST.

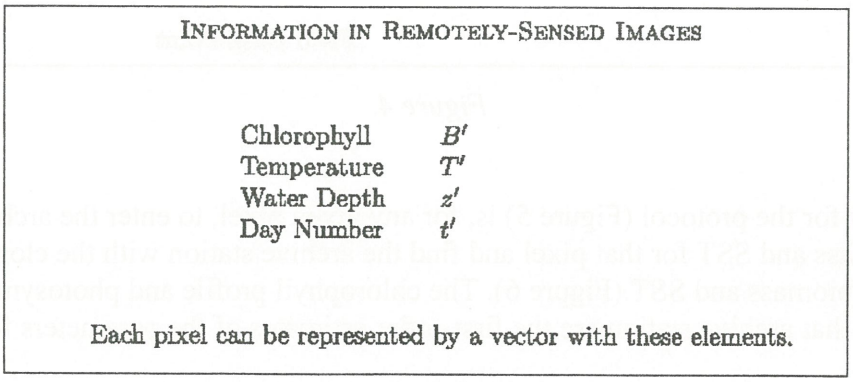

Figure 2.

We also know the water depth and the date (day number). In the archived data (Figure 3), over and above the properties already mentioned for the images, we know the parameters of the photosynthesis-light curve and the parameters of the chlorophyll profile, when it is fitted to a standard shape. We must then consider the intersection between these data sets (Figure 4).

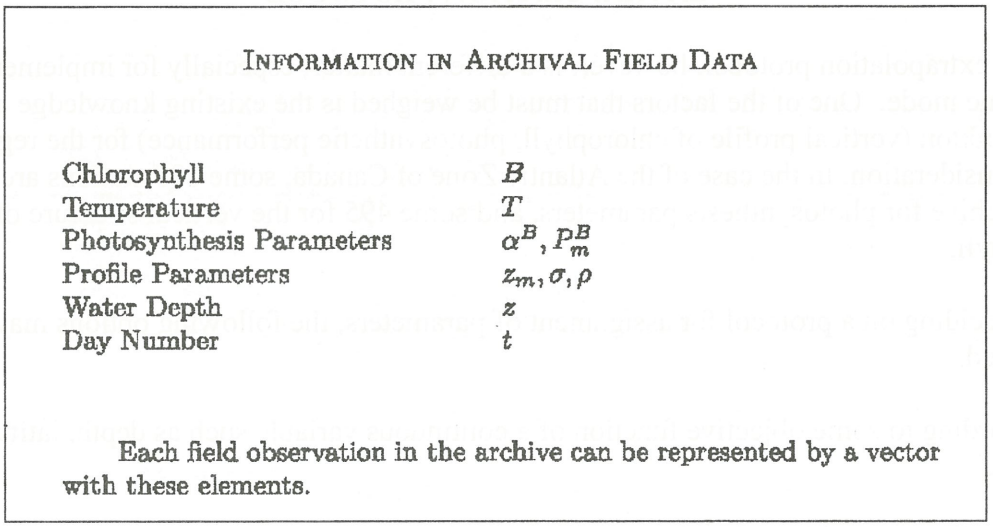

Figure 3.

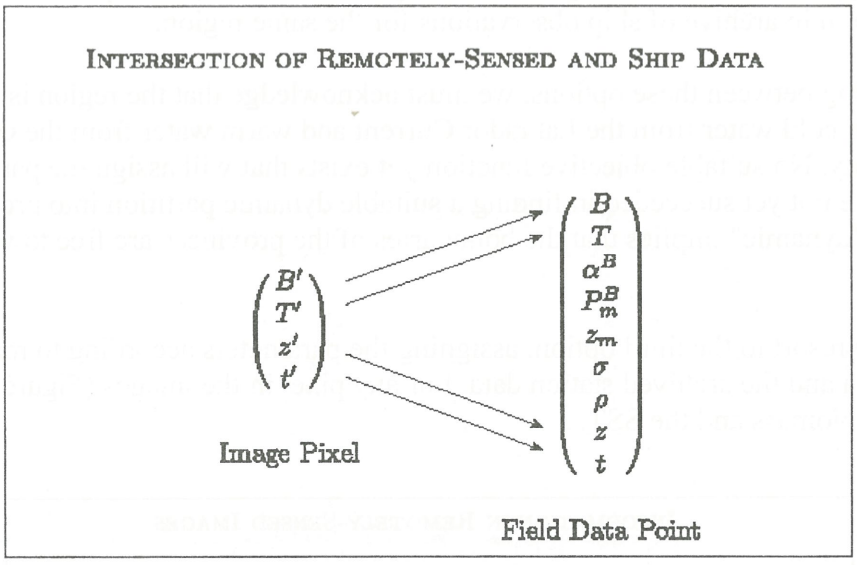

Figure 4.

The strategy for the protocol (Figure 5) is, for any given pixel, to enter the archive with the values of biomass and SST for that pixel and find the archive station with the closest coordinates of biomass and SST (Figure 6). The chlorophyll profile and photosynthesis parameters for that archive station are the first-order estimates of the parameters for that pixel.

ASSIGNMENT OF PARAMETERS FROM ARCHIVE FILE

Let $\mathbf{x}$ be the vector of parameters required to calculate primary production on a given pixel $\mathbf{x} = (\alpha^B, P_m^B, z_m, \sigma, \rho)$.

Map from images to archive to parameter vector:

$$(B', T') \rightarrow (B, T) \rightarrow (B, T, \mathbf{x})$$

In the archive, search in the local neighbourhood of (B, T).

Figure 5.

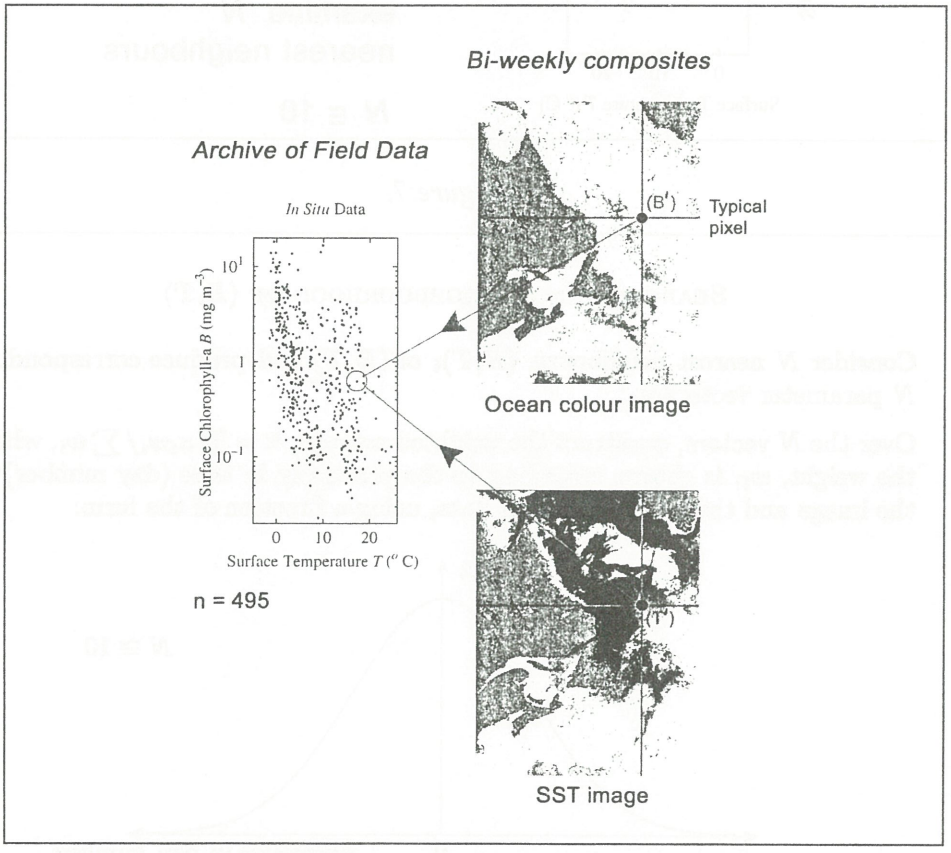

Figure 6.

Certain refinements can now be made. Instead of taking the parameters from only the single archive point with the closest coordinates, we can use also a number (ten, say) of its nearest neighbours, and calculate the average parameter values over this set (Figure 7). Then, we take into consideration that the archive station and the image may have been taken in different seasons, so we can weight the utility of the archived station according to the difference in day number between it and the image, constructing a weighted average of the parameters over the nearest neighbour set (Figure 8). This is the procedure that is in use

in our laboratory. Further refinements may be possible based on water depth, but these have not yet been explored.

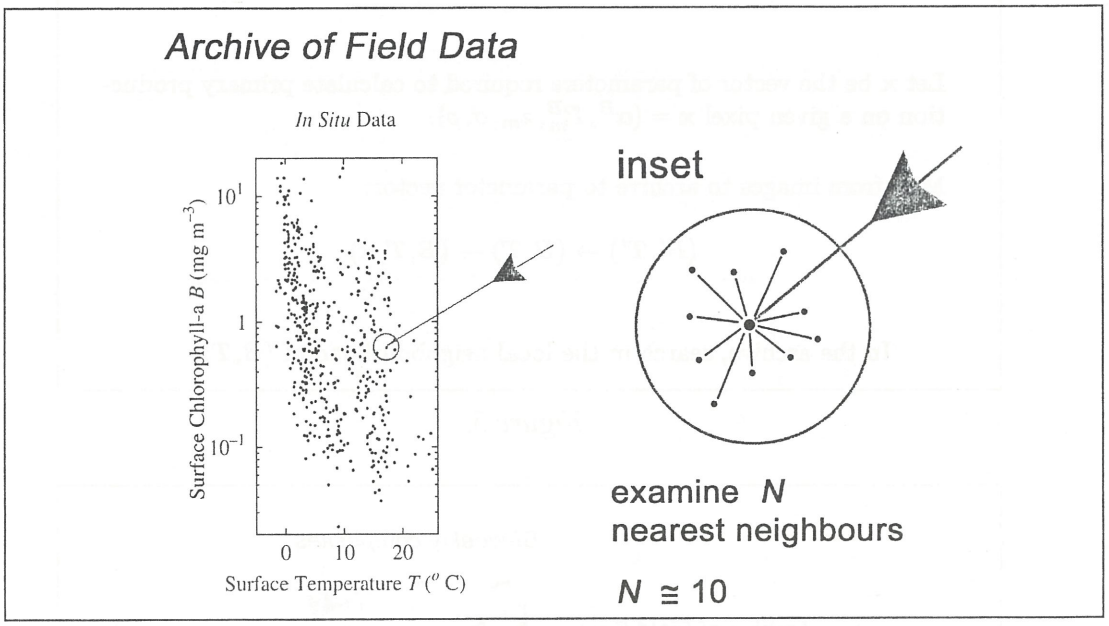

Figure 7.

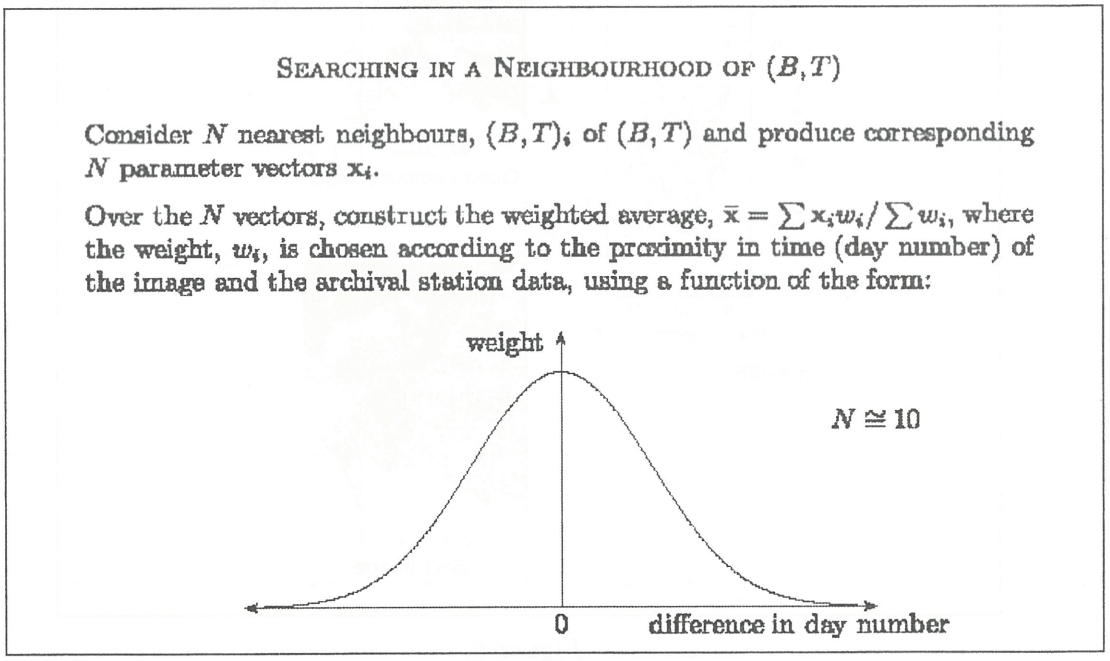

Figure 8.

The advantage of the method is that it exploits fully the intersection between the image data and the archive data, using information from both the ocean-colour and the SST images. It is also an objective procedure. It is now being evaluated for computing efficiency. At the earliest opportunity it will be tested against independent field data.

Chlorophyll and Primary Production in a Cyclonic Eddy off the Island of Hawaii

Carrie L. Leonard and Robert R. Bidigare

Department of Oceanography
1000 Pope Rd.
University of Hawaii
Honolulu, HI 96822 USA
carrie@soest.hawaii.edu; bidigare@soest.hawaii.edu

Abstracts

Both cyclonic and anti-cyclonic eddies formation are a common occurrence in the lee of the Island of Hawaii due to disruption of the trade winds between Maui and Hawaii to the north and the Kilauea volcano to the south. Recently, these eddies have been successfully tracked using GOES satellite imagery of sea surface temperature (SST). During an eddy spin up in March 1999, an increase in SeaWiFS surface chlorophyll was associated with cooler SSTs as recorded by GOES.

Estimates of primary production inside and outside of the eddy were computed using a full-spectral depth-dependant primary production model with the satellite chlorophyll as input. New production was also estimated using field data from a similar eddy sampled in a previous year. New production increased 10-fold inside the eddy, while total primary production simply doubles and surface chlorophyll was only 2.5 times the outside values. It appears that eddies off the Big Island may contribute substantially to local new production rates, and that ocean color can be successfully used to track and calculate production due to these eddies.

In situ measurement of chlorophyll *a* specific absorption coefficient in the sea

S. Kobara[1], M. Kishino[2], and S. Taguchi[1].

1: Department of Bioengineering, Soka University,
1-236 Tangi-cho, Hachioji, Tokyo 192-8577, JAPAN
E-mail: skobara@edu.t.soka.ac.jp
staguchi@t.soka.ac.jp

2: RIKEN (The Institute of Physical and Chemical Research)
2-1 Hirosawa, Wako, Saitama 351-0198, JAPAN
E-mail: kishino@postman.riken.go.jp

Abstract

The total absorption coefficient is important in determining the magnitude and the spectral shape of the light field in an aquatic medium. Furthermore, accurate estimates of phytoplankton absorption are necessary to determine the chlorophyll *a* specific absorption coefficient, which is central to the bio-optical model for primary production. However, the presence of detrital and dissolved matter in seawater complicates the direct measurement of phytoplankton absorption coefficient in the sea.

The most widely used method for determining absorption coefficient is the quantitative filter technique (QFT). It can be used to determine the chlorophyll *a* specific absorption coefficient. However, these provide the information at discrete depths only. In recent years, reflective-tube absorption and attenuation meter (ac-9: Wetlabs) and fluorometer (WETStar: Wetlabs) have been developed and provide the continuous vertical profiles of *in situ* absorption, attenuation, and fluorescence.

The present study is aimed to estimate the vertical profile of chlorophyll *a* specific

absorption coefficient using an *in situ* method that was tested against QFT method.

Data were collected in Sagami Bay from April to July 1999. The particulate absorption coefficient using *in situ* method were obtained by subtracting the absorption of dissolved organic matter determined with a 0.2μm filter placed at the intake port of ac-9 from the total absorption coefficient using *in situ* method. In the present study we chose to use absorption at 676nm to estimate phytoplankton absorption *in situ* due to negligible contribution by detrital absorption to particulate absorption at 676nm. *In vivo* bottle samples were taken from Niskin bottle casts at discrete depths. Seawater samples were filtered through Whatman GF/F glass-fiber filters for analysis of chlorophyll *a* concentrations with fluorometric method after extraction in DMF. The continuous profile of chlorophyll *a*, matched well with those collected at discrete depths, provided information on the fine structure of the vertical pigment profile.

There was a good agreement between absorption coefficients at 676nm measured by QFT and ac-9 at the subsurface depths. The significant relationship between specific absorption coefficient at 676nm and the average absorption coefficient from 400 to 700nm was obtained for the QFT method. Estimation of the specific absorption coefficient at 676nm using *in situ* method and *in situ* chlorophyll *a* concentration is able to give continuous information on the vertical variation of chlorophyll *a* specific absorption coefficient for PAR region of the spectrum.

In conclusion, *in situ* method for measuring chlorophyll *a* specific absorption coefficient at 676nm developed can be used to continuously determine vertical profile of the chlorophyll *a* specific absorption coefficient in the spectral region from 400 to 700nm for depths below 10m.

Variations in the Absorption Characteristics of Phytoplankton: Implications for Remote Sensing

Shubha Sathyendranath[1,2], Trevor Platt[2], Venetia Stuart[1,2] and Heidi Maass[2]

[1]*Oceanography Department*
Dalhousie University, Halifax, Nova Scotia,
B3H 4J1 Canada

[2]*Biological Oceanography*
Bedford Institute of Oceanography, Dartmouth, Nova Scotia
B2Y 4A2 Canada

Email:shubha@is.dal.ca

Abstract

Over the course of the last ten years, our laboratory has acquired a data base of about 800 absorption spectra of natural phytoplankton samples collected from several oceanic regions. These data have been analysed, along with concurrent information on pigment composition estimated using High Performance Liquid Chromatography (HPLC) techniques. The analysis highlights some general trends in the absorption characteristics and in pigment composition with changes in the phytoplankton biomass, as indexed by the concentration of the main pigment, chlorophyll-a. An empirical, three-parameter model can be used to estimate the absorption coefficient of phytoplankton at a given wavelength as a function of chlorophyll-a concentration. But such models fail to account for deviations in the absorption characteristics from the main trend. The implications for the estimation of both phytoplankton biomass and primary production from remotely-sensed data are examined.

Introduction

In the bi-partite optical classification scheme formulated by Morel and Prieur (Morel and Prieur 1977; Morel 1980; Sathyendranath and Morel 1983), oceanic waters are classified as Case 1 waters, if phytoplankton can be considered to be the major, independent variable responsible for changes in the optical properties of the water. If this condition does not hold, then the waters are classified as Case 2 waters. In Case 1 waters, a suite of parameterisations have been developed, for computing phytoplankton absorption and scattering properties as functions of a single variable, the concentration of chlorophyll-a (Prieur and Sathyendranath 1981; Morel 1988; Sathyendranath and Platt 1988; Sathyendranath et al. 1999). It would, however, be wrong to assume from these developments that chlorophyll-a concentration is the only property that is modified when there is a change in the concentration of phytoplankton. The factors that cause variations in the optical properties of phytoplankton merit more attention, particularly in the context of developing biomass algorithms for quantitative interpretation of ocean-colour data in Case 1 waters. This is the topic of our paper.

What causes variations in ocean colour in Case 1 waters? As shown schematically in Figure 1, the optical properties of phytoplankton, and hence of the waters, will of course depend on the concentration of chlorophyll-a, which is present in all phytoplankton, either in its regular form,

or as the variant divinyl chlorophyll-a. However, it must not be overlooked that changes in chlorophyll-a concentration are typically accompanied by variations in the relative concentrations of auxiliary pigments, and in the size structure of the phytoplankton population, both of which can affect the optical properties of phytoplankton. Pigment composition and size structure vary with the species composition of the phytoplankton population. Therefore, one may expect the optical properties to differ depending on whether the population is dominated by a single species or class, or by many species belonging to many classes. In the case of multi-species populations, the optical properties would depend on the species composition, whereas in the case of mono-specific blooms, they would depend on the dominant species present.

If indeed so many changes accompany variations in phytoplankton concentration, how is it that we have been able to develop successful models that employ a single variable, chlorophyll-a, to parameterise the optical properties of phytoplankton in Case 1 waters? The success of these models implies that many of the changes listed above follow certain predictable trends, which follow changes in chlorophyll-a. In this paper we analyse a data base of phytoplankton absorption spectra and pigment composition, to highlight general trends in species succession that accompany changes in phytoplankton concentration (as indexed by chlorophyll-a concentration), and the implications for modelling. We also examine the modifications in pigment composition that occur along with changes in chlorophyll-a concentration, and the possibilities for deriving pigment composition from absorption data.

A certain amount of yellow substance or coloured dissolved organic matter is also expected to be present in Case 1 waters, and to modify ocean colour by its presence (Fig. 1). But in this paper, we focus our attention exclusively on the absorption characteristics of phytoplankton, their variability in oceanic waters, and their implications for remote sensing.

Data and Methods

The absorption data were collected over the course of the last ten years or so, using the filter technique (Yentsch 1962) as modified by Kishino et al. (1985). The measured absorption values were corrected for pathlength amplification on the filters, using the results of Hoepffner and Sathyendranath (1992) and Moore et al. (1995), as outlined in Kyewalyanga et al. (1998) and Stuart et al. (1998). Pigment composition was measured using High Performance Liquid Chromatography (HPLC) technique, following the protocol of Head and Horne (1993). All the data were collected using consistent techniques, during 13 cruises, with the total number of samples numbering about 750.

Results

Species-related Variations in Absorption Spectra: Analysis of diagnostic pigments measured by HPLC technique suggested that prochlorophytes often tended to dominate in very oligotrophic waters, cyanophytes increasing in importance with increase in the chlorophyll-a concentration. Diatoms tended to be the dominant group in high-chlorophyll environments, with prymnesiophytes being present in high concentrations in a diversity of environments. The specific absorption coefficient at 440 nm was very high for the small-

celled prochlorophytes, dropping off to a minimum for the relatively large-celled diatom populations.

The corresponding variations in pigment composition introduced changes in the shapes of the absorption spectra. These changes were found to have non-negligible effects on light absorption by phytoplankton at the base of the euphotic zone (the depth of the 1% light level), in computations that employed a spectral model of light penetration to estimate the spectral quality of light at the 1% light level. At this optical depth, prochlorophytes appear to be most efficient at light absorption in oligotrophic waters, and diatoms in eutrophic waters.

General Trends in the Concentrations of Some Major Auxiliary Pigments Relative to Chlorophyll-a: The concentration of chlorophyll-b relative to chlorophyll-a dropped off with increasing concentrations of phytoplankton, whereas the relative concentration of chlorophyll-c tended to increase with phytoplankton concentration. We also examined the trends in non-photosynthetic carotenoids (diadinoxanthin, diatoxanthin, zeaxanthin, alloxanthin, β-carotene) and in photosynthetic carotenoids (fucoxanthin, 19'-hexanoyloxyfucoxanthin, 19'-butanoyloxyfucoxanthin, peridinin, prasinoxanthin, α-carotene). The concentrations of non-photosynthetic carotenoids relative to chlorophyll-a tended to fall off with depth, and with latitude, with highest values (predominantly zeaxanthin) appearing in surface waters of oligotrophic tropical oceans. On the other hand, the relative concentrations of photosynthetic carotenoids (mostly fucoxanthin) showed a tendency to increase with increase in phytoplankton concentration. Some of these trends were weak, and there was a certain amount of variability around them. A consequence of the variations in the size structure and in the pigment composition of phytoplankton with change in concentration was that the relationship between phytoplankton absorption at 440 nm and the chlorophyll-a concentration was non-linear, requiring empirical fits that involved two or three parameters. The variability around these trends was reflected in the fact that chlorophyll-a was able to explain only about 72% of the variance in the data, even with a non-linear fit.

Relationships between Pigments and Phytoplankton Absorption: If one used linear relationships, then chlorophyll-a by itself was able to explain only 68% of the variance in phytoplankton absorption at 440 nm. The explained variance increased to 79% if the concentrations of chlorophylls-b and -c and photosynthetic and non-photosynthetic carotenoids were included in a multiple linear regression.

From the perspective of remote sensing, it is also interesting to pose the question from the opposite angle, and examine whether information on phytoplankton absorption at multiple wavelengths can be used to derive any information on pigment composition, over and above information on chlorophyll-a concentration. In fact, multiple linear regression of various pigments on SeaWiFS wavelengths in the visible showed that these absorption values could be used to derive some information on pigments other than chlorophyll-a (Table 1). Of all the major pigments examined, the results were poorest for chlorophyll-b. But, as mentioned earlier, the relative concentration of chlorophyll-b tended to decrease with increase in chlorophyll-a concentration, and it is possible that the methods would work better in waters where chlorophyll-b was present in significant amounts. To examine this idea further, the data set were split into two groups, based on the relative concentration of chlorophyll-c to chlorophyll-a. Table 2 shows the results for analyses on the sub-set of data for which the

chlorophyll-c:chlorophyll-a ratio was less than 0.2. In fact, for this subset, the variances explained are higher, not just for chlorophyll-b, but for all pigments.

Discussion and Conclusion

Models of phytoplankton absorption in Case 1 waters rely on a suite of changes in phytoplankton cell size and pigment composition that typically accompany variations in chlorophyll-a concentration. Fluctuations around these general trends can introduce significant effects on the performance of algorithms for interpretation of ocean-colour data, as demonstrated by Sathyendranath et al. (1999), using data on the absorption characteristics of diatom and prymnesiophyte blooms from the Labrador Sea. The results reported here, preliminary as they are, suggest that it may be possible to overcome some of the limitations of present-day algorithms by making use of multiple wavelengths to distinguish between some of the major pigments. Partitioning the data based on an index of pigment composition (say the ratio of chlorophyll-c to chlorophyll-a) appears to improve the results, suggesting that branching algorithms may perform better than universal algorithms, and that the criteria for branching might be based on remotely-detectable signals.

The analysis presented here is based on absorption data, and has not broached the additional problems associated with the non-linearity in the relationships between absorption and ocean colour or those problems associated with the influence of substances such as yellow substances on ocean colour. In this sense, the results presented here must be considered to be preliminary, from the point of view of interpretation of remotely-sensed data on ocean colour.

References

Head, E. J. H., and Horne, E. P. W. (1993). Pigment transformation and vertical flux in an area of convergence in the North Atlantic. Deep-Sea Res. II. 40: 329-346.

Hoepffner, N., and Sathyendranath, S. (1992). Bio-optical characteristics of coastal waters: Absorption spectra of phytoplankton and pigment distribution in the western North Atlantic. Limnol. Oceanogr. 37: 1660-1679.

Kishino, M., Takahashi, M., Okami, N., and Ichimura, S. (1985). Estimation of the spectral absorption coefficients of phytoplankton in the sea. Bull. Mar. Sci. 37: 634-642.

Kyewalyanga, M. N., Platt, T., Sathyendranath, S., Lutz, V. A., and Stuart, V. (1998). Seasonal variations in physiological parameters of phytoplankton across the North Atlantic. J. Plankton Res. 20: 17-42.

Moore, L. R., Goericke, R., and Chisholm, S. W. (1995). Comparative physiology of *Synechococcus* and *Prochlorococcus*: influence of light and temperature on growth, pigments, fluorescence and absorptive properties. Mar. Ecol. Prog. Ser. 116: 259-275.

Morel, A. (1980). In-water and remote measurement of ocean color. Boundary-Layer Meteorol. 18: 177-201.

Morel, A. (1988). Optical modeling of the upper ocean in relation to its biogenous matter content (Case I waters). J. Geophys. Res. 93: 10,749-10,768.

Morel, A., and Prieur, L. (1977). Analysis of variations in ocean color. Limnol. Oceanogr. 22: 709-722.

Prieur, L., and Sathyendranath, S. (1981). An optical classification of coastal and oceanic waters based on the specific spectral absorption curves of phytoplankton pigments,

dissolved organic matter, and other particulate materials. Limnol. Oceanogr. 26: 671-689.

Sathyendranath, S., and Morel, A. (1983). Light emerging from the sea - interpretation and uses in remote sensing. In: Remote Sensing Applications in Marine Science and Technology, A. P. Cracknell (ed.), D. Reidel Publishing Company, Dordrecht, 323-357.

Sathyendranath, S., Stuart, V., Cota, G., Maass, H., and Platt, T. (1999). Remote sensing of phytoplankton pigments: a comparison of empirical and theoretical approaches. Int. J. Remote Sensing. In press.

Stuart, V., Sathyendranath, S., Platt, T., Maass, H., and Irwin, B. D. (1998). Pigments and species composition of natural phytoplankton populations: Effect on the absorption spectra. J. Plankton Res. 20: 187-217.

Yentsch, C. S. (1962). Measurement of visible light absorption by particulate matter in the ocean. Limnol. Oceanogr. 7: 207-217.

What Determines the Colour of Case 1 Waters?

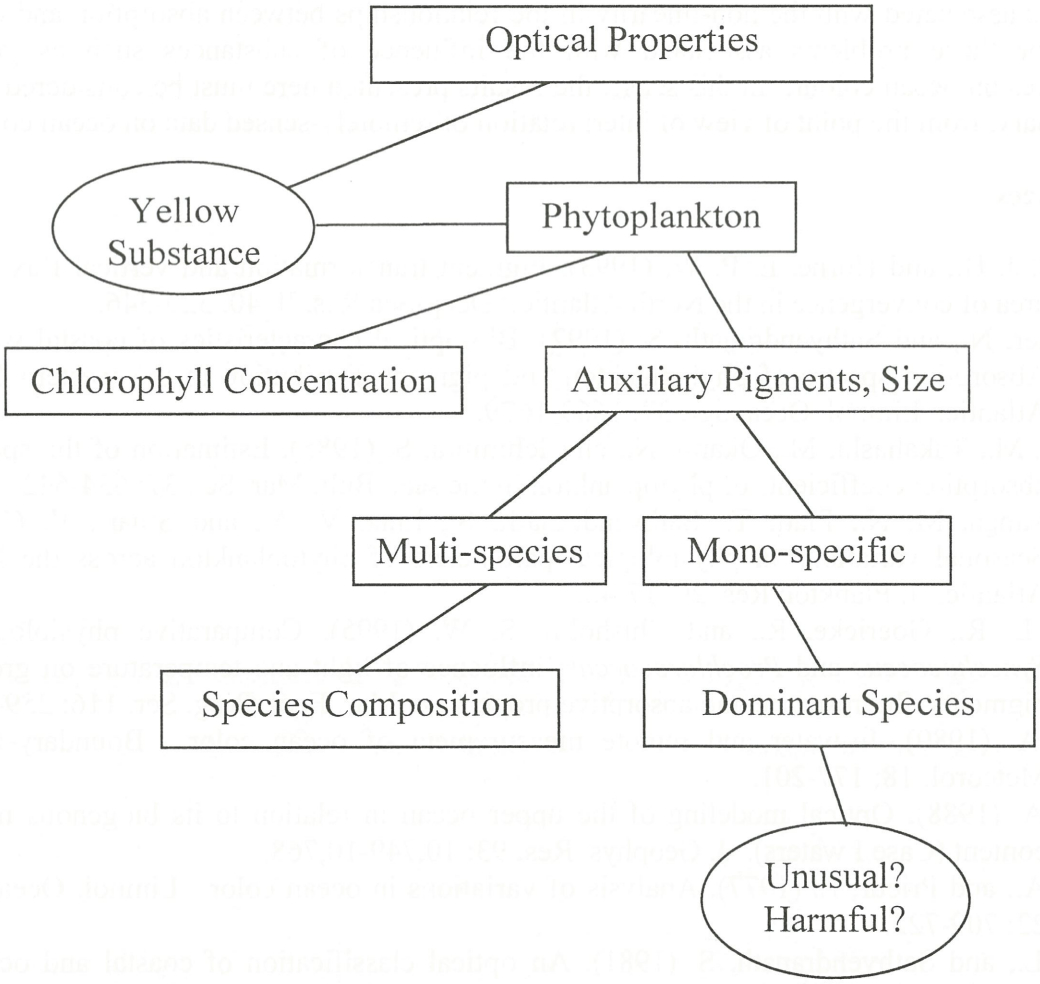

Figure 1: Schematic diagram showing sources of variations in phytoplankton absorption characteristics in the aquatic environment. These in turn influence ocean colour.

Table 1. Results of multiple linear regression analysis of HPLC-derived pigment concentration on phytoplankton absorption at SeaWiFS wavelengths in the visible region of the spectrum, using the entire database (n = 757). Wavelengths used in the multiple regression are indicated by tick marks. All the coefficients associated with these wavelengths were significant (p = 0.0000). Extending the multiple regression to include all six SeaWiFS wavelengths in the visible did not result in any marked increase in the reported r^2 values. 19-Hex = 19'-Hexanoyloxyfucoxanthin; PC = photosynthetic carotenoids; NPC = non-photosynthetic carotenoids (see text for list of carotenoids in each group).

	SeaWiFS wavelengths used						
Pigment	**412 nm**	**443 nm**	**490 nm**	**510 nm**	**555 nm**	**670 nm**	r^2
Chl-*a*			✓	✓		✓	0.86
Chl-*b*	✓		✓	✓	✓		0.47
Chl-*c*	✓					✓	0.74
Fucoxanthin			✓	✓		✓	0.87
19-Hex	✓	✓	✓			✓	0.53
PC			✓	✓	✓		0.86
NPC		✓	✓	✓	✓		0.72

Table 2. Results of multiple linear regression analysis of HPLC-derived pigment concentration on phytoplankton absorption at SeaWiFS wavelengths in the visible region of the spectrum, similar to the analyses presented in Table 1 in all respects, except that only samples with chlorophyll-a:chlorophyll-c ratios < 0.2 (n = 450) are used here.

	SeaWiFS wavelengths used						
Pigment	**412 nm**	**443 nm**	**490 nm**	**510 nm**	**555 nm**	**670 nm**	r^2
Chl-*a*	✓	✓			✓	✓	0.91
Chl-*b*		✓	✓	✓		✓	0.66
Chl-*c*	✓	✓	✓		✓	✓	0.94
Fucoxanthin	✓	✓			✓	✓	0.93
19-Hex	✓		✓			✓	0.65
PC	✓	✓			✓	✓	0.92
NPC	✓	✓		✓	✓	✓	0.75

Oceanic chlorophyll *a* algorithm for several cases of waters

Toru Hirawake

Center for Antarctic Environment Monitoring, National Institute of Polar Research
9-10 Kaga 1, Itabashi, Tokyo 173-8515, Japan
hirawake@nipr.ac.jp

Abstract: Characteristics of bio-optical relationships (chlorophyll *a* versus remote-sensing reflectance) for oceanic, turbid, high chlorophyll and polar region waters (n=129) were confirmed and an algorithm using a ratio of four bands (ratio of sum of two bands) was developed . The band-ratio algorithm performed well for oceanic waters and high chlorophyll waters (RMSE = 0.161). However, only the data in the southern ocean and the yellow sea of less than 1.5 mg chl.*a* m^{-3} were not combined with the other one and were needed to deal with separately. Filtering the data using remote-sensing reflectance ratios was effective for the separation.

Introduction

Main primary producer in the ocean is phytoplankton. Although biomass of phytoplankton is extremely less than terrestrial plants, aquatic primary production by phytoplankton almost corresponds to those of the latter (Schimel, 1995). Therefore global accurate estimation of phytoplankton biomass and their primary production in the ocean is required to predict the global carbon flux and global climate change such as the greenhouse effect.

Ocean color remote sensing is effective procedure to estimate chlorophyll *a* concentration as an index of phytoplankton biomass widely, simultaneously, repeatedly and continuously. However, bio-optical algorithms to estimate chlorophyll *a* concentration have some problems. One of the problems is that the most of historic algorithms consisted of small number of data from limited geographic region. Indeed the standard algorithm for the Coastal Zone Color Scanner (CZCS) (Gordon *et al.*, 1983) was developed with the bio-optical data around the North American Continent.

Ocean color which is spectrum of radiance or reflectance depend on the inherent optical properties (IOPs) such as absorption and scattering coefficient. The relationship between absorption coefficient and chlorophyll *a* concentration and also the scattering coefficient is not constant in the world ocean. Therefore the relationship between ocean color and chlorophyll is not invariable.

Although it has been suggested that the polar region water and turbid case 2 (Morel and Prieur, 1977) water occur the large error in the chlorophyll estimation, the bio-optical algorithm for new sensors, SeaWiFS and OCTS did not be taken these waters into consideration. In this study, the global algorithm for some cases of waters was developed.

Materials and Methods

Chlorophyll a concentration and underwater spectral radiation was carried out in the Indian Ocean, Persian Gulf, Southern Ocean, East China Sea, Japan Sea, Pacific Ocean, Osaka Bay, and Yellow Sea (Fig. 1). Total number of data utilized for analysis was 129.

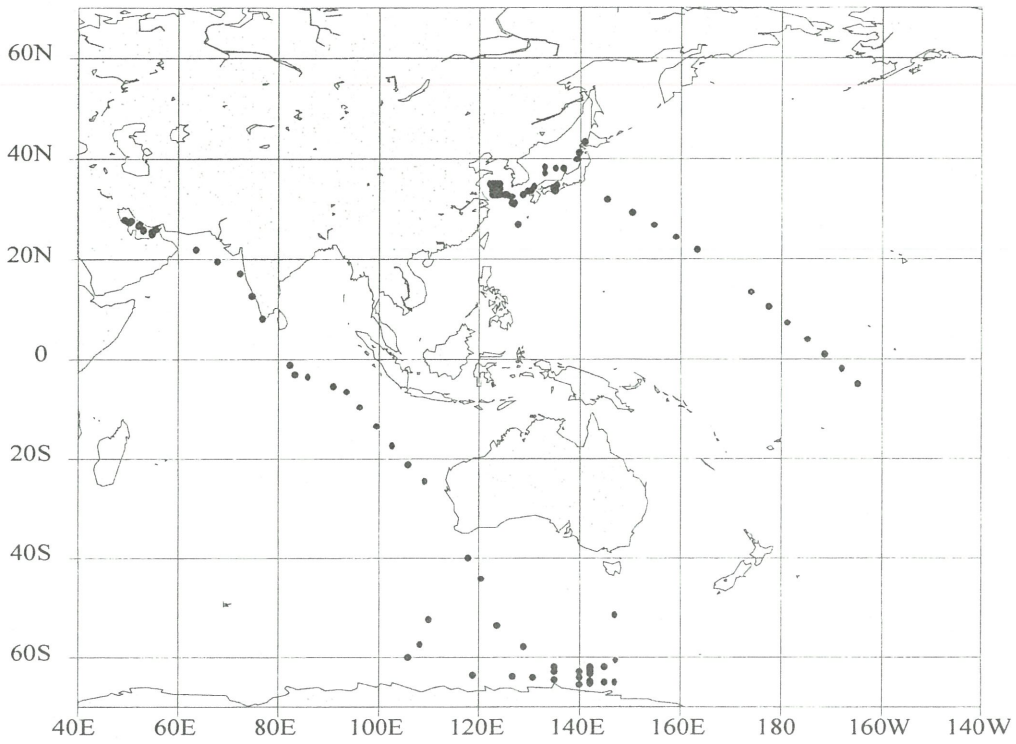

Fig. 1. Sampling station

Chlorophyll *a* concentration was determined fluorometricaly (Parsons et al., 1984) with a fluorometer (Turner Designs). Spectral downwelling irradiance, $E_d(\lambda, z)$ and upwelling radiance $L_u(\lambda, z)$ was measured with spectroradiometers, MER-2020A, MER-2040 and PRR-600 (Biospherical Instruments).

Normalized water-leaving radiance $L_{wn}(\lambda)$ and remote sensing reflectance $R_{rs}(\lambda)$ were calculated from measured $E_d(\lambda, z)$ and $L_u(\lambda, z)$ for development of bio-optical algorithm.

Results and Discussions

The two-bands ratio algorithm of the CZCS was tested for the data set in this study to know the overview of the relationship (Fig. 2).

Based on the distribution in Fig. 2, five cases were determined as following:

(1) Indian Ocean, Japan Sea and Pacific Ocean (Clearer Case 1 waters)
(2) Clearer Case 1 waters + Persian Gulf and Osaka Bay (Case 1 waters)
(3) Southern Ocean and JARE (Southern Ocean)
(4) Yellow Sea and Osaka Bay (Case 2 waters)

(5) All oceanic region.

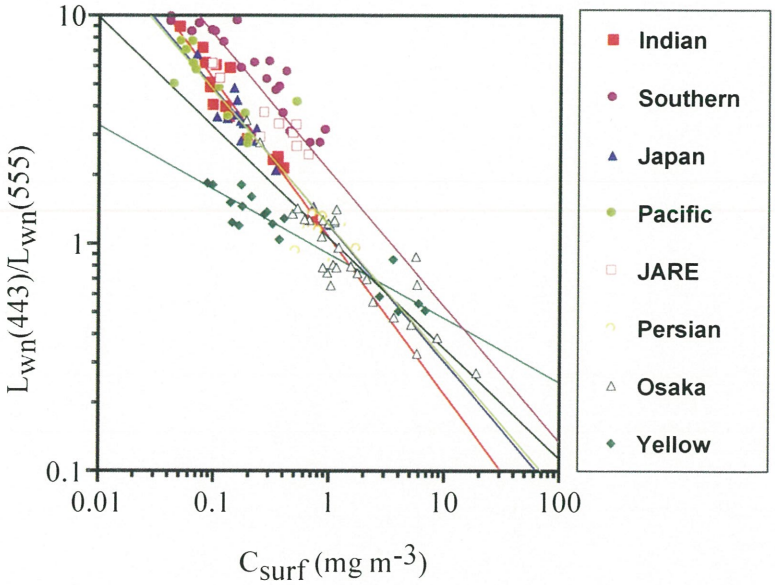

Fig. 2. Relationship between chlorophyll *a* concentration and two-bands ratio (443:555)

For these five cases, tow bands (λ_1 and λ_2) with the highest R^2 value (Table 1) were found with least square fitting to consider the wavelength which should be used in the new algorithm.

Table 1. Tow bands with the highest R^2 value

Area	λ_1	λ_2	R^2	a	b
Clear Case I	443	510	0.877	0.592	-2.317
Southern Ocean	443	510	0.879	1.770	-3.353
Case I	443	555	0.917	1.164	-1.517
Case II	490	555	0.783	1.720	-2.834
ALL	443	555	0.748	1.057	-1.293

λ_1 and λ_2 smoothly shifted from 443 to 490 nm and from 510 to 555 nm, respectively. Therefore, these shifts should be applied and the new bio-optical algorithm was developed as following:

$$C_{surf} = a \times \{[R_{rs}(\lambda_1) + R_{rs}(\lambda_2)] / [R_{rs}(\lambda_3) + R_{rs}(\lambda_4)]\}^{b}, \quad (1)$$

where C_{surf} is chlorophyll a concentration at the sea surface, R_{rs} is remote sensing reflectance, λ_1 to λ_4 are 443, 490, 510 and 555 nm. This algorithm performed well for the all data except the Southern Ocean and Yellow Sea data, and its equation was,

$$C_{surf} = 1.291 \times \{[R_{rs}(443) + R_{rs}(490)] / [R_{rs}(510) + R_{rs}(555)]\}^{-2.621}$$
$$RMSE=0.161, R^2 = 0.924 \quad (2)$$

The results of the analysis using the semi-analytical method (Carder et al., 1999) suggested that the incorrect estimation in the Southern Ocean and the Yellow Sea in the concentration less than 1.5 mg m^3 was attributed to:

(1) Low specific absorption coefficient of phytoplankton and non co-variation of absorption coefficients of non-algal matters with chlorophyll *a* concentration in the Southern Ocean

(2) High specific absorption coefficients of phytoplankton and non-algal matter in the Yellow Sea.

Therefore, variation of the band ratio $R_{rs}(443)/R_{rs}(555)$ indicating chlorophyll *a* concentration and $R_{rs}(412)/R_{rs}(443)$ indicating non-algal matter with their concentrations depend on the waters. This variation can be utilized to separate the waters (Fig. 3).

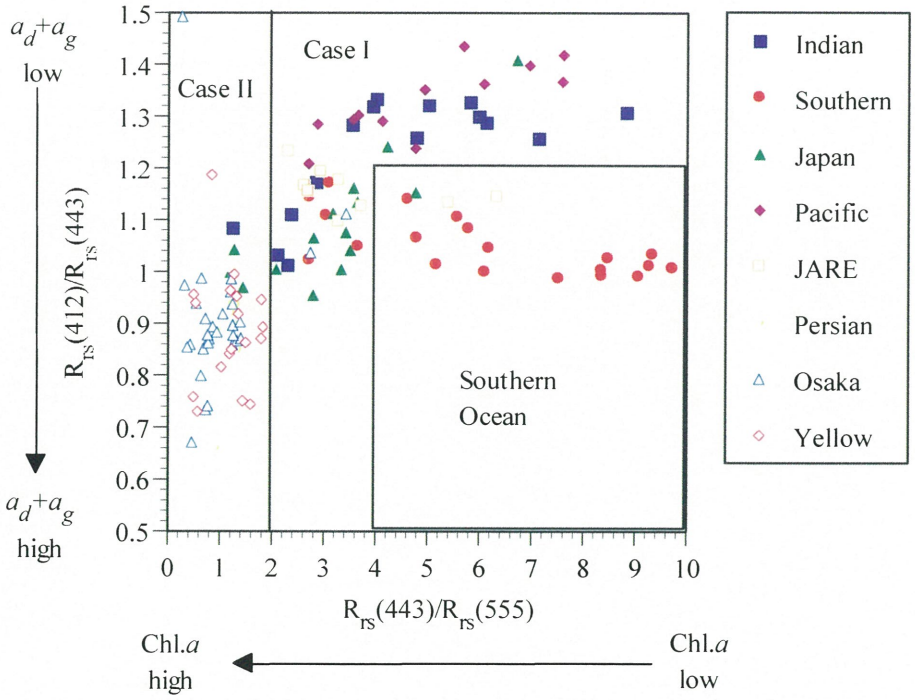

Fig. 3. Separation of waters using the bands ratios $R_{rs}(443)/R_{rs}(555)$ and $R_{rs}(412)/R_{rs}(443)$

In this study, the waters were determined as $R_{rs}(443)/R_{rs}(555) \leq 2$ for case 2 waters, and $R_{rs}(443)/R_{rs}(555) \geq 4$ and $R_{rs}(412)/R_{rs}(443) \leq 1.2$ for the Southern Ocean, respectively. When the each separated data was input to their local algorithm (Fig. 4), the estimation of chlorophyll *a* concentration for all data was largely improved (RMSE=0.236, R^2=0.834).

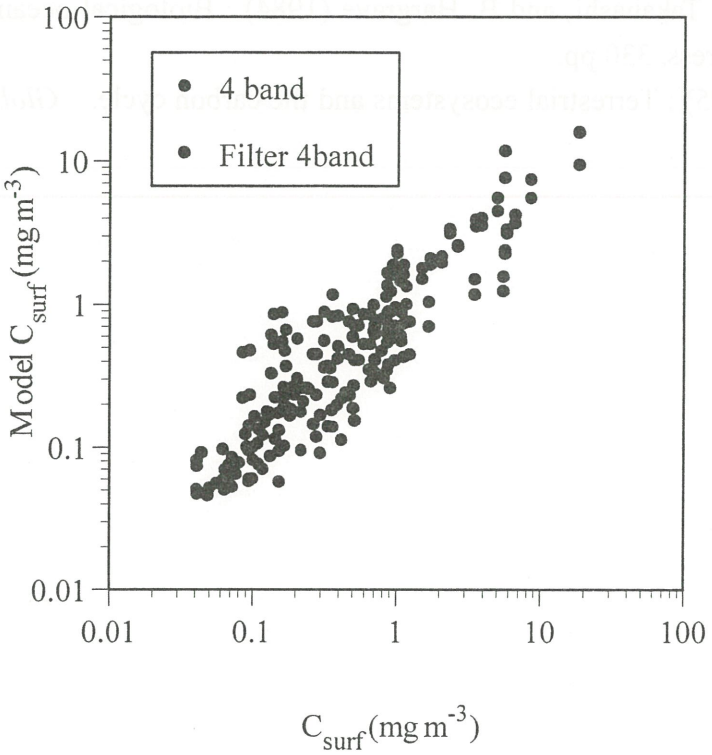

Fig. 4. Relationship between measured and modeled chlorophyll *a* concentration.

This procedure was effective for the global estimation of chlorophyll *a* concentration, because it needs only remotely sensed data.

Acknowledgements

We thank the officers and crews of the T/V Umitaka-maru III and Shinyo-maru, Tokyo University of Fisheries, for their cooperation during the cruise

References

Carder, K. L., F. R. Chen, Z. P. Lee, S. K. Hawes, and D. Kamykowski (1999) : Semianalytic Moderate-Resolution Imaging Spectrometer algorithms for chlorophyll a and absorption with bio-optical domains based on nitrate-depletion temperatures. *J. Geophys. Res.*, **104**, 5403-5421.

Gordon, H. R., D. K. Clark, J. W. Brown, O. B. Brown, R. H. Evans, and W. W. Broenkow (1983) : Phytoplankton pigment concentrations in the Middle Atlantic Bight: comparison of ship determinations and CZCS estimates. *Appl. Opt.*, **22**, 20-36.

Morel, A. and L. Prieur (1977) : Analysis of variations in ocean color. *Limnol. Oceanogr.*, **22**, 709－722.

Parsons, T. R., M. Takahashi, and B. Hargrave (1984) : Biological oceanographic processes. Pergamon Press, 330 pp.

Shimel, D. S. (1995) : Terrestrial ecosystems and the carbon cycle. *Global Change Biol.*, **1**, 77-91.

Air-sea carbon flux simulated in an upper ocean biogeochemical model

Yoshikazu Sasai and Motoyoshi Ikeda

Graduate School of Environmental Earth Science, Hokkaido University,
Sapporo, 060-0810, Japan,
E-mail: mikeda@ees.hokudai.ac.jp

Introduction

The partial pressure of CO_2 (pCO_2) in the surface ocean shows spatial and temporal variations larger than the atmospheric counterparts, caused by the mixed-layer development and biological productivity. In the subpolar regions of the oceans, observations show that the oceanic pCO_2 and the concentration of total inorganic carbon are higher during winter than summer. The ocean is a CO_2 source for the atmosphere in winter and a CO_2 sink in summer. This seasonal evolution may be mainly accounted for by the winter mixing of deep waters, which are rich in total inorganic carbon, and the biological production in summer. On the other hand, in the subtropical region, the ocean is a CO_2 sink in the winter and a CO_2 source in the summer. This variation is governed primarily by temperature.

Method

In this study, we focus the mechanism of carbon cycle in the surface ocean. We employ a three-dimensional ocean model including the bulk mixed-layer model [*Kraus and Turner,* 1967; *Niiler and Kraus,* 1977]. Air-sea carbon flux is calculated using a this model, in which the distributions of total inorganic carbon, phosphate, and carbonate alkalinity are simulated. The model has the upper 300 m of the ocean. The model is initialized with historical data in the North Pacific and forced by European Centre for Medium-Range Weather Forecasts (ECMWF) data and National Centers for Environmental Prediction (NCEP)/ National Center for Atmospheric Research (NCAR) data. Velocity structures are obtained from wind driven Ekman transport and geostrophic ocean currents diagnostically induced by the observed density structures. This model retains the following processes: air-sea carbon flux at the sea surface, the biological pump, the development of mixed layer, horizontal and vertical advections and horizontal and vertical diffusions. The mixed layer development occurs by cooling and wind stress through the sea surface. The entrainment velocity, W_e, is determined from the energy balance. A gain of potential energy at the base of the mixed layer balances with a sum of the turbulent kinetic energy and the potential energy input at the surface. When the atmospheric cooling changes to the heating (e.g. summer), the entrainment velocity is set to zero.

The equations for conservation of total inorganic carbon C_m, carbonate alkalinity A_m, and phosphate P_m in the mixed layer are

$$\frac{\partial C_m}{\partial t} = W_e \frac{\triangle C}{h} - \frac{F_{CO_2}}{h} - \frac{106}{1} S_{P_m} - \left(u + u_e \frac{h_e}{h}\right) \frac{\partial C_m}{\partial x} - \left(v + v_e \frac{h_e}{h}\right) \frac{\partial C_m}{\partial y} + K_H \left(\frac{\partial^2 C_m}{\partial x^2} + \frac{\partial^2 C_m}{\partial y^2}\right), \quad (1)$$

$$\frac{\partial A_m}{\partial t} = W_e \frac{\triangle A}{h} - \frac{106}{1} \frac{1}{10} S_{P_m} - \left(u + u_e \frac{h_e}{h}\right) \frac{\partial A_m}{\partial x} - \left(v + v_e \frac{h_e}{h}\right) \frac{\partial A_m}{\partial y} + K_H \left(\frac{\partial^2 A_m}{\partial x^2} + \frac{\partial^2 A_m}{\partial y^2}\right), \quad (2)$$

$$\frac{\partial P_m}{\partial t} = W_e \frac{\triangle P}{h} - S_{P_m} - \left(u + u_e \frac{h_e}{h}\right) \frac{\partial P_m}{\partial x} - \left(v + v_e \frac{h_e}{h}\right) \frac{\partial P_m}{\partial y} + K_H \left(\frac{\partial^2 P_m}{\partial x^2} + \frac{\partial^2 P_m}{\partial y^2}\right), \quad (3)$$

where $\triangle C$, $\triangle A$ and $\triangle P$ are the discontinuities in total inorganic carbon, carbonate alkalinity, and phosphate at the base of the mixed layer. u, v and w are the horizontal and vertical velocity components, u_e and v_e are the Ekman velocities, w_e is the vertical velocity (Ekman pumping or suction) associated with convergence or divergence of the Ekman transport, h is the mixed-layer depth, h_e is the Ekman depth, and K_H is the horizontal diffusion ($= 10^2$ m^2 s^{-1}). The formula for the air-sea carbon flux, F_{CO_2} is

$$F_{CO_2} = k_s \gamma (pCO_{2oc} - pCO_{2atm}), \quad (4)$$

where k_s (cm h^{-1}) is the piston velocity [*Wanninkhof*,1992], γ (mol kg^{-1} atm^{-1}) is the solubility of CO_2 in seawater, and pCO_{2oc} (μatm) and pCO_{2atm}(μatm) are the partial pressures of CO_2 in the surface ocean and in the atmosphere, respectively. The oceanic pCO_2 is related to total inorganic carbon and carbonate alkalinity under the assumptions of chemical equilibrium.

The biological pump S_{P_m} is considered as a function of phosphate concentration in the mixed layer :

$$S_{P_m} = \frac{L}{T_e} P(t) \frac{30}{h}, \quad (5)$$

where L is the coefficient at which the biological production occurs ($L = 1$) or does not occur ($L = 0$), and the T_e is the e-folding time scale of phosphate reduction (or biological production). The coefficient L is 1 in summer and 0 in winter, with the transition times given as a function of the latitudes. The values of L and T_e control the magnitude and the period of the biological production, respectively. The values of T_e are set as 60 days west of 165°E and 180 days east of 165°E.

The equations for total CO_2 C_l, carbonate alkalinity A_l, and phosphate P_l in the lower layer are

$$\begin{aligned}\frac{\partial C_l}{\partial t} &= \frac{106}{1} S_{P_l} \\ &\quad -u\frac{\partial C_l}{\partial x} - v\frac{\partial C_l}{\partial y} - (w + w_e)\frac{\partial C_l}{\partial z} \\ &\quad +K_H\left(\frac{\partial^2 C_l}{\partial x^2} + \frac{\partial^2 C_l}{\partial y^2}\right) + K_Z\left(\frac{\partial^2 C_l}{\partial z^2}\right), \end{aligned} \tag{6}$$

$$\begin{aligned}\frac{\partial A_l}{\partial t} &= \frac{106}{1}\frac{1}{10} S_{P_l} \\ &\quad -u\frac{\partial A_l}{\partial x} - v\frac{\partial A_l}{\partial y} - (w + w_e)\frac{\partial A_l}{\partial z} \\ &\quad +K_H\left(\frac{\partial^2 A_l}{\partial x^2} + \frac{\partial^2 A_l}{\partial y^2}\right) + K_Z\left(\frac{\partial^2 A_l}{\partial z^2}\right), \end{aligned} \tag{7}$$

$$\begin{aligned}\frac{\partial P_l}{\partial t} &= S_{P_l} \\ &\quad -u\frac{\partial P_l}{\partial x} - v\frac{\partial P_l}{\partial y} - (w + w_e)\frac{\partial P_l}{\partial z} \\ &\quad +K_H\left(\frac{\partial^2 P_l}{\partial x^2} + \frac{\partial^2 P_l}{\partial y^2}\right) + K_Z\left(\frac{\partial^2 P_l}{\partial z^2}\right), \end{aligned} \tag{8}$$

where K_Z is the vertical diffusion coefficient ($= 10^{-5}$ m^2 s^{-1}). The vertical profile of the mineralization S_{P_l} is given by

$$S_{P_l} = \frac{S_{P_m} h}{1000} exp(-(z - h)/1000), \tag{9}$$

where z is the depth of water. Thus, the organic carbon flux reduces exponentially to 1/e at 1000 m.

Results

We describe the result of difference of the effect of the biological production between the eastern and western regions. The horizontal map of annual mean air-sea carbon flux is shown in Figure 1 (a). Positive values denote the region where the ocean is a CO_2 sink in one year. Especially, in the vicinity of the Japan coast, the ocean is a strong CO_2 sink because the strong biological production occurs in summer. In the limited position of the subpolar region, the ocean is a CO_2 source where vertical mixing of deep waters, which are rich in total inorganic carbon, occurs rapidly in winter.

In the mean balance, the biological pump is nearly canceled by the advection effects in the subpolar region, and the minor residual takes the atmospheric CO_2 to the ocean (Figure 1(b)). The advection effects in the subpolar region are mainly due to the Ekman upwelling, increasing CO_2 by transporting the high CO_2 from the lower layer. To the subtropical region, the large CO_2 in the subpolar region is transported by the southward Ekman flow. All three components are smaller in the subtropical region. The seasonal variability of air-sea carbon flux is controlled by the biological pump in spring and summer and vertical mixing to the mixed layer in winter along with the secondary effect of the Ekman upwelling which is stronger in winter (Figure 2).

References

Kraus,E.B., and J.S.Turner, A one-dimensional model of the seasonal thermocline, II. The general theory and its consequences, *Tellus*, *1*, 98-105, 1967.

Niiler,P.P., and E.B.Kraus, One-dimensional models of the upper ocean, in *Modelling and Prediction of Upper Layers of the Ocean*, edited by E.B.Kraus, pp. 143-172, Pergamon, Tarrytown, N. Y., 1977.

Wanninkhof,R, Relationship between wind speed and gas exchange over the ocean, *J. Geophys. Res.*, *97*, 7,373-7,382, 1992.

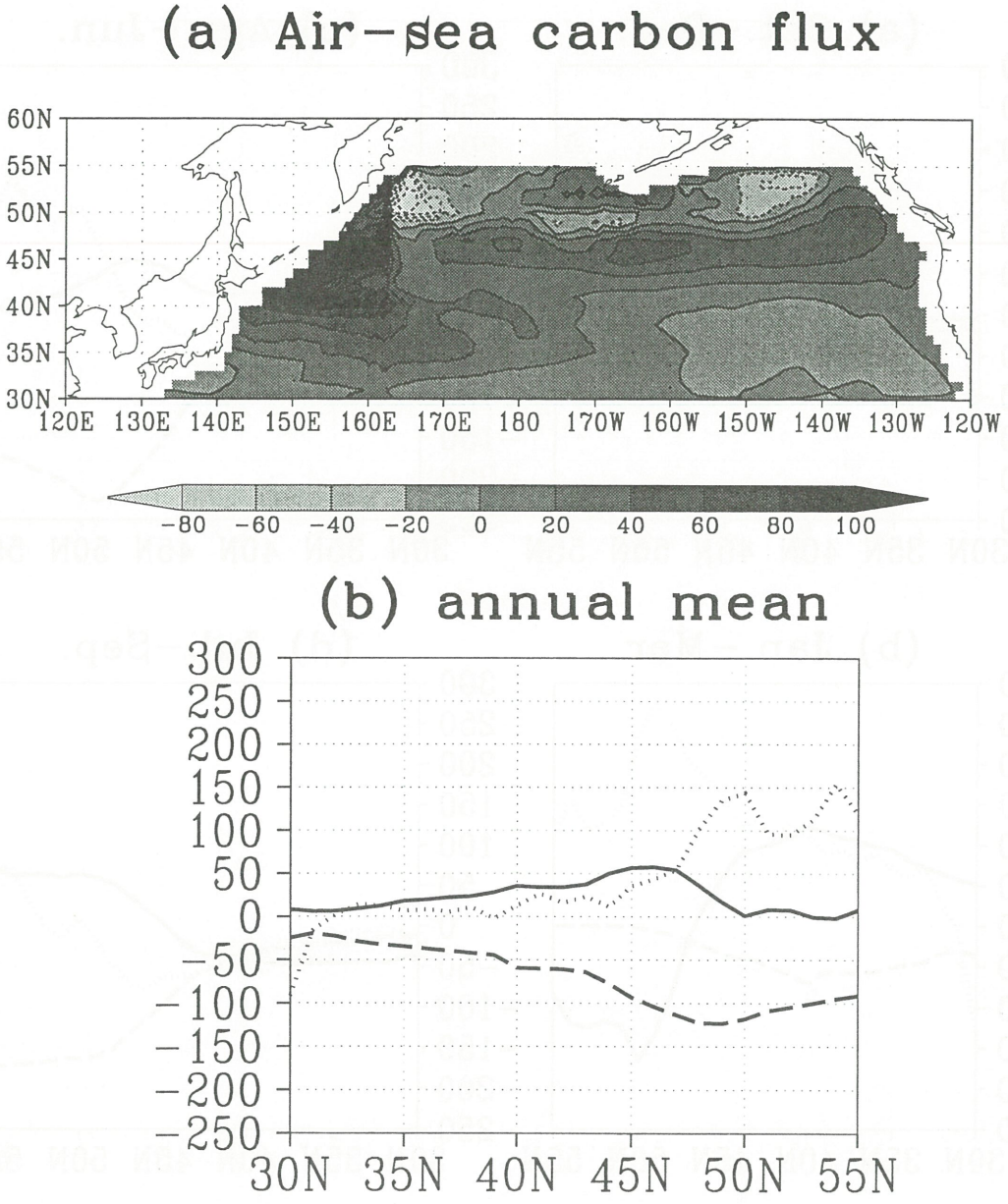

Figure 1. Annual mean distribution of (a) air-sea carbon flux (mgC m^{-2} d^{-1}) in the North Pacific. The contour interval is 20 mgC m^{-2} d^{-1}. Positive values are where the ocean is a CO_2 sink, and negative values are where the ocean is a CO_2 source. (b) Annual mean carbon flux (mgC m^{-2} d^{-1}), which vertical integrated from sea surface to 200 m depth, along the latitude. The solid line denotes air-sea carbon flux. The short dashed line denotes biological pump which exports organic carbon for the lower layer. The dots line denotes the advections which transports carbon in the surface layer.

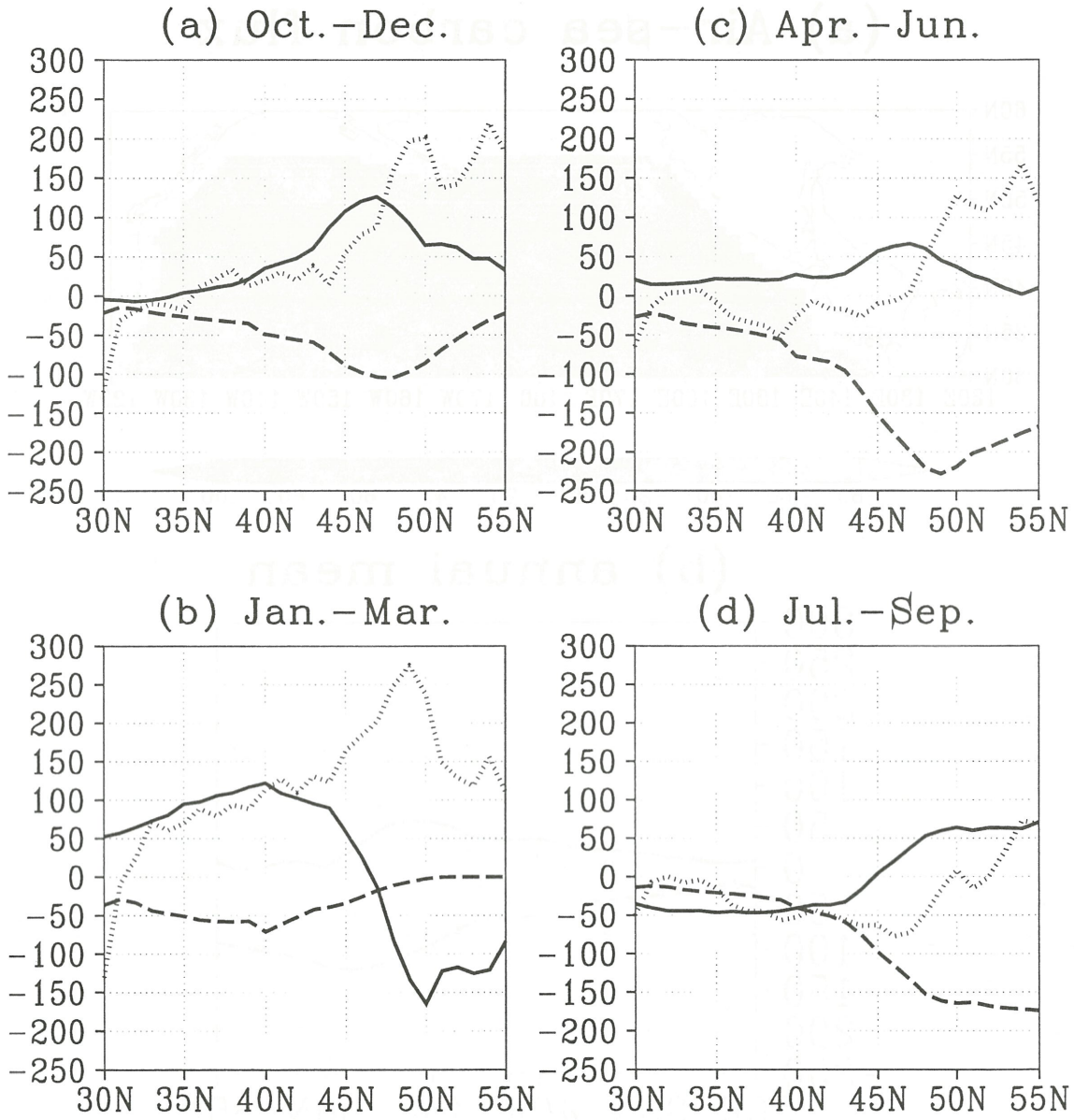

Figure 2. Same as Figure 1 (b) but for the seasonal mean carbon flux (mgC m^{-2} d^{-1}).

(a) Air-sea carbon flux

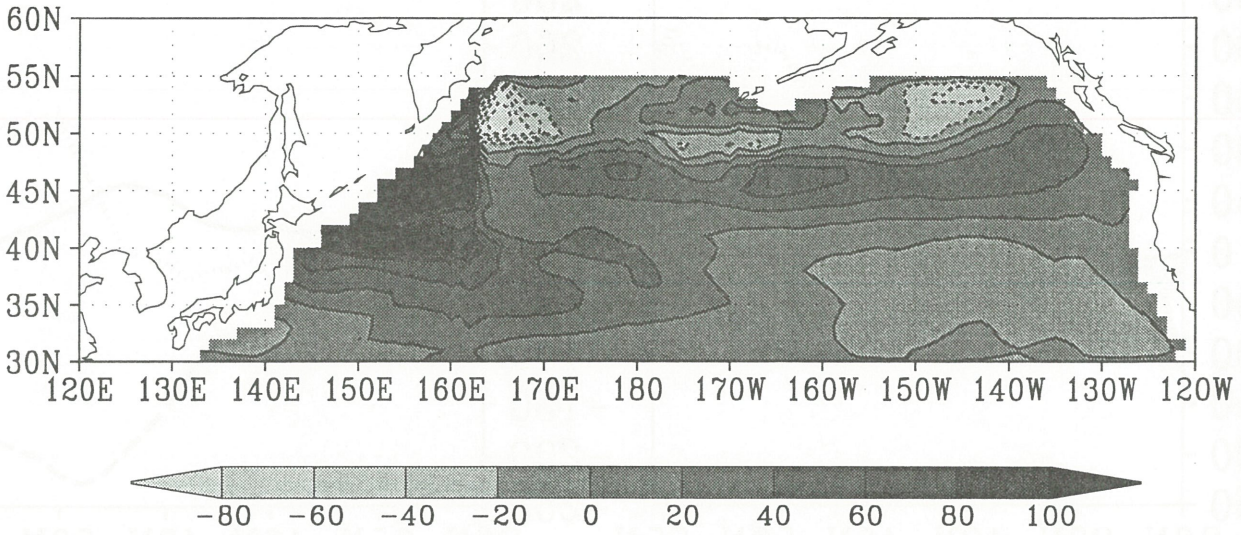

(b) annual mean

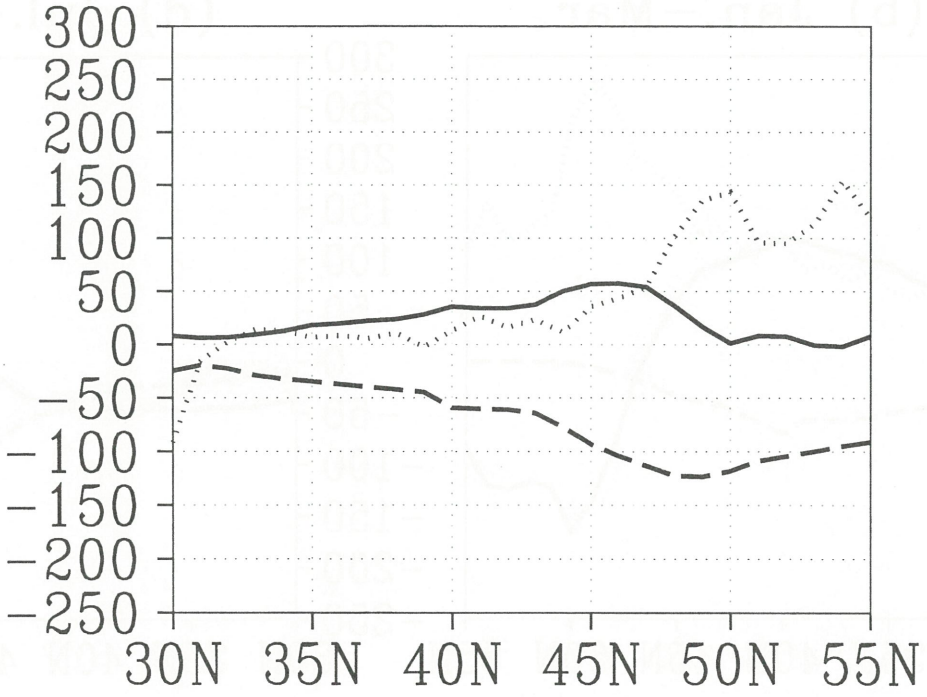

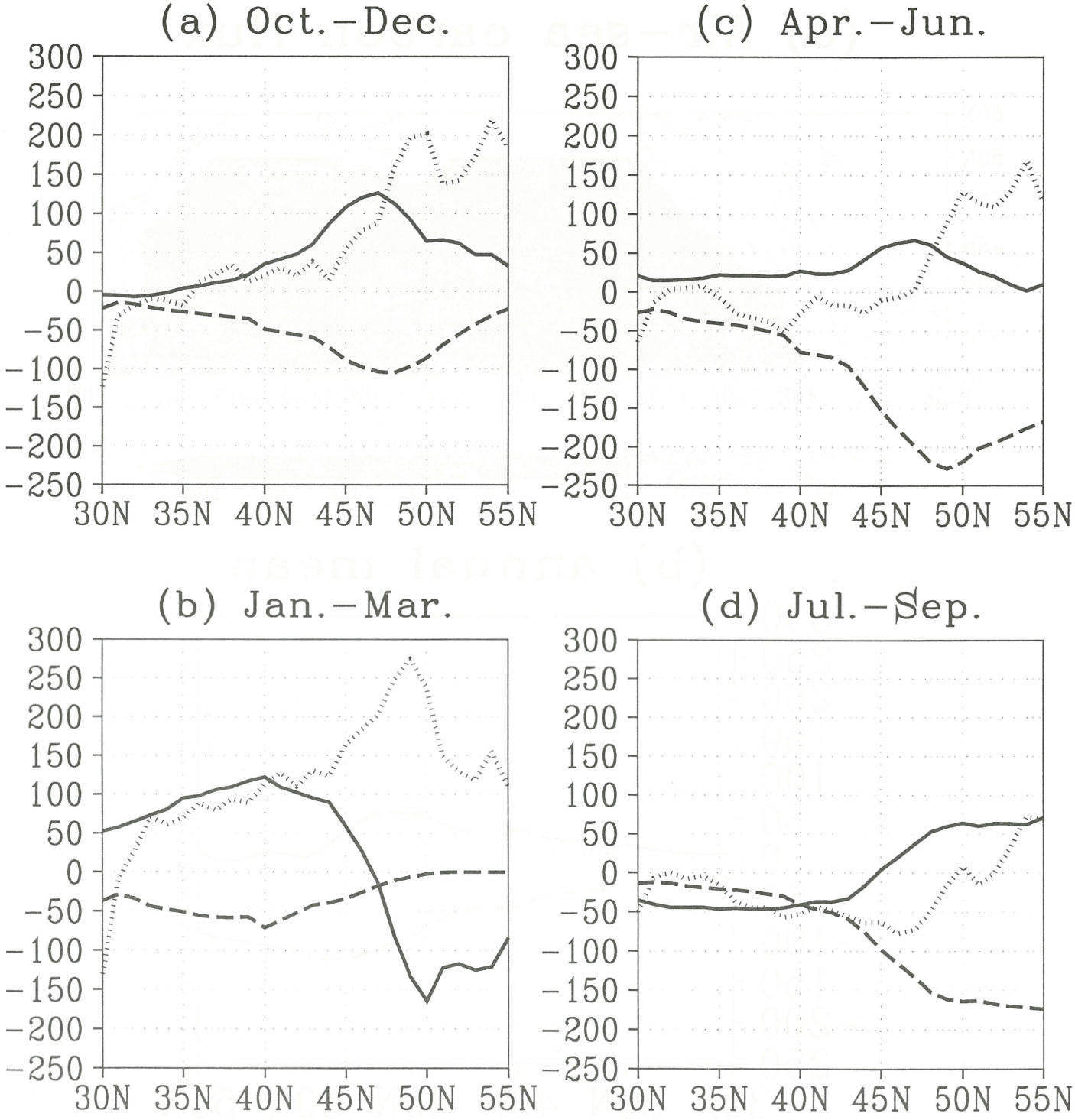
(a) Oct.−Dec.
(c) Apr.−Jun.
(b) Jan.−Mar.
(d) Jul.−Sep.
300
250
200
150
100
50
0
−50
−100
−150
−200
−250
30N 35N 40N 45N 50N 55N

Variations in CO_2 outflux from the central and western equatorial Pacific

Hisayuki Y. Inoue, Masao Ishii, Hidekadzu Matsueda, Takayuki Tokieda, Shu Saito, Ichio Asanuma, Takeshi Kawano*, and Akihiko Murata**

Geochemical Research Department, Meteorological Research Institute

Nagamine 1-1, Tsukuba, Ibaraki 305-0052, Japan. e-mail: INOUE<hysohsika@mri-jma.go.jp>

** Ocean Research Department, Japan Marine Science and Technology Center*

Natsushima 2-15, Yokosuka, Kanagawa 237-0061, Japan. e-mail: ASANUMA<asanumai@jamstec.go.jp>

Introduction

Equatorial Pacific is known as a strong natural source for atmospheric CO_2. CO_2 outflux from the equatorial Pacific has been estimated to be 1-2 Gt-C/yr (Tans et al., 1990). Depending on the oceanic conditions, CO_2 outflux varies considerably on time scale of months: following the occurrence of El Niño event, the CO_2 outflux has been reported to decrease significantly (Feely et al., 1987, Inoue and Sugimura 1992, Wong et al., 1993). Francey et al., (1995) have reported the interannual changes in oceanic/biospheric CO_2 uptake on the basis of measurements of $^{13}C/^{12}C$ of atmospheric CO_2. In order to investigate effects of temporal variations in CO_2 outflux from the central and western equatorial Pacific to the growth rate of atmospheric CO_2, measurements of partial pressure of CO_2 (pCO_2^W) in surface seawater were made in the central and western equatorial Pacific during the period from 1987 to 1997.

Results and Discussion.

Figure 1 shows the longitudinal distributions of pCO_2^W in surface seawater in

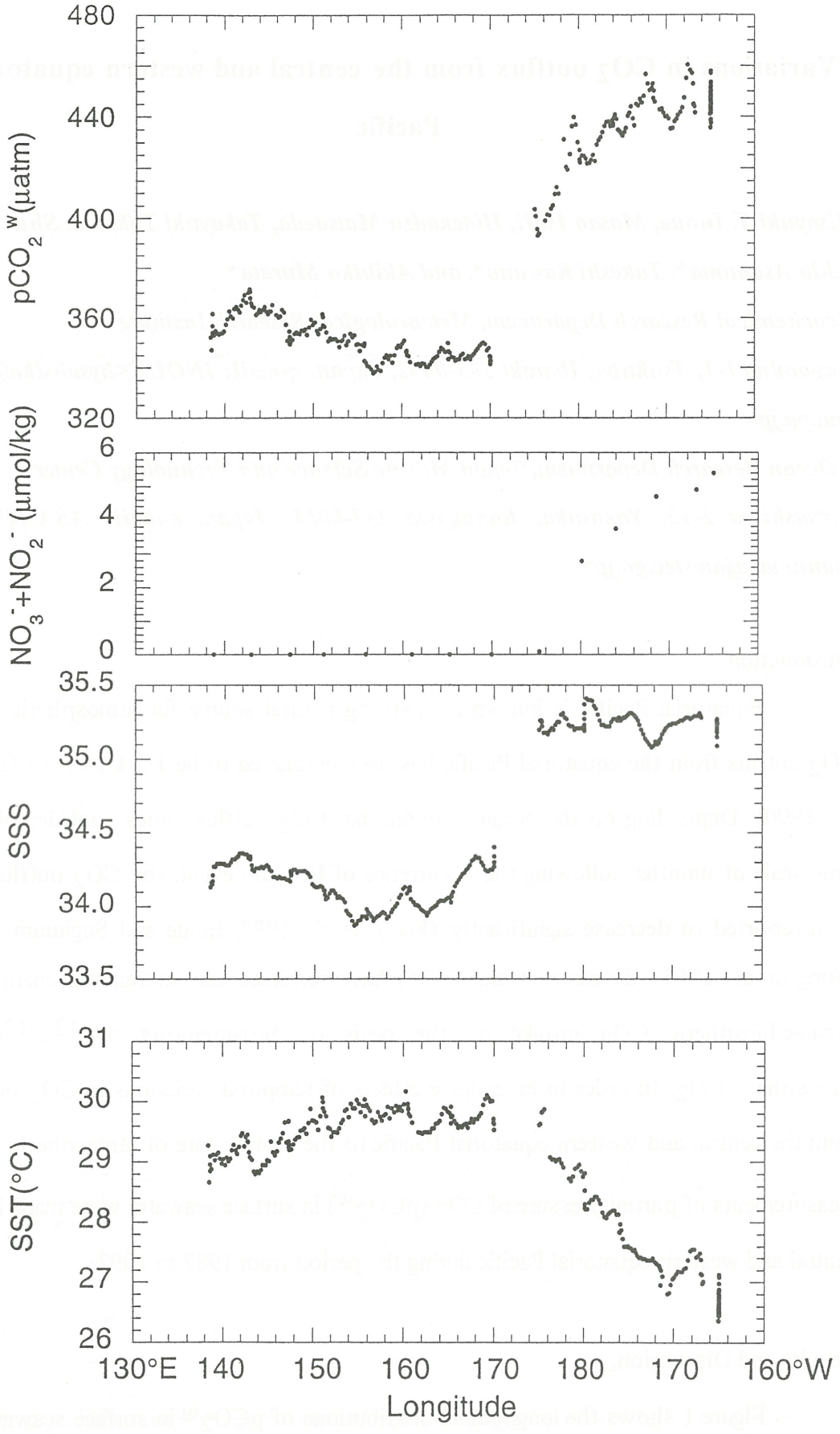

Fig. 1 Longitudinal distributions of $pCO_2{}^w$, $NO_2^-+NO_3^-$, SSS, and SST along the equator in January 1994.

November 1994. In the area of warm water pool having characteristics of high sea surface temperature (SST), low sea surface salinity(SSS) and low nutrient concentrations, the pCO_2 is nearly equal to or slightly supersaturated with respect to that of pCO_2 in the air (pCO_2^a). This could be caused by shallow mixed layers that are insulated from the cold water reservoir of the thermocline by underlying barrier layers (Lukas and Lindstrom, 1991). Vertical stratification in the water column resulted from a salinity gradient above the thermocline (see for example, Ando and McPhaden, 1997).

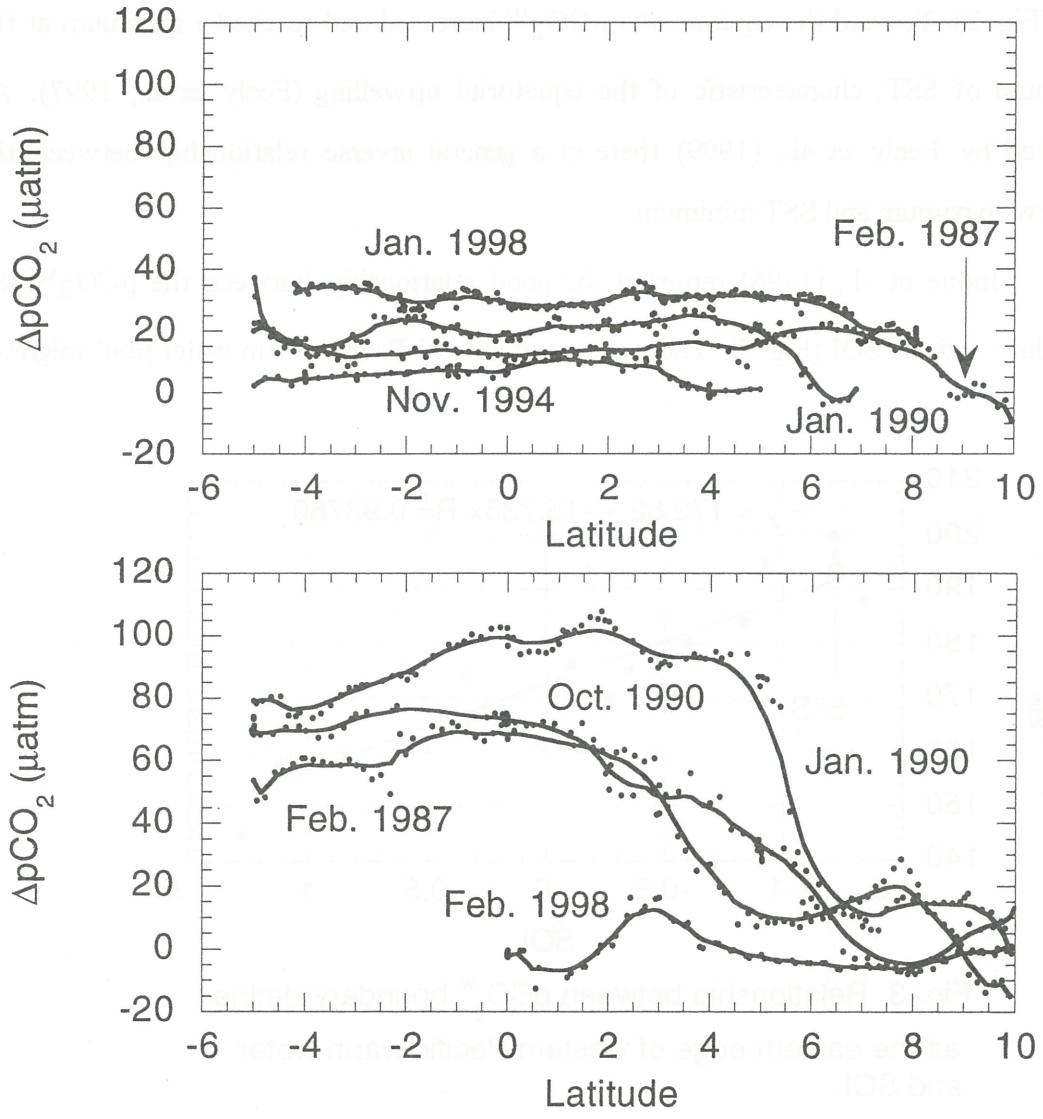

Fig. 2 Latitudinal dsitributions of pCO_2^w along 160°E and 160°W.

Latitudinal distributions of ΔpCO_2 (pCO_2^W - pCO_2^a) along 160°E show fairly low and constant values for both non-El Niño and El Niño periods (Fig. 2). East of the western equatorial Pacific warm water, known as the area of "cold-tongue", the pCO_2^W is highly supersaturated with respect to that of the air, and tends to increase with the increase of SSS, and the decrease of SST. The latitudinal distribution of pCO_2^W is strongly dependent on the position of the eastern edge of warm water pool. The pCO_2^W sometimes occurred a steep change at the boundary (~5°N) between the NECC and the SEC (Fig. 2). Toward the equator, the pCO_2^W increased and reached a maximum at the minimum of SST, characteristic of the equatorial upwelling (Feely et al., 1997). As reported by Feely et al., (1999) there is a general inverse relationship between the pCO2w maximum and SST minimum.

Inoue et al., (1996) reported the good relationship between the pCO_2^W/SSS boundary and the SOI (Fig. 3). The western equatorial Pacific warm water pool migrates

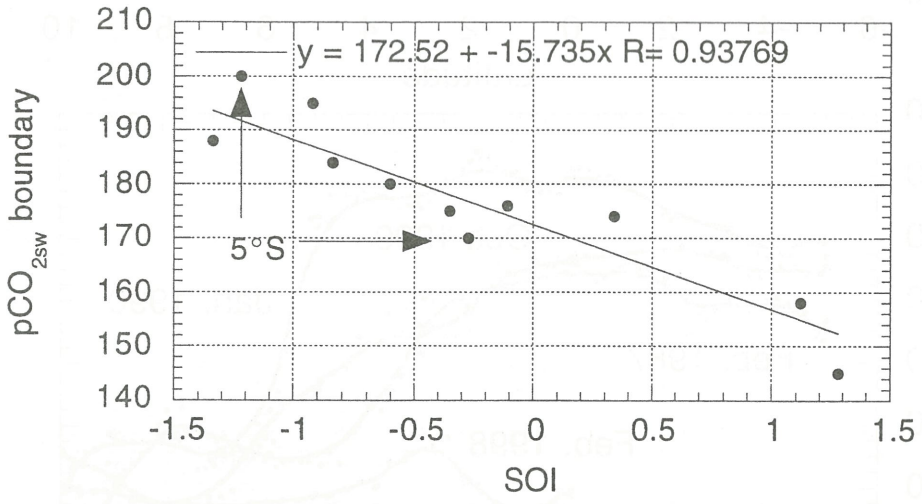

Fig. 3. Relationship between pCO_2^W boundary defined as the eastern edge of western Pacific warm water and SOI.

to the east during El Niño period and conversely to the west during La Niña period, which leads to the intra/interannual changes in CO_2 outflux on time scales of a few months. A good correlation between the pCO_2^W/SSS and SOI allows us to estimate variations in CO_2 outflux from the central and western equatorial Pacific (Inoue, 1999). In order to know temporal variations in CO_2 outflux, we examined the relationship

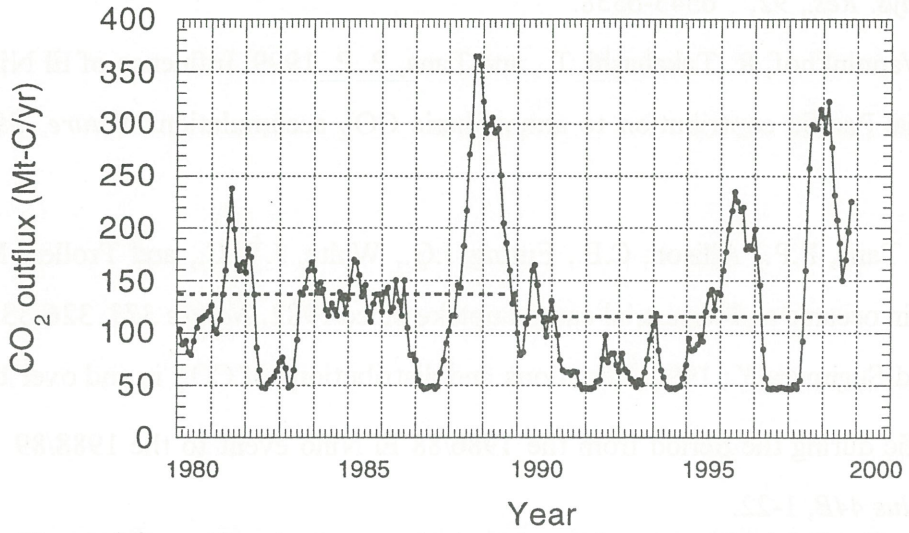

Fig. 4 CO_2 outflux in the central and western equatorial Pacific (5.5°S-5.5°N, 139.5°E-159.5°W) during 1980 to 1999. Dotted line shows a mean flux over 1980sand 1990s.

between CO_2 outflux and SOI (Fig. 4). On the basis of the relationship in Fig. 4, temporal variations in CO_2 outflux from the central and western equatorial Pacific were drawn: over the 1980s, the average annual CO_2 outflux from the central and western equatorial Pacific was estimated to be 137 Mt-C/yr, while from January 1990 to October 1999 115 Mt-C/yr because of a prolonged El Niño over early 1990s that could be linked to decadal changes in climate throughout the Pacific basin (Trenberth and Hoar, 1996).

References

Ando, K. and McPhaden, M. J. 1997. Variability of surface layer hydrography in the tropical Pacific Ocean. *J. Geophys. Res., 102*, 23,063-23,078.

Feely, R.A., Gammon, R.H., Taft, B.A., Pullen, P.E., Waterman, L.S., Conway, T.J., Gendron, J.F., and Wisegarver, D.P. 1987. Distribution of chemical tracers in the eastern equatorial Pacific during and after the 1982-83 El Niño/Southern Oscillation Event, *J. Geophys. Res., 92*, 6545-6558.

Feely, R. A., Wanninkhof, R. Takahashi, T., and Tans, P. P. 1999. Influence of El Niño on the equatorial Pacific contribution to atmospheric CO_2 accumulation. *Nature, 398*, 597-601.

Francey, R. J., Tans, P.P., Allison, C.E., Enting, I.G., White, J.W.C., and Troller, M. 1995. Changes in oceanic and terrestrial carbon uptake since 1982. *Nature 373*, 326-330.

Inoue Y. H., and Sugimura Y., 1992. Variations and distributions of CO_2 in and over the equatorial Pacific during the period from the 1986/88 El Niño event to the 1988/89 La Niña event. *Tellus 44B*, 1-22.

Inoue Y. H., M. Ishii, Matsueda H., Ahoyama M., and Asanuma I. 1996. changes in longitudinal distribution of the partial pressure of CO_2 (pCO_2) in the central and western equatorial Pacific., west of 160°W. *Geophys. Res. Lett.* , 23, 1781-1784.

Inoue, H. Y. 1999. CO_2 exchange between the atmosphere and the ocean. Carbon cycle studies of the Meteorological Research Institute since 1968. In *Dynamics and Characterization of Marine Organic Matter* (edited by N. Handa, E. Tanoue and T. Hama). TerraPub, Tokyo, in press.

Ishii, M. and Inoue, H. Y. 1995. Air-sea exchange of CO_2 in the central and western equatorial Pacific in 1990. *Tellus, 47B*, 447-460.

Lukas, R. and Lindstrom, E. 1991. The mixed layer of the western equatorial Pacific Ocean, J. *Geophys Res., 96*, 3,343-3,357.

Tans, P.P., Fung,I., and Takahashi, T. 1990. Observational constrains on the global atmospheric CO_2 budget. *Science, 247*, 1431-1438.

Trenberth, K. E. and Hoar, T. J., 1996. The 1990-1995 El Niño-Southern Oscillation event: Longest on record. *Geophys. Res. Lett., 23*, 57-60.

Wong, C.S., Chan, Y.-H., Page, J.S., Smith, G.E., and Bellegay, R.D., 1993. Changes in equatorial CO_2 flux and new production estimated from CO_2 and nutrient levels in Pacific surface waters during the 1986/87 El Niño. *Tellus 45B*, 64-79.

Comparison between carbon flux collected by time-series sediment trap experiment and the primary productivity estimated with satellite data

Makio C. Honda* [1], Masashi Kusakabe [1], Fumiko Hoshi [1], Toshikatsu Sugawara [2], and Ichio Asanuma [1]

1) Japan Marine Science and Technology Center, Ocean Research Department
2-15 Natsushima, Yokosuka, 237-0061 Japan
* e-mail: hondam@jamstec.go.jp
2) Marine Works Japan, Ltd., 2-15 Natsushima, Yokosuka, 237-0061 Japan

1. Introduction

Till quite recently, a sediment trap experiment had been only one method for time-series observation of biogeochemistry in the ocean. Recent progress in the remote sensing technology has also enable us to understand seasonal variability in the sea surface temperature, chlorophyll-a, solar irradiance, and wind velocity which data can be utilized for the research of air-sea exchange of CO_2, primary production, and so on. This report is the preliminary result of comparison between carbon flux collected by time-series sediment trap and the primary productivity estimated with satellite data for the northwestern North Pacific (NWNP).

2. Methods

2.1 Sediment trap experiment

Sediment trap mooring systems were deployed at three stations (stn. KNOT: 44°N, 155°E; stn. 50N: 50°N, 165°E, stn. 40N: 40°N, 165°E) in the NWNP from Dec. 1997 and May 1999. Time-series sediment traps with 21 rotary cups were installed at ~ 1000, 3000, 5000 m depths on mooring system. In laboratory, organic carbon and inorganic carbon of samples with size less than 1 mm were measured with an elemental analyzer, and silica, calcium and aluminum were determined with Inductively Coupled Plasma-Atomic Emission Spectrometry.

2.2 Satellite data

Ocean color data were observed by SeaWiFS aboard the Orv View-2 and concentrations chlorophyll-a (chl-a) were calculated with analysis software "Seadas ver 3.3" supplied by NASA. Sea surface temperature (SST) were obtained from NOAA-AVHRR-MCSST. As most of data during the experimental period were not available because of cloud cover over the NWNP, SST data interpolated by "Seadas ver 3.3" were used for this study. SST data obtained during 1 week and within approximately 1

degree square around three sediment trap stations were compiled. Solar irradiance data observed by VISSR aboard GMS-5 were supplied by Japan Meteorological Agency. One week data of dairy irradiance ($MJ/m^2/day$) for each 1 degree were compiled and averaged with standard deviation.

3. Results

3.1 Sediment trap experiment

Total mass flux increased in the late spring to summer at stn. KNOT and stn. 50N, and in the early spring at stn. 40N. Collected materials consisted of, mainly, biogenic materials (organic matter, $CaCO_3$, and opal), and opal was major component, annual average of which was ~ 50 % for stn. KNOT and stn. 50N. Seasonal variability in carbon flux synchronized well with total mass flux and the ratio of organic carbon flux to inorganic carbon flux (Co/Ci ratio) increased in summer at stns. KNOT and 50N and in autumn at stn. 40N. Opal flux at stn. KNOT and stn. 50N increased drastically from the late spring to summer, and seasonal variability in opal flux was larger than that in $CaCO_3$. Opal/$CaCO_3$ ratio correlated well with Co/Ci ratio. It implies that the increase of the Co/Ci ratio was attributed to the increase of plankton with opal test such as diatom. Average values of carbon flux, Co/Ci ratio and opal/$CaCO_3$ ratio at stn. KNOT were the highest among three stations, which is indicative of that the biological pump at stn. KNOT might work the most efficiently for the uptake of atmospheric CO_2 in this region.

3.2 Satellite data

(1) Chl-a

Surface Chl-a concentrations were approximately 0.8 ± 0.3 mg/m^3 around stn. KNOT and 0.6 ± 0.2 mg/m^3 around stn. 40N in Dec. 1997 and 1998. Chl-a concentrations were low in winter, decreased by the middle of March, and increased toward summer and autumn. Maximum of weekly mean of chl-a concentration around stn. KNOT, stn. 50N, and stn. 40N were 1.7 ± 3.5 mg/m^3 (observed in October), 1.1 ± 0.1 mg/m^3 (in September), and 1.1 ± 0.2 mg/m^3 (in July), respectively. Mean values during the experimental period were 0.6 mg/m^3 for KNOT, 0.4 mg/m^3 for stn. 50N, and stn. 0.4 mg/m^3 for stn. 40N.

(2) SST

SST around stn. KNOT in February was low (~ 2 deg-C) and high in August (~ 17 deg-C). Seasonal variability in SST around stn. 50N synchronized with that around stn. KNOT although the maximum of SST was ~ 5 deg-C lower than KNOT. Compared with other two stations, seasonal variability in SST around stn. 50N showed smooth curve. It is likely that station 50N is located in the North Pacific Subarctic Gyre

and the water mass is comparatively stable. SST around 40N were higher than other two stations and SST in the late summer or the early autumn increased by ~ 25 deg-C.

(3) Solar irradiance

Weekly mean of daily solar irradiance had large standard deviation for respective stations. It should be attributed to that this value significantly depends on the intense of cloud coverage, which is ubiquitous and changeable within object areas. Seasonal variation in solar irradiance around stn. KNOT was low in December and January and became the highest in June. Around stn. 50N, the mean values of experimental period was lower than other two stations (8.2 MJ/m^2). In 1998, solar irradiance around stn. 50N was the highest in July, when was approximately one month after the highest period around stn. KNOT. The mean value around stn. 40N was higher than other two areas (10.3 MJ/m^2). The highest solar irradiance of approximately 20 MJ/m^2 was observed in July. According to seasonal variability in SST, solar irradiance and photoperiod, period with SST maximum appeared in two or three months after period with maximum solar irradiance or photoperiod.

4. Discussions

4.1 Primary productivity

Seasonal variability in the primary productivity (PP) was calculated with chl-a, SST and solar irradiance which obtained from SeaWiFS, AVHRR, and VISSR, respectively, and using empirical equations proposed by (a) Berger (1989) and (b) Behrenfeld and Falkowski (1997).

(a) $\mathrm{Log}(PP) = 2.793 + 0.559\,\mathrm{Log}(\text{Chl-a})$ ---------- (1)

(b) $PP = 0.66125 * Popt * [E0 / (E0+4.1)] * Zeu * \text{Chl-a} * Dirr$ ---------- (2)

where, Chl-a is sea surface chl-a concentration. Popt is maximum PP (mg-C/mg-Chl-a/day) within a water column, which is estimated with SST empirically. E0 is the sea surface photosynthesis available radiation (PAR: mol quanta/m^2/day). In this study, E0 is assumed that 1 MJ/m^2/day is equal to 2.0 mol quanta/m^2/day (Kishino, personal communication with Ishizaka, 1998). Zeu is the physical depth receiving 1 % of E0 (m) and estimated with a function of chl-a proposed by Morel and Berthon (1989). Dirr is photoperiod (hours) per day and supplied by Hydrographic Department, Japan Maritime Safety Agency.

Fig. 1 shows time-series PP estimated with both equations for respective stations (solid lines). In this figure, the maximum and minimum values estimated with boundary values of standard deviation are also shown (broken lines) (Note that vertical axis are logarithm scale). PP estimated with equation of Behrenfeld and Falkowski

("B&F" equation) show larger seasonal variability than PP estimated with Berger's equation ("B" equation). In general, PP for respective areas was higher during summer and lower in winter. Average value of PP by "B&F" equation around stn. KNOT increased by 1,900 mg-C/m^2/day in September and decreased by 120 mg-C/m^2/day in winter, while the maximum and minimum values by "B" equation were 800 mg/m^2/day and 300 mg-C/m^2/day, respectively. Around stn. 50N, the maximum of PP by "B&F" equation was at most 1,000 mg-C/m^2/day in summer and PP decrease by 80 mg-C/m^2/day in winter. PP appeared in August around 40N was the highest (2,200 mg-C/m^2/day) among three stations. PP in the NWNP have been observed on board previously. Compared our estimated values with values reported previously, although winter PP estimated by "B&F" in this study was comparable to that observed on board, our PP are significantly higher, especially in summer and autumn.

4.2 Comparison between estimated PP and organic carbon flux by sediment trap

It has been reported that organic carbon flux collected by sediment trap reflected ocean PP, in other words, high organic carbon flux was observed in the high productivity area. Fig. 1 compares seasonal variability in organic carbon flux observed by sediment traps (bar graph) with that in estimated PP (axis is expressed as logarithm scale). Although PP estimated with "B" equation were not correlated with organic carbon flux, PP estimated with "B&F" equation correlated well with organic carbon flux for respective stations. Although absolute values still remain uncertain, it can be said that organic carbon flux observed by sediment traps correlated positively with PP.

4.3 The export ratio and vertical change in organic carbon flux

One of the goal of our study is the estimation of carbon flux at the lower boundary of the surface mixed layer (biological carbon pump) with carbon flux observed by sediment trap moored in the deep sea in order to quantify the role of biological pump in the uptake of atmospheric CO_2. For the sake of this, empirical equation for the export ratio (the ratio of carbon flux at the lower boundary of mixed layer to PP) and vertical change in organic carbon flux should be proposed. Following empirical equation proposed previously (*e.g.* Suess, 1980; Betzer *et al.*, 1984; Pace *et al.*, 1987), we expressed the equation for PP and vertical change in organic carbon as following exponent function;

$$Fc(z) = a * PP^b * Z^c \quad \text{---------- (3)}$$

where, Fc(z) is organic carbon flux at z m depth. From equation (3), organic carbon flux at z m (Fc(z)) and at z1 m (Fc(z1)) have following relation;

$$\text{Log}(Fc(z)) - \text{Log}(Fc(z1)) = C*(\text{Log}(z) - \text{Log}(z1)) \quad \text{---------- (4)}$$

At first, we calculated constant C using organic carbon flux collected at ~ 1000 m, 3000m, and 5000 m for respective stations.

Equation (3) can be converted to

$$\text{Log}(Fc(z)) = b*\text{Log}(PP) + (\text{Log}(a) + C*\text{Log}(z)) \quad \text{---------- (5)}$$

Sequentially, we calculated "a" and "b" using organic carbon flux at 1000 m and organic carbon flux at 1000 m estimated with flux at 3000 m and 5000 m using equation (4).

As a result of these calculation, equations proposed this study leads that the export ratio is ~ 8 % for KNOT and ~ 15 % for 50N and this ratio decreases with increasing PP. Vertical change in organic carbon flux estimated this study is smaller than other studies. Approximately 50 %, 26 %, and 36 % of organic carbon flux exported from the upper 100 m reached 1000 m depth around stn. KNOT, 50N, and 40N, respectively.

5. Conclusion

PP estimated with satellite data (Chl-a, SST, PAR) and using an empirical equation by Behrenfeld and Falkowski (1997) showed positive correlation with organic carbon flux collected by sediment traps although absolute PP values remains still questionable. Based on empirical equations for the export ratio (organic carbon at 100 m / PP) proposed this study, the annual mean of export ratio in the northwestern North Pacific (NWNP) is ~ 10 % and decreases with increasing PP. Vertical change in organic carbon flux was smaller in the NWNP than other area. For more detail discussion on biological pump in the NWNP, the development of algorithm for estimation of PP with satellite data for the NWNP and the time-series observation of organic carbon fluxes in the upper layer with ST are strongly requested.

References

Behrenfeld, M.J. and Falkowski, P.G. (1997), *Limnol. Oceanogr.*, **42(1)**, 1-20.

Berger, W.H. (1989), *Productivity of the Ocean: Present and Past*, 429-455.

Betzer, P.R., Shower, W.L., Laws, E.A., Winn, C.D., Ditullio, G.R., Kroopnick, P.M. (1984), *Deep-Sea Res.*, **31**, 1-11.

Ishizaka, J. (1998), *J. Oceanogr.*, 54, 553-564.

Morel, A. and Berton, J.F. (1989), *Limnol. Oceanogr.*, **34(8)**, 1545-1562.

Pace, M.L., Knauer, G.A., Karl, D.M., and Martin, J.D. (1987), *Nature*, **325**, 803-804.

Suess, E. (1980), *Nature*, **288**, 260-263.

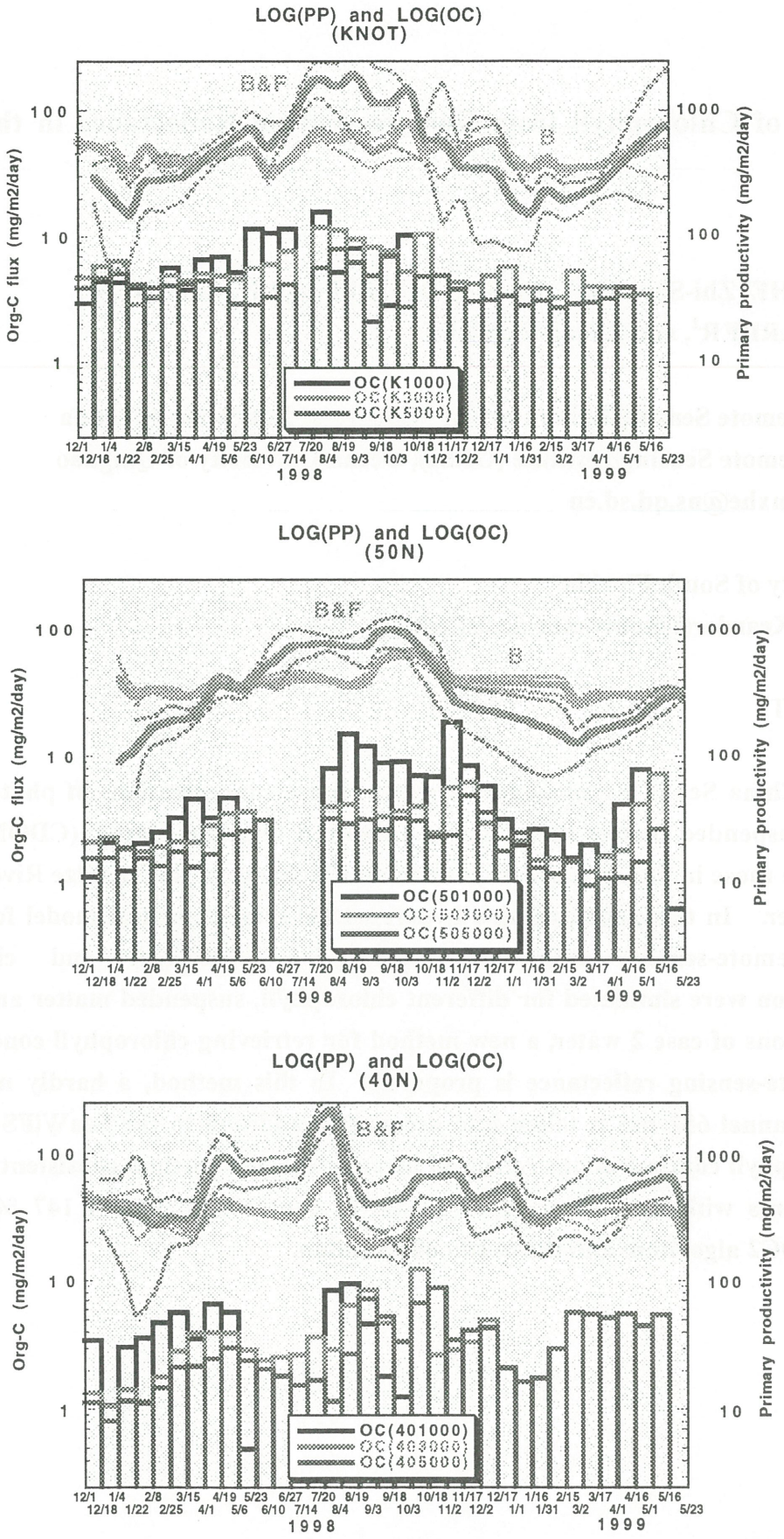

Fig. 1 Seasonal variability in primary productivity (PP) estimated with satellite data using empirical equations proposed by Behrenfeld and Falkowski (1997) (B &F) and Berger (1989) (B) (line graph), and organic carbon flux (OC) observed by sediment traps at ~ 1000, 3000, and 5000 m (bar graph). Solid lines and broken lines for PP show average and maximum / minimum, respectively. Note that OC and PP values are in logarithm scale.

Retrieval of Chlorophyll from Remote-Sensing Reflectance in the China Seas

Ming-Xia[1] HE, Zhi-Shen LIU[1], Ke-Ping DU[1], Li-Ping LI[1], Rui CHEN[1], Kendall CARDER[2], and Zhong-Ping LEE[2]

1: Ocean Remote Sensing Laboratory of Ministry of Education of China
Ocean Remote Sensing Institute (ORSI), Ocean University of Qingdao
E-Mail: mxhe@ns.qd.sd.cn

2: University of South Florida
E-Mail: Kcarder@monty.marine.usf.edu

ABSTRACT

The East China Sea is a typical case 2 water whose concentrations of phytoplankton pigment, suspended matter and Colored Dissolved Organic Matter (CDOM) are all higher than those in the open oceans, due to the discharge of the Yangtze River and the Yellow River. In this paper, using a hyperspectral semi-analytical model for shallow waters, remote-sensing reflectance, absorption coefficient and chlorophyll concentration were simulated for different chlorophyll, suspended matter and CDOM concentrations of case 2 water, a new method for retrieving chlorophyll concentration from remote-sensing reflectance is proposed. In this method, a hardly neglectable spectral channel 682 nm is taken into account in addition to the SeaWiFS channels. The chlorophyll concentrations retrieved through the new method consistent with field measurements with a small error of 18 %, in contrast to that of 147 % between SeaWiFS OC2 algorithm and the *in situ* observation.

Chlorophyll Control of Surface Temperature in the Arabian Sea

R. Frouin[1] and S. Nakamoto[2]

1. Scripps Institutions of Oceanography, UCSD

2. Earth Science & Technology Organization, Japan

Abstracts

A general ocean circulation model is used to investigate the effect of solar radiation absorption by phytoplankton on surface temperature. The model, an updated version of Oberhuber's (1993) OPYC model, solves primitive equations, uses isopycnals as Lagrangian vertical coordinates, and includes a fully coupled mixed layer. The vertical profile of heating rate is parameterized as a function of remotely-sensed chlorophyll concentration. The model is run for 50 years without chlorophyll (control run) and an additional 10 years with chlorophyll (experimental run). The difference between experimental and control runs gives the biological effect. In January, sea surface temperature anomalies are positive in the northern hemisphere and negative in the southern hemisphere. In July, the opposite result is obtained. This suggests that, on a global scale, phytoplankton acts at moderating meridional temperature gradients. In the Arabian Sea, along a zonal strip centered at 20N, positive anomalies reaching 0.6K appear twice a year, from March through June and from September through November, and are associated with the two maxima of solar radiation over the annual cycle. The anomalies are smaller by 0.2K during the fall inter-monsoon season despite a 5-fold increase in chlorophyll abundance, because of reduced solar radiation. Increased chlorophyll during the southwest monsoon causes surface warming and sub-surface cooling consistent with JGOFS observations during the 1994-1995 Arabian Sea experiment.

Ocean Color Detection of Chanjang Plume in the East China Sea on 1998

Joji Ishizaka

Faculty of Fisheries, Nagasaki University
Nagasaki 852-8521, Japan

Abstract

Flood of the Chanjiang River on summer of 1998 discharged large amount of materials into the East China Sea. Time series of ocean color remote sensing data showed that the greenish water of the plume extended to the east and flew into the Japan Sea on September. Although the ocean color may be affected by suspended matter from the river at the mouth, fairly well correlation between the sea-truth and satellite chlorophyll concentrations indicates that chlorophyll concentration in the East China Sea is enhanced by the plume.

Key words: East China Sea, Chanjiang River, Ocean Color, Chlorophyll

1. Introduction

Chanjiang River is one of the largest rivers in the world and about 10,000-50,000 m^3 s^{-1} of freshwater is discharged to the East China Sea (Ning et al., 1998), and large amount of dissolved and suspended materials supplied to the East China Sea. Heavy rain in the mid-China on the summer of 1998 caused one of the worst floods of the surrounding area of the Chanjiang River. It is expected that the discharged freshwater and materials also increased during the time.

Ocean color remote sensing is one of the powerful tools to detect the large river discharge. Muller-Karger et al. (1988) used Coastal Zone Color Scanner (CZCS) data to show the effect of the Amazon River extended to east, middle of the Atlantic Ocean. Ning et al. (1998) described general pattern of ocean color in the East China Sea with relation to the general circulation, using the monthly composite of CZCS data during 1978-1986. Ocean color remote sensor is absent for about 10 years after the CZCS, and the Japanese Ocean Color and Temperature Scanner was on-board of Advanced Earth Observation Satellite (ADEOS) launched on August 1996 and collected about 8 months of global data. Although the ADEOS was shut-down on June 1997, NASA SeaWiFS was launched on September 1998 and the data is available since then.

In this paper, monthly composite SeaWiFS ocean color data of 1998 was used to

identify the plume of Chanjiang River in the East China Sea during the flood period

2. Methods

NASA monthly chlorophyll a (hereafter chlorophyll) and normalized water leaving radiance of 555 nm were used. Normalized water leaving radiance is the water leaving radiance, which varies with incident incoming irradiance, normalized to the extra-terrestrial irradiance. Those data are provided from NASA Goddard Space Flight Center. The chlorophyll concentrations were calculated from the ratio of 413, 490, and 560 nm of water leaving radiance with an empirical relationship indicating high chlorophyll water is green. Ship-measured sea surface chlorophyll data was provided from Kagoshima Univeristy, Seikai National Fisheries Research Institute, National Research Institute of Far Seas Fisheries and Japan Meteological Agency.

3. Distribution of Satellite Chlorophyll

Figure 1 showed the monthly chlorophyll data detected by SeaWiFS. The chlorophyll distribution indicated that high chlorophyll water extended from the mouth of the Changjang River to the east in the East China Sea. About 2 $\mu g\ l^{-1}$ line was located only at 123°E on June, and moved to 125°E on July, and further extended to 128°E on August. During these three months, the high chlorophyll plume moved to the east. However, on September the plume moved to the northeast, flew along the coast of the South Korea and moved into the Japan Sea through the Korea Strait (western channel of Tsushima Strait). The high chlorophyll (>2 $\mu g\ l^{-1}$) region decreased on October.

4. Accuracy of Chlorophyll Concentration

Although the satellite-derived chlorophyll concentration was fairly well correlated with the sea-truth data in the open ocean, presence of suspended solid and colored dissolved organic materials are know to be interfered the chlorophyll estimation in the coastal area (Fukushima and Ishizaka, 1993). In the East China Sea, Kiyomoto et al. (1998) compared OCTS data with the past chlorophyll measurements and found the overestimation of OCTS. Water leaving radiance on 555 nm is known as an good indicator of high reflectance of suspended materials, thus the radiance distributions were examined.

The distribution of normalized water leaving radiance of 555 nm derived from SeaWiFS data showed that the high reflectance water corresponded to the high-chlorophyll region around 125°E and 32°N during winter period (Fig. 2). Since this high reflectance area was corresponded to the shallow water area off the Changjiang River mouth on the

continental shelf, the strong mixing during the winter period caused the resuspension of the bottom sediment and increased the suspended materials. On the other hand, the high reflectance water distributed only along the coast of the China and Korea, and the high SeaWiFS chlorophyll water does not corresponded to the high reflectance water during summer. This indicates that the suspended materials are not important for the greenish water mass extended to the middle to east of the East China Sea during the 1998 flood.

In order to further verify the chlorophyll concentrations estimated by the SeaWiFS, ship-measured sea surface chlorophyll data in the East China Sea was collected during the spring to summer of 1998 and compared with the monthly SeaWiFS chlorophyll data (Fig. 3). The comparison indicated that there is no large bias for the chlorophyll data and that the SeaWiFS data is fairly well corresponded to the actual sea surface chlorophyll concentrations.

5. Discussion

Satellite chlorophyll data indicates that plume of the Changjiang River extended to the east in the East China Sea from June and reached to the Korea Strait (western channel of Tsushima Strait) on September during 1998 when the heavy rain caused serious floods to the river. Extension of the high chlorophyll plume is far more east than the one detected by CZCS 1978-1996 composite shown by Ning et al. (1998). Unfortunately, OCTS data was only available from November 1996 to June 1997 and SeaWiFS data from 1999 is not available yet, and year-to-year comparison is difficult.

It is certain that the Chagjiang river plume covered large area of the East China Sea, including the water around Cheju Island, and the effect extended to the Japan Sea through the Korea Strait (western channel of Tsushima Strait). It is known that the decrease of the salinity may have affected to the local fisheries.

Distributions of the normalized water leaving radiance of 555 nm indicate that the water in the plume did not show high reflectance and that the suspended materials from the river are negligible. Fairly well correlation between the satellite and ship chlorophyll indicates that the plume is actually high chlorophyll water. It is not known how the high chlorophyll was maintained during the plume extended to the east. The time scale of the plume is at least one month, and it is unlikely that the nutrients contained in the water of the Changjiang river can maintain the high chlorophyll. The extension of the high chlorophyll plume may also affect to the ecosystem in the East China Sea. It is further expected that such an event may affect to the ecosystem of the Japan Sea.

Acknowledgement

I would like to thank Prof. Toshihiro Ichikawa of Kagoshima Univeristy, Ms. Yoko Kiyomoto and Mr. Kazumaro Okamura of Seikai National Fisheries Research Institute, and Dr. Akihiro Shiomoto of National Research Institute of Far Seas Fisheries for their permission to use their chlorophyll data for the sea-truth of SeaWiFS data. I also thank Ms. Yoko Kiyomoto and Mr. Kazumaro Okamura for their discussion.

References

Fukushima, H. and J. Ishizaka (1993): Special features and applications of CZCS data in Asian waters. In "Ocean Colour: Theory and applications in a decade of CZCS experience", Eds. V. Barale and P.M. Schlittenhardt, 213-236pp.

Kiyomoto, Y., K. Okamura, K. Iseki, and H. Nagata (1998): Variability of chlorophyll distribution in the East China Sea using shipboard measurements and ocean color satellite imagery. AGU 1998 Fall Meeting.

Muller-Karger, F.E., C.R. McClain, and P.L. Richardson (1988): The dispersal of the Amazon's water. Nature 333, 56-59.

Ning, X, Z. Liu, Y. Cai, M. Fang and F. Chai (1998): Physicobiological oceanographic remote sensing of the East China Sea: Satellite and in situ observations. J. Geophysic. Res., 103, 21,623-21,635.

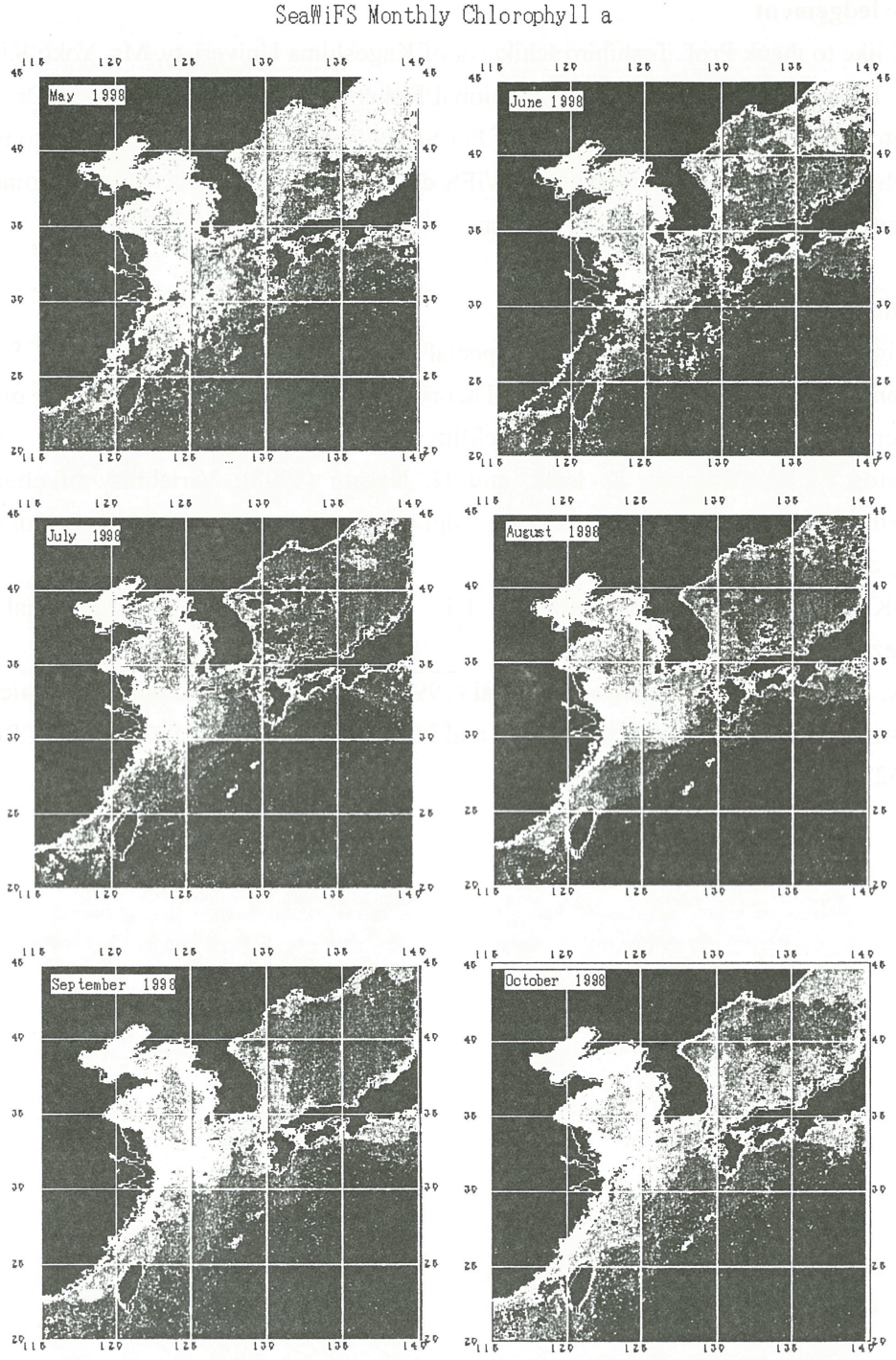

Figure 1 Chlorophyll distribution in the East China Sea from May to October 1998 detected by SeaWiFS. High and low concentrations of chlorophyll is expressed as bright and dark color, respectively, and black area indicates land and clouds.

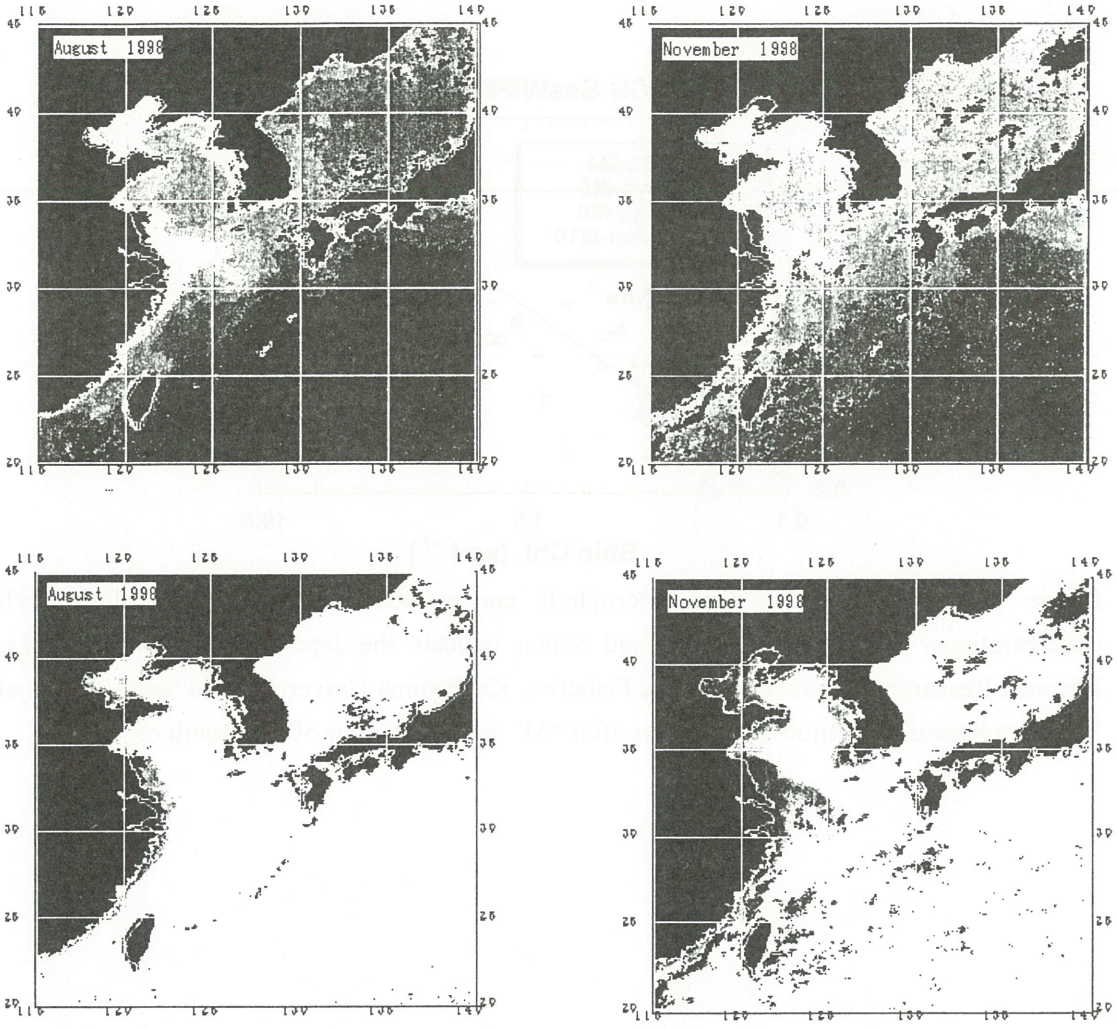

Figure 2 Chlorophyll (upper panels) and normalized water leaving radiance of 555 nm (lower panels) in the East China Sea on August and November, 1998. High and low concentrations of chlorophyll is expressed as bright and dark color, respectively. High and low normalized water leaving radiance is expressed as dark and bright color, respectively. Black area indicates land and clouds.

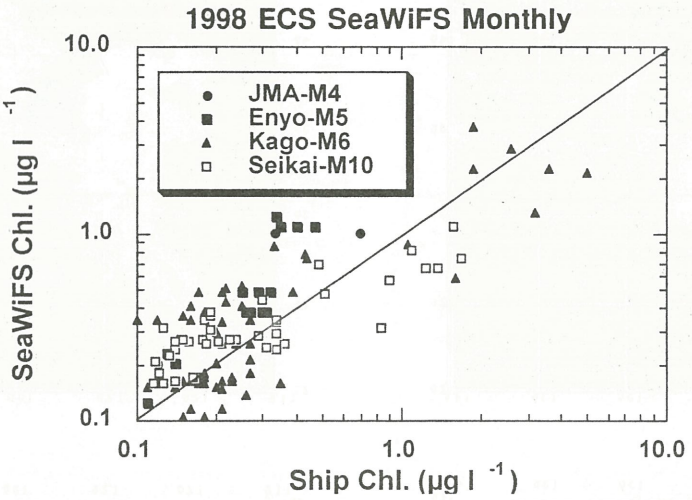

Figure 3 Comparison of ship chlorophyll concentration and SeaWiFS chlorophyll concentrations. JMA, Enyo, Kago, and Seikai indicate the Japan Meteological Agency, National Research Institute of Far Seas Fisheries, Kagoshima University, and Seikai National Fisheries Research Institute. Numbers after "M" are the number of the month of the year.

Blooming Mechanism off Lombok Strait

Ichio Aasanuma, Kazuhiko Matsumoto, Hirofumi Okano, and Takeshi Kawano
Japan Marine Science and Technology Center
E-Mail: asanumai@jamstec.go.jp

Abstracts

A series of ocean color sensors, OCTS on ADEOS and SeaWiFS on OrbView-2, provided images of chlorophyll-a distribution along the Sunda Islands. A limited number of sea surface wind observation by NSCAT on ADEOS showed the important contribution of the sea surface wind to the distribution of chlorophyll-a. The sea surface topography observation by SAR on J-ERS-1 also supported the surface flow from the Lombok strait and contribution of flows to the phytoplankton distribution. From satellite observation, it is confirmed that the irregular wind, which is different from the major monsoon wind, determines the distribution of phytoplankton. The southeast wind in February 1997 regulated the runoff from the Lombok Strait. The phytoplankton bloom was started when the southeast wind has stopped. From in-situ observation in March 1998, the spatial distribution of the phytoplankton bloom was made clear. The surface layer up to 30 m with a lower density around 21.5 kg m^{-3} and slightly higher nitrate around 0.5 uM L^{-1} maintains the phytoplankton bloom along the coast.

1. Introduction

The Indonesian through flow runs from the Pacific to the Indian Ocean through Indonesian Islands. The North Equatorial Current in the Pacific is the major source of the Indonesian through flow, which enters the Indonesian sea through the Mindanao strait, passing the Celebes Sea, Jawa Sea, the Banda Sea, the Arafura Sea, the Timor Sea and runs into the Indian Ocean. Also the South Equatorial Current in the Pacific is another source of the Indonesian through flow, which is running into the Salam Sea and the Maluka Sea. Figure 1 shows the major route of the Indonesian through flow and related flows on the Java Sea including the minor flows through straits. Although the major part of the Indonesian through flow runs into the Indian Ocean through the Timor Sea, the small portion of the Indonesian through flow runs into the Indian Ocean through the Lombok strait and other minor straits. The intensities of these flows or currents are dependent on the southeast or western monsoon. During the southeast monsoon, from May to September, the Indonesian through flow from the Timor Sea and the South Equatorial Current run along the Sunda Islands toward the West. On the contrary, the northwest monsoon from October to April, the South Equatorial Current runs southern off of the Sunda Islands, while the eastward coastal current, called the Java coastal current, runs along the Sunda Islands. Many scientists discussed these changes with observation and numerical models. [*Gordon et al.*, 1994, *Gordon*, 1995, *Fieux et al.* 1994].

We selected the southern off of the Lombok strait for the research region, where the runoff from the Lombok Strait may have a contribution to the distribution of phytoplankton with related to the seasonal variation of currents in the Indian Ocean. We repeated the expeditions as a joint research between Japan and Indonesia in this region to study the mechanism of the primary

production related to the Indonesian through flow using research vessels of the Indonesian government. In these expeditions, we had series of observation by the satellite born color sensors and other sensors, although it was difficult to synchronize between the in-situ measurement and the satellite observation.

2. Remote Sensors

2-1. Ocean Color Thermal Scanner

In August of 1996, the National Space Development Agency of Japan (NASDA) launched the ADEOS. Unfortunately, ADEOS stopped its mission in June of 1997 because of the trouble on the solar panel. During its mission life, OCTS had provided images of chlorophyll-a and sea surface temperature distribution over the globe. The OCTS covers 1400 km in the swath range from the altitude of 800 km. The swath range varies with the tilting function of the scanning mirror, which is designed to avoid a solar glitter from the surface. The OCTS has a spatial resolution of 700 m at a nadir. Figure 2-a shows a chlorophyll-a distribution observed and Figure 2-b shows a sea surface temperature distribution observed by OCTS. These images show a beginning of the chlorophyll-a bloom off the Lombok strait.

2-2. Sea Wide Field of View Sensor

Shortly after the ADEOS mission, the NASA and the OrbImage cooperation launched the OrbView-2 polar orbiting satellite with the SeaWiFS. The SeaWiFS provides images of chlorophyll-a distribution as much as the OCTS. The SeaWiFS covers 2000 km in swath from the altitude of 800 km. The SeaWiFS has a spatial resolution of 1.4 km at a nadir, although it varies with a tilting angle. Figure 3-a shows a chlorophyll-a distribution observed by SeaWiFS and Figure 3-b shows a sea surface temperature distribution observed by AVHRR. These images show a plume of chlorophyll-a from the Lombok strait.

3. Mechanism of chlorophyll bloom

It was possible to classify the water layers into four layers in the offshore water and three layers in the coastal water judging from the vertical distribution of chlorophyll-a. Figure 4-a shows a vertical cross section of chlorophyll-a along 116 degree-East between 9 degree-South to 12 degree-South. Figure 4-b is a vertical cross section of nitrate (NO3). Figure 4-c is a vertical cross section of Density. Figure 4-d is a vertical cross section of current vectors observed by ADCP.

The offshore water is classified into four different water layers. The top layer is the surface mixed layer with showing a lower density and with a depleted nitrate. In this top layer, the chlorophyll-a concentration is around 0.1 mg m^{-3}, which is lower than the surface water near the Islands. The nitrate is supplied by the runoff from the Lombok strait, but the nitrate cannot be supplied to the offshore through the surface layer, where the nitrate is consumed by the phytoplankton immediately. The second layer is the pycnocline with a depleted nitrate. The pycnocline is the stable water layer under the mixed layer and over the nitracline with preventing a penetration or a mixing of waters between both sides. In this second layer, the chlorophyll-a concentration is very low, less than 0.1 mg m^{-3}, because of low nitrate. The third layer is the nitracline, where the higher density water and the chlorophyll maximum are observed. The

chlorophyll maximum shows the chlorophyll-a concentration around 0.4 mg m^{-3}, which is lower concentration than the chlorophyll maximum near the coast. The forth layer is the high density and the high nitrate water mass under the chlorophyll maximum. The second and deeper layers showed the stable flows.

The coastal water is classified into three different water layers. The top layer is the surface mixed layer with the lower density and with the slightly higher concentration of the nitrate. In this top layer, the chlorophyll-a concentration is around 0.2 mg m^{-3}. This top layer is supposed to be the water mass from straits along the Sunda Islands. The second layer is the stable water mass with the pycnocline and the nitracline. In this second layer, the chlorophyll maximum is observed with the chlorophyll-a concentration around 1.0 mg m^{-3}. The third layer is the high density and the high nitrate water mass under the chlorophyll maximum. The second and deeper layer is the westward Indonesian through flow along the Islands, because of the steady westward current. This also suggests that the structures of the water mass in the second and deeper layer are that of the Indonesian through flow along the Sunda Islands.

In this section, we classified the water masses into the offshore and the coastal type. From this classification, it is possible to address that the surface mixed layer is observed in all sections. The surface mixed layer near the coast is slightly deeper than that of the offshore. The observation depth of the satellite ocean color sensor is in the order of the inverse of K, the attenuation coefficient of the water. Except the coastal turbid waters, the observation depth of the water in this area is corresponding to the surface-mixing layer. This means that the chlorophyll-a distribution observed by the ocean color sensor only explains the water characteristics only in the surface-mixing layer.

The chlorophyll-a blooming in this region, especially observed by the satellite sensor, is the phenomenon in the surface-mixing layer, which is influenced by the flows from the straits along the Sunda Islands, the tidal currents, and the sea surface winds. The major westward stream of the Indonesian through flow along the Sunda Islands did not make a significant contribution to the surface-mixing layer with running under the surface-mixing layer.

4. Conclusion

In the previous studies, there were two hypotheses on the bloom of phytoplankton in the Indian Ocean on two different seasons. *Nontiji* [1977] proposed the hypothesis that the nutrient rich water originated from the westward SEC during the southeast monsoon produced the bloom. *Setiapermana* [1992] proposed the hypothesis that the divergence between the eastward Java coastal current and the westward SEC during the northwest monsoon produced the bloom. These two hypotheses explain the blooms for two seasons, the southeast monsoon and the northwest monsoon.

In this study, the continuous observation by satellite, especially using the ocean color sensors, revealed the mechanism of primary production along the Sunda Islands. Those data described that the runoff from the straits along the Sunda Islands are continuously running into the Indian Ocean except the period while the strong southeast wind suppress the flow into the Indian Ocean.

The OCTS provided the data set to understand the mechanism of the primary production. The NSCAT supported the understanding of the current field with the wind data. Although the satellite observation in March 1997 was in the western monsoon period, the strong southeast wind prevented the flows from the Lombok strait to the Indian Ocean. It is suggested that the southeast

wind on the both side of the Sunda Islands regulated the flows, especially the southeast wind along the northern side of the Sunda Islands regulated the outgoing flow into the Indian Ocean. Following to the southeast wind period, the west wind was dominant as in the western monsoon period. During this west wind period, the flows from the Lombok strait were continuously observed.

The synchronized observations between the satellites and the research vessel were realized in March of 1998. In this period, the flow from the Lombok strait was continuously observed. The water sampling from the water column revealed the structure of the water mass along the Sunda Islands. The water layers are classified into four layers in the offshore water and into three layers in the coastal water.

In the offshore, the top layer is a surface mixed layer with a low density and a low nitrate concentration, where a chlorophyll-a concentration was less than 0.1 mg m^{-3}. The second layer is a pycnocline with a low chlorophyll-a concentration and a low nitrate concentration. The third layer is a nitracline with higher density water and a chlorophyll-a maximum around 0.4 mg m^{-3}. The fourth layer is high density and nitrate rich water under a chlorophyll-a maximum.

Along the coast, the top layer is a surface mixed layer with a low density and a slightly higher nirate, where a chlorophyll-a concentration was around 0.2 mg m^{-3}. This top layer is water mass from the Lombok strait and observed by satellite sensors. The second layer is a stable water mass with a pycnocline and nitracline, where a chlorophyll-a maximum was observed in the order of 1.0 mg m^{-3}. The third layer is high density and nitrate rich water under a chlorophyll-a maximum.

The surface mixed layer in the offshore and the coastal area showed a different nitrate concentration. The nitrate is supplied by the runoff from the Lombok strait, but the nitrate cannot be supplied to the offshore through the surface layer, as the nitrate is consumed by the phytoplankton immediately.

This mechanism is also observed by the SAR image as the distribution of the surface roughness. The surface roughness indicated the runoff of the coastal water from the Lombok strait and the water mass scattered to the offshore.

For these distribution of the water mass and the distribution of chlorophyll-a bloom in the surface, this study made clear the influence of the southeast wind to regulate the flow of the water from the straits along the Sunda Islands and the less influence of the west wind. The southeast wind along the Sunda Island will regulate the water mass in the both side of the Sunda Island, the Java Sea and the Indian Ocean, with reducing the outgoing flows into the Indian Ocean. On the contrary, the west wind along the Sunda Island may push the water mass in the Java Sea into the Indian Ocean through the straits along the Sunda Islands.

5. References

Fieux,M., C.Andrie, P.Delecluse, A.G.Ilahude, A.Kartavtseff, F.Mantisi, R.Molcard and J.C.Swallow, Measurements within the Pacifi-Indian oceans throughflow region, *Deep-Sea Res., 41*, 1091-1130, 1994.

Gordon, A.L., A.Ffield, and A.G.Ilahude, Thermocline of the Flores and Banda Seas, *J.Geophys. Res., 99*, 18235-18242, 1994.

Gordon, A.L., When is Appearance Reality? A Comment on Why Does the Indonesian

Throughflow Appear to Originate from the North Pacific, *J.Physical Oceanog., 25*, 1560-1567, 1995.

Hsu,C.S., *Ocean Wind Products CD-ROM User's Manual*, Jet Propulsion Laboratory, D-14766, 62pp., 1997.

Nontji A., Notes on the Chlorophyll Distribution around Jawa, *Oseanologi di Indonesia, 7*, 43-47, 1992.

Setiapermana D., Santoso, and S. H. Riyono, Chlorophyll Content in Relation to Physical Structure in East Indian Ocean, *Oseanologi di Indonesia, 25*, 13-29, 1992.

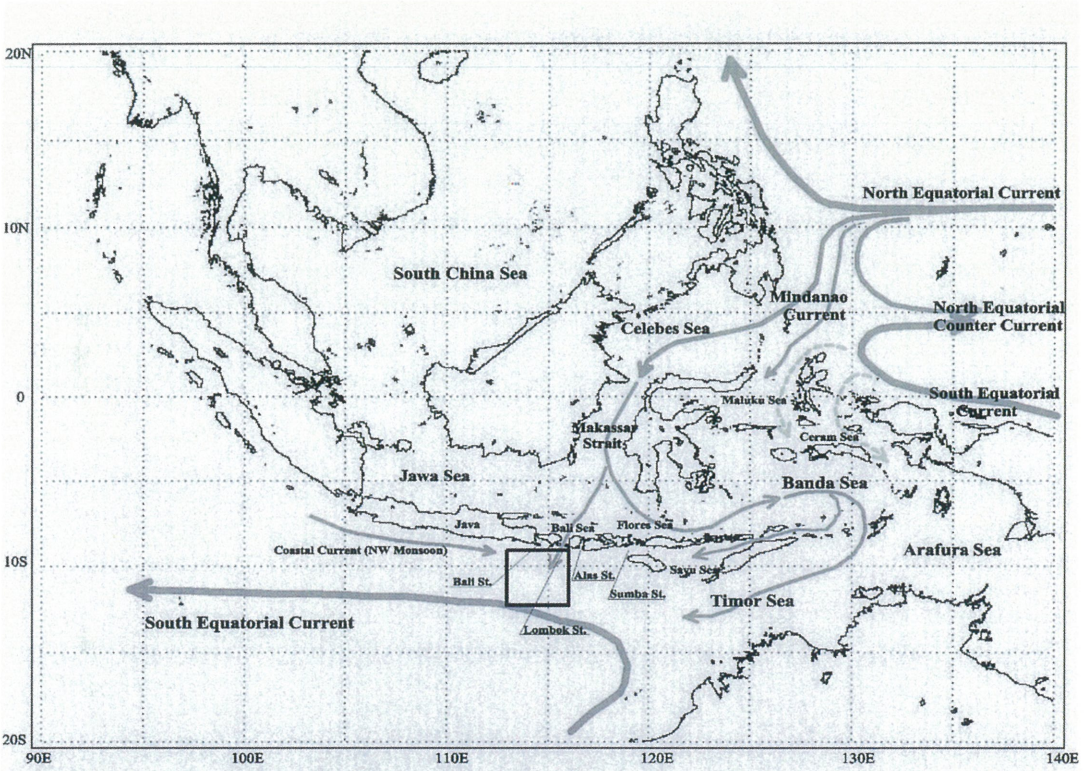

Fig.1 Currents around Indonesian Islands

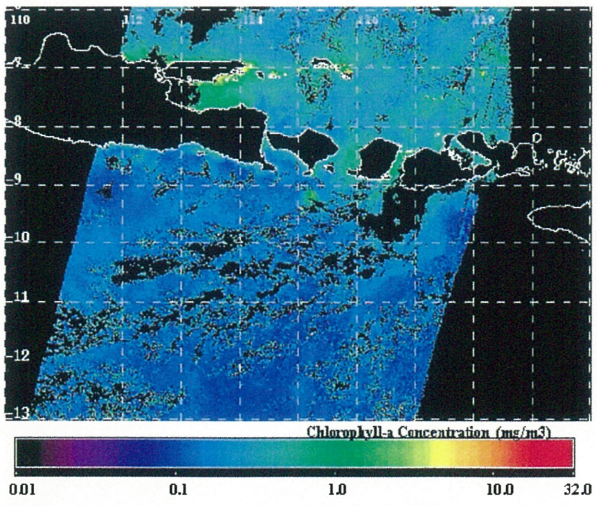

Fig.2a Chlorophyll-a on Mar.14,97 by OCTS

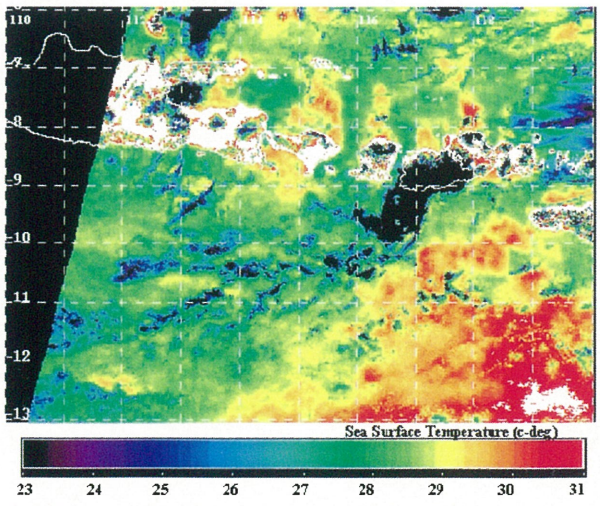

Fig.2b Sea Surface Temp. on Mar.14,97 by OCTS

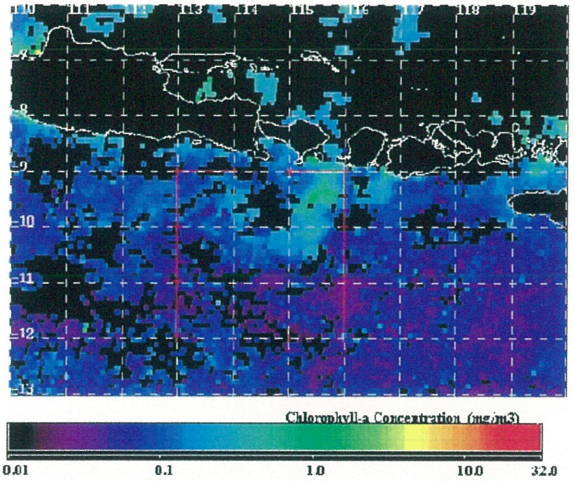

Fig.3-a Chl-a 14-Mar-98 to 21-Mar-98 by SeaWiFS

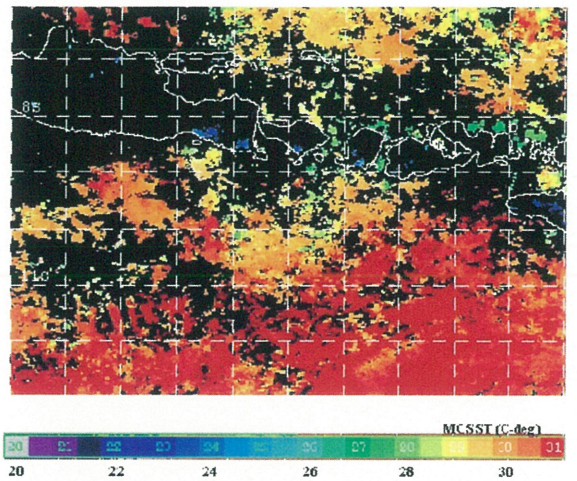

Fig.3-b MCSST from 14-Mar-98 to 21-Mar-98 by AVHRR

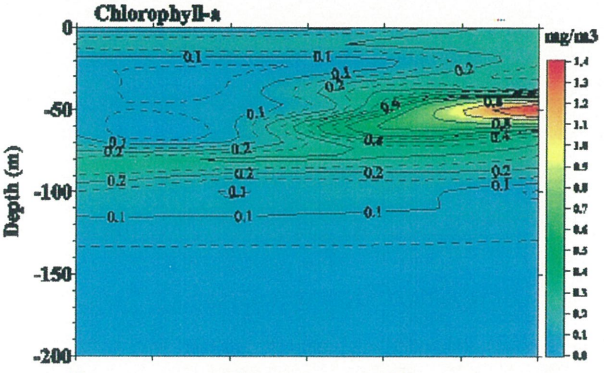

Fig.4-a Chlorophyll-a Cross Section along 116E

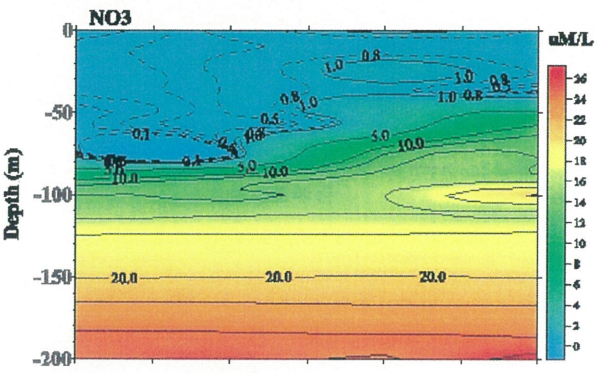

Fig.4-b Nitrate Cross Section along 116E

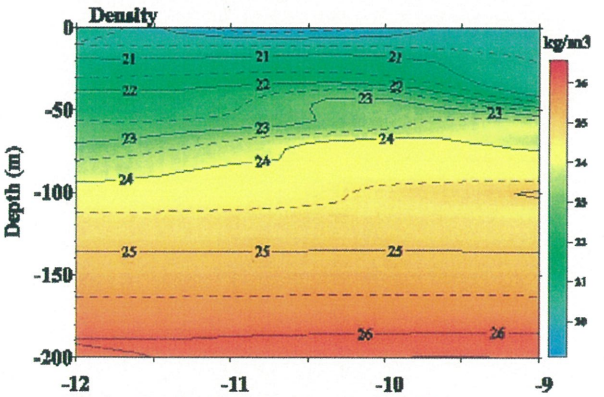

Fig.4-c Density Cross Section along 116E

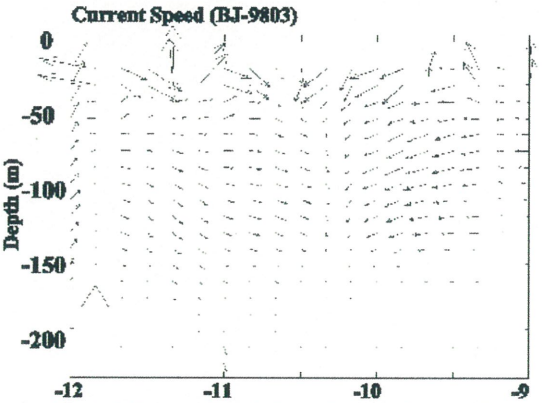

Fig.4-d Current Speed Cross Section along 116E
(Left bottom arrow=2kt)